Chemical Science

ROYAL SOCIETY OF CHEMISTRY

REVIEW

View Article Online
View Journal | View Issue

Check for updates

Cite this: *Chem. Sci.*, 2025, **16**, 11768

Oriented design and engineering of advanced metal–organic frameworks for light hydrocarbon separations

Hujun Zhang,†[b] Jie Tang,†[a] Chunze Yu,†[b] Muyu Zhang,[a] Jiaqi Wang[a] and Jingui Duan *[ab]

Light olefins, such as ethylene (C_2H_4) and propylene (C_3H_6), are essential feedstocks for the production of chemical products. However, the current purification strategy of distillation is energy-intensive and results in high carbon emissions. Adsorptive separation, the selective capture of gas from mixtures by porous materials, is considered a promising alternative or transitional technology. Metal–organic frameworks (MOFs), a kind of porous material with highly tunable nature, have emerged as an innovative chemistry in the past two decades, offering solutions for separating these small gases. This review highlights recent advances in the design and engineering of advanced MOFs, with a focus on precise control over their pore structure and functionality for the adsorption-based purification of C_2H_4 and C_3H_6 from the corresponding hydrocarbons with the same carbon number. The importance of rational design in achieving specific functionalities, such as functional sites and molecular sieving in rigid MOFs and local/global dynamics in soft MOFs, is underscored, with examples demonstrating enhanced performance in selective adsorption separation. Additionally, methods and examples of large-scale synthesis of MOFs are briefly described. The goal is to present the state-of-the-art chemistry and applications of MOFs and to offer an outlook towards discovering and designing further new materials.

Received 5th March 2025
Accepted 1st June 2025

DOI: 10.1039/d5sc01755f

rsc.li/chemical-science

Open Access Article. Published on 02 June 2025. Downloaded on 5/21/2026 10:40:29 PM.
This article is licensed under a Creative Commons Attribution-NonCommercial 3.0 Unported Licence.

1. Introduction

The global production and demand for light olefins, especially polymer-grade ethylene (C_2H_4) and propylene (C_3H_6), exceed that of all other commodity organic compounds. The majority of these products are widely used in chemical manufacturing, such as plastics, synthetic rubber, and synthetic fibers.[1] Additionally, they are essential raw materials for agriculture and fine chemicals. Currently, C_2H_4 and C_3H_6 are isolated from the cracking units through the strategies of energy-intensive catalytic hydrogenation and cryogenic distillation methods, which account for nearly 3% of all separation energy.[2,3] Furthermore, the high pressure and low temperature bring significant risks during the separation process. Therefore, there is a strong need to develop energy-efficient separation technologies, such as

[a]State Key Laboratory of Materials-Oriented Chemical Engineering, College of Chemical Engineering, Nanjing Tech University, Nanjing 211816, China. E-mail: duanjingui@njtech.edu.cn

[b]State Key Laboratory of Chemistry and Utilization of Carbon-Based Energy Resources, College of Chemistry, Xinjiang University, Urumqi, 830017, China

† These authors contributed equally to this work.

Hujun Zhang

Hujun Zhang obtained his master's degree from Xinjiang University in 2022. Now, he is a PhD candidate at Xinjiang University, under the supervision of Prof. Jingui Duan. His current research interests include the design and synthesis of porous coordination polymers and their applications in gas separation.

Jie Tang

Jie Tang graduated from the Anhui University of Science and Technology of China with a BS Degree in Chemical Engineering and Technology. She is currently a PhD student under the supervision of Prof. Jingui Duan at Nanjing Tech University. Her research focuses on the design and synthesis of porous coordination polymers for gas separation.

© 2025 The Author(s). Published by the Royal Society of Chemistry

Open Access Article. Published on 02 June 2025. Downloaded on 5/21/2026 10:40:29 PM. This article is licensed under a Creative Commons Attribution-NonCommercial 3.0 Unported Licence.

Table 1 Properties of C2 and C3 hydrocarbons

	Molecular dimensions (Å^3)	Kinetic diameter (Å)	Polarizability (×10–24 cm^{-3})	Boiling point (K)
C_2H_2	3.32 × 3.34 × 5.70	3.3	3.33–3.93	188.4
C_2H_4	3.28 × 4.18 × 4.82	4.16	4.25	169.45
C_2H_6	3.81 × 4.08 × 5.70	4.44	4.43–4.47	184.6
C_3H_4	4.16 × 4.01 × 6.51	4.2	5.55	249.95
C_3H_6	4.65 × 4.16 × 6.44	4.6	6.26	225.45
C_3H_8	4.20 × 4.60 × 6.80	4.3//5.12	6.29–6.37	231.05

non-thermally driven processes, for downstream processing of cracked gas.[4–6]

Adsorption separation is often considered as an alternative technology due to its ability to separate gas molecules based on their chemical nature or size, rather than their boiling points. This non-thermal process can be carried out under mild conditions, such as at room temperature, resulting in significantly reduced energy inputs. However, the main challenge of this technology lies in the construction or selection of optimal porous materials that can achieve the desired uptakes and separation factors. This is particularly difficult due to the extremely similar molecular properties of light hydrocarbons, especially when dealing with mixtures containing the same number of carbon atoms (Table 1). This similarity in properties, both physical and chemical, makes the efficient separation of these molecules a highly challenging task.

Porous materials, such as zeolites and activated carbons, have long been studied for their potential in separating light hydrocarbons.[7–10] For example, silver ZK-5 zeolite, known for its unique pore structure and surface chemistry, has shown promise in separating C_2H_4 and C_2H_6. However, the strong interaction between the host and guest molecules makes it difficult to desorb them at higher temperatures (>200 °C), limiting their practical applications.[11] Activated carbons, on the other hand, have an irregular pore system with meso- or macropores, leading to co-adsorption and making it challenging to obtain pure C_2H_4. In summary, these traditional porous materials, lacking structural diversity and design flexibility, are not suitable for meeting the demands of industrial hydrocarbon separations.

Metal–organic frameworks (MOFs), also known as porous coordination polymers (PCPs), are a new class of crystalline porous materials, which are built from the coordination assembly of organic linkers and inorganic nodes in two or three dimensions.[12–21] MOFs are emerging porous materials due to their charming diversity, exceptional porosity, functional pore surface and tunable nature (pore size, shape and distribution).[22–29] Over the past two decades, there have been numerous reports on MOFs, with many designs specifically targeting the separation of light hydrocarbon mixtures (Scheme 1). These designs have led to significant improvements in key properties, such as capacity and selectivity (Table 2). Typically, as a kind of rigid framework with open Cu sites, HKUST-1 was investigated as the first MOF for the separation of C_2H_4/C_2H_6 mixtures as early as 2002.[30] After modifying the isolated open metal sites to a linear configuration, Fe_2(dobdc) (dobdc: 2,5-dioxido-1,4-benzenedicarboxylate) demonstrated a sharply promoted separation performance of C_2H_4/C_2H_6 and C_3H_6/C_3H_8 at 318 K, as the linear Fe atoms exhibited a strong affinity towards C_2H_4 and C_3H_6.[31] Since the prediction of structural dynamics by Prof. Kitagawa in 1998,[75] active research shifted to design and synthesis of soft MOFs for such separation, given the structural sensitivity of these structures to the tiny difference in the light hydrocarbons.[76] With a rational pyridyl ring (also called

Chunze Yu

Chunze Yu graduated from Yili Normal University with a B.S. degree in 2024. In the same year, he joined Xinjiang University as a master's student under the supervision of Prof. Jingui Duan. His main interests are in the field of porous coordination polymers for efficient light hydrocarbon separation.

Jingui Duan

Jingui Duan obtained his PhD from the Coordination Chemistry Institute of Nanjing University in 2011. He was subsequently awarded a JSPS fellowship at Kyoto University, under the supervision of Professor S. Kitagawa, from 2011 to 2014. In 2015, he joined Nanjing Tech University. He was promoted to a full professor in 2018, and subsequently moved to Xinjiang University in 2024. His current research interests focus on the design and synthesis of porous coordination polymers and membranes for gas separations.

Open Access Article. Published on 02 June 2025. Downloaded on 5/21/2026 10:40:29 PM. This article is licensed under a Creative Commons Attribution-NonCommercial 3.0 Unported Licence.

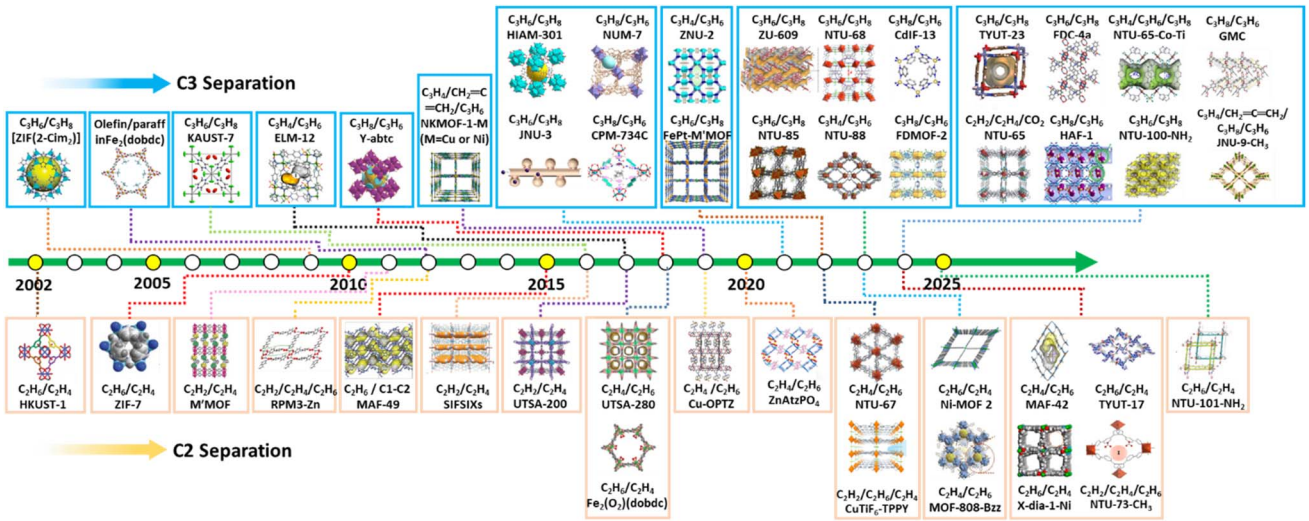

Scheme 1 The representative MOFs for the separation of light hydrocarbons.[6,30–74]

a confined-rotational shutter) in the confined nanospace, NTU-88 creates a maximum aperture of 4.4 Å, allowing dedicated propyne C_3H_4 (4.4 Å) adsorption from a C_3H_6 (5.4 Å) containing mixture under ambient conditions.[69] Moreover, the dynamic nature of the molecular pockets in JNU-3a is pivotal for achieving molecular sieving of C_3H_6 and C_3H_8.[65] In this regard, MOFs have shown significant advantages over traditional materials in the separation of light hydrocarbons. Consequently, the present review outlines recent advances in MOF chemistry in the separation of light hydrocarbons, with a particular focus on the oriented design strategy, including functional sites in rigid MOFs, molecular sieving in rigid MOFs, and local dynamics and global flexibility in soft MOFs. The discussion will incorporate computational modelling and gas-loaded crystallographic structure to reveal the host–guest interaction and emerging functions in the most promising and innovative achievements. In addition, the strategies for large-scale MOF synthesis were also analysed. Separations of methane and carbon dioxide from light hydrocarbons are not included.

2. Design strategies

In the context of the continuous advancement of sophisticated MOFs for the separation of gases, a range of design strategies have been put forward. These can be broadly categorized into two groups based on their principles of gas molecular adsorption separation: (1) functional sites, molecular sieving and diffusion strategies using rigid MOFs, and (2) framework dynamics strategies in soft MOFs (Fig. 1). And, we compare the advantages and limitations of each strategy in order to provide clear suggestions and guidance for the synthesis of future MOFs (Table 3). Furthermore, the incorporation of host–guest interactions has been comprehensively examined in relation to these design strategies.

2.1 Oriented design strategies in rigid MOFs

2.1.1 Open metal sites. Open metal sites are defined as the vacant sites of metal ions or metal clusters within a metal organic framework (MOF) that have unsaturated coordination numbers and are therefore open and reactive.[77,78] These sites have the capacity to coordinate or interact with gas molecules, organic molecules and ions. When metal sites are exposed in the pores or surfaces of the framework, they are susceptible to contact and react with molecules or ions in the external environment. The regulation of the types, quantities, and distributions of these sites can be achieved through the manipulation of the composition and structure of MOFs, thereby enabling selective recognition and separation of different molecules or ions.[79] This selective recognition capability renders MOFs promising candidates for application in the separation of light hydrocarbons.

Given the finding that HKUST-1 can separate C_2H_4/C_2H_6,[30] the configuration of open metal sites has been investigated. This has been achieved by altering the transition metal ions in M-MOF-74 (M = Co, Mn, and Mg), resulting in varying abilities of the rod-shaped and high-density open metal sites to interact with C_3H_6 through π-complexation.[22] It is worth noting that Co sites exhibit the largest difference in binding energies between C_3H_6 and C_3H_8. As pressure increases, the open Co sites become increasingly occupied by C_3H_6, leading to a strong suppression of C_3H_8 adsorption and a significant increase in C_3H_6/C_3H_8 selectivity (Fig. 2a). Following the alteration of the redox-active Fe(II) within the same MOF platform, the material exhibits olefin adsorption selectivity that surpassed that of paraffin.[31] The neutron diffraction data confirmed that the unsaturated hydrocarbons such as C_2H_2, C_2H_4 and C_3H_6 exhibited side-on binding modes, with Fe–C distances of 2.42(2) to 2.60(2) Å. A comparison with the shorter distance of 2.020(5) to 2.078(4) Å observed in the diamagnetic complex $[Fe(C_2H_4)^4]^{2-}$ indicated that the Fe centres within Fe-MOF-74 maintain a high spin electron configuration when binding these unsaturated gases. The interactions of both C_2H_6 and C_3H_8 with Fe in Fe-MOF-74 are even weaker, as evidenced by the longer Fe–C distance of ~3 Å (Fig. 2b).

In the context of the larger channel aperture of 11–12 Å in the MOF-74-series, a microporous framework, Fe(pyrazine)$Pt(CN)_4$,

© 2025 The Author(s). Published by the Royal Society of Chemistry

Open Access Article. Published on 02 June 2025. Downloaded on 5/21/2026 10:40:29 PM.
This article is licensed under a Creative Commons Attribution-NonCommercial 3.0 Unported Licence.

Table 2 Structural properties and adsorption separation performance of some key MOFs from Scheme 1

Typical MOFs	Structural properties	C2/C3 separation	Adsorption uptake (mmol g^{-1})	Selectivity	T/P	Ref.
HKUST-1	3D-channel with Cu sites	C_2H_6/C_2H_4	5.0/5.9 mol kg^{-1}	—	295 K 0.8 bar	30
[ZIF(2-Cim_2)]	SOD network	C_3H_6/C_3H_8	160/155 mg g^{-1}	—	303 K 0.8 bar	45
ZIF-7	SOD network	C_2H_6/C_2H_4	2.24/2.2	1.75	298 K 1 bar	38
M-MOF-3	Hexagonal network	C_2H_2/C_2H_4	6.56/1.35	25.5	195 K 1 bar	59
MAF-49	3D framework with narrow 1D zigzag channels	C_2H_6/C_2H_4	1.73/1.7	9	316 K 1 bar	49
SIFSIXs-2-Cu-i	Cubic topology	C_2H_2/C_2H_4	4.02/2.19	44.54	298 K 1 bar	34
KAUST-7	3D framework with square-shaped channels	C_3H_6/C_3H_8	1.4/0.04	—	318 K 1 bar	32
Y-abtc	Ftw network and cage-like pores	C_3H_8/C_3H_6	2.0/0.07	—	318 K 1 bar	6
UTSA-200	Doubly interpenetrated nets	C_2H_2/C_2H_4	3.65/0.63	6320	198 K 1 bar	44
UTSA-280	1D Ca–C_4O_4 chain with pentagonal bipyramidal structure	C_2H_4/C_2H_6	2.5/0.098	>10 000	298 K 1 bar	70
$Fe_2(O_2)$(dobdc)	Iron–peroxo sites	C_3H_8/C_3H_6	3.32/2.53	4.4	298 K 1 bar	46
JNU-3	1D diffusion channel with dynamic molecular pockets	C_3H_6/C_3H_8	58.6/42.5 cm^3 g^{-1}	513	303 K 1 bar	65
$ZnAtzPO_4$	2D pillared framework with pocket-bottleneck channels	C_2H_4/C_2H_6	1.1/0/3	31	273 K 1 bar	35
$CuTiF_6$-TPPY	Pillared semi-cage 1D channels	$C_2H_2/C_2H_6/C_2H_4$	3.62/2.82/2.42	1.50 C_2H_2/C_2H_4 1.17 C_2H_6/C_2H_4	298 K 1 bar	67
NTU-85	Square-apertured H_2O channels	C_3H_6/C_3H_8	0.45/0.003	1570	298 K 1 bar	37
NTU-88	Sql layer and rhombic pores	C_3H_4/C_3H_6	86.0/2.0 cm^3 g^{-1}	—	298 K 1 bar	69
FDMOF-2	3D framework	C_3H_8/C_3H_6	5.04/4.15	2.18	298 K 1 bar	73
CdIF-13	SOD network	C_3H_8/C_3H_6	2.56/2.32	2.04	288 K 1 bar	43
MOF-808Bzz	Octahedral morphologies	$C_2H_2/C_2H_6/C_2H_4$	2.98/2.20/1.43	3.15 C_2H_2/C_2H_4 1.90 C_2H_6/C_2H_4 1.92 C_2H_6/C_2H_4	298 K 1 bar	53
ZU-609	3D networks with large 1D channels	C_3H_6/C_3H_8	2.0	>10	298 K 1 bar	33
HAF-1	3D framework with channels and molecular pockets	C_3H_8/C_3H_6	101.61 cm^3 cm^{-3}/—	1.67×10^7	298 K 1 bar	55
X-dia-1-$Ni_{0.89}Co_{0.11}$	Flexible diamondoid networks	C_2H_4/C_2H_6	4.96/0.54	—	273 K 1 bar	56
TYUT-17	Spindle-like cages	C_2H_6/C_2H_4	67.4/61.3 cm^3 g^{-1}	—	298 K 1 bar	66
$NTU101-NH_2$	H-bond-tuned interpenetrated pcu framework	C_2H_6/C_2H_4	40.1/15.2 cm^3 g^{-1}	—	328 K 0.5 bar	62
NKMOF-1-Ni	3D framework with 1D channels and dual gas-binding sites	$C_3H_4/CH_2{=}C{=}CH_2/C_3H_6$	3.5/2.1/—	1271.6(C_3H_4)	298 K 1 bar	52
JNU-9-CH_3	3D framework with cubane SBUs	$C_3H_4/CH_2{=}C{=}CH_2$/ C_3H_8/C_3H_6	3.6/3.4/2.95/2.9	1.5 (C_3H_8/C_3H_6) 2.1 (C_3H_4/C_3H_6) 1.3 (propadiene/C_3H_6)	298 K 1 bar	60

© 2025 The Author(s). Published by the Royal Society of Chemistry

Open Access Article. Published on 02 June 2025. Downloaded on 5/21/2026 10:40:29 PM.
This article is licensed under a Creative Commons Attribution-NonCommercial 3.0 Unported Licence.

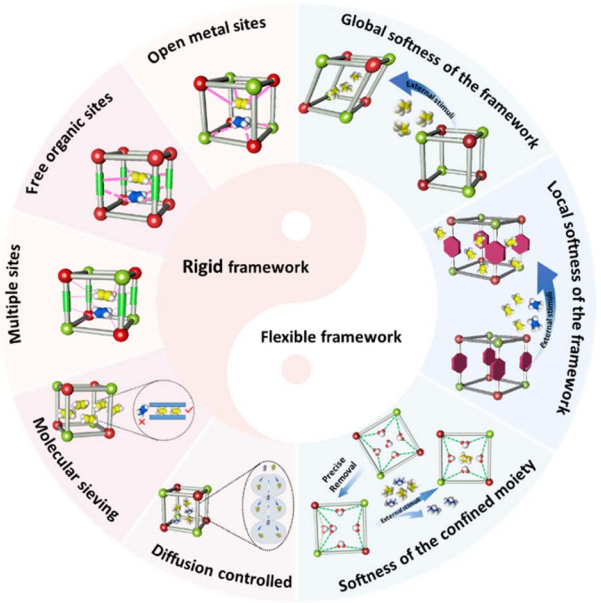

Fig. 1 Oriented design and engineering strategies of advanced MOFs.

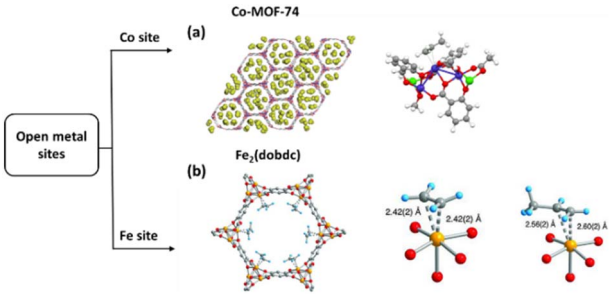

Fig. 2 (a) A snapshot from a GCMC simulation for C_3H_6 adsorption in Co-MOF-74, and the propylene molecule binds to the Co atom. (b) A portion of the solid-state structure of $Fe_2(dobdc)\cdot 2C_2D_4$, and C_2H_4, and C_3H_6 coordination with $Fe_2(dobdc)$. Reprinted with permission from ref. 22. Copyright 2012 John Wiley & Sons, ref. 31. Copyright 2012 The American Association for the Advancement of Science, respectively.

with a channel size of 4.0 Å and mixed open metal sites was designed and prepared for the separation of C_3H_6/C_3H_8. C_3H_6 was located between two pyrazine rings, forming π–π interactions. Notably, the distance between $C_{C_3H_6}$ and the face-to-face packed open Pt sites is short, ranging from 2.8–3.2 Å. In

Table 3 The advantages and limitations of each design strategy for light hydrocarbon separation-oriented MOFs

Design strategy	Advantages	Limitations
Open metal sites	High selectivity	Synthesis and scale-up challenges
	Highly adjustable	Stability issues
	High adsorption capacity	Vulnerability to impurity gases
Free organic sites	Highly selective	Diffusion resistance
	Highly adjustable	Difficulty and cost of synthesis
	Good stability to avoid toxicity of metal sites	Vulnerable to other impurity gases
	Low regenerative energy consumption	Selectivity may be low
Multiple sites	Synergistically enhanced selectivity	Synthesis complexity increase
	Broadening the applicable separation system	Risk of site-to-site interference
	Balancing adsorption strength and regeneration energy	Challenging kinetic balance
	Improve stability	
Molecular sieving	Highly selective separation	Aperture regulation is difficult
	Gentle operating conditions	Low pressure adsorption capacity
	High stability (not dependent on chemisorption)	Limited separation of similar-sized molecules
	Low energy consumption for regeneration	Diffusion kinetic limitations
	Suitable for kinetic separations	
Diffusion controlled	Highly dynamic selectivity	Highly sensitive to an orifice structure.
	Low energy consumption for regeneration	Low pressure separation efficiency
	High stability	Limited separation of similar sized molecules
	Gentle operating conditions	May be affected by the 'blocking effect'
Global softness of the framework	High selectivity and dynamic adaptability	Structural stability issues
	Low energy consumption and efficient regeneration	High material preparation requirements
	Outfield response characteristics	Representation challenge
Local softness of the framework	Highly selective	Complex interaction mechanisms
	Fast adsorption kinetics	Difficult to synthesize
	Good stability	Industrial scale-up challenges
	Precise molecular recognition	
	Low energy consumption	
Softness of the confined moiety in the framework	Highly selective	Synthesis is complex
	Energy saving potential	Difficulty in industrial scale-up
		Regeneration difficulties

© 2025 The Author(s). Published by the Royal Society of Chemistry

Open Access Article. Published on 02 June 2025. Downloaded on 5/21/2026 10:40:29 PM. This article is licensed under a Creative Commons Attribution-NonCommercial 3.0 Unported Licence.

contrast, the $C_{C_3H_6}\cdots$Ni distance becomes longer (3.5 Å) in FeNi-M'MOF. The finely tailored pore size of 4.0 Å facilitates the passage of C_3H_6 through the channel, but significantly hinders the movement of the larger C_3H_8 molecule.

2.1.2 Free organic sites. As an essential building block of MOFs, the functionalization of organic ligands is also expected to achieve efficient separation. Typically, the polar groups containing electronegative F and N elements are incorporated into the organic linker. In addition, amino and nitro groups, which act as electron donors or acceptors, have been investigated for their ability to selectively capture olefins from mixtures containing paraffins *via* supramolecular interactions. Interestingly, the metal-oxo species, formed by coordinating O_2 to open metal sites have shown preferable interactions with paraffin. Furthermore, comparison of open metal site strategies may show reduced separation efficiency in the presence of moisture, and the use of organic sites not only achieves the desired separations, but also maintains good cycling stability even in the presence of moisture.

Supramolecular interactions derived from organic sites and light hydrocarbons are visualized and understood in the case of NOTT-300.[80] The results of neutron scattering, synchrotron X-ray and neutron diffraction, and computational modelling revealed that the free OH and benzene ring are simultaneously incorporated with C_2H_2 through stronger hydrogen-bonding (C$\cdots$H = 2.96–3.64 Å), $\pi\cdots\pi$ stacking interactions (C≡C$\cdots$C6 = 3.81 Å) and intermolecular dipole interactions ($C^{I}\cdots H^{II}$ = 3.24 Å, $C^{II}\cdots H^{I}$ = 3.12 Å). However, the reduced π-electron density of C_2H_4 compared to that of C_2H_2 enables a longer $C_{C_2H_4}\cdots$HO distance (4.62 Å), which suggests a weaker hydrogen bonding. Despite the $\pi\cdots\pi$ interactions between C_2H_4 and phenyl rings of the ligand, C_2H_4 was displaced towards the centre of the cavity and interacted majorly with C_2H_2 molecules (captured by OH), upon the introduction of an equimolar mixture of the two gases to the system (Fig. 3a).

By changing the OH group into COOH, we recently found the unique ability for the adsorption of C_2H_2 from C_2H_4 containing mixtures by a MOF with crab-like carboxylic pincers. On a new platform of a 6-c topology network, pore size engineering of the carboxylic-functionalized MOFs was finely tuned by altering the MF_6^{2-} pillars (M = Si, Ti and Zr).[81] Following the increased distance of the M–F, the pincer distance increased gradually from 5.02 to 5.91 Å, yielding a fitted nanospace in NTU-72 for selective recognition of a C_2H_2 tetramer. The O_{COOH} interacts with terminal $H_{C_2H_2}$ with a short distance of 2.309 Å, while the OH_{COOH} chelates to two C_2H_2 through O–H$\cdots C_{C_2H_2}$. The formation of a C_2H_2 tetramer with C_{2h} symmetry is characterised by these two groups of gas molecules, which is distinctly different from the S_4 symmetric C_2H_2 tetramer in SIFSIX-Cu-i.[34] In contrast, two types of longer hydrogen bonds are observed between COOH$\cdots C_2H_4$, reflecting the relative weak carboxylic–C_2H_4 interaction. Importantly, the captured C_2H_2 tetramer not only facilitates the direct harvesting of highly pure C_2H_4 at the adsorption step, but also benefits the collection of pure C_2H_2 during the desorption step (Fig. 3b).

To promote the ability for purification of C_2H_4 from C2 ternary hydrocarbons, fine material design is highly required as

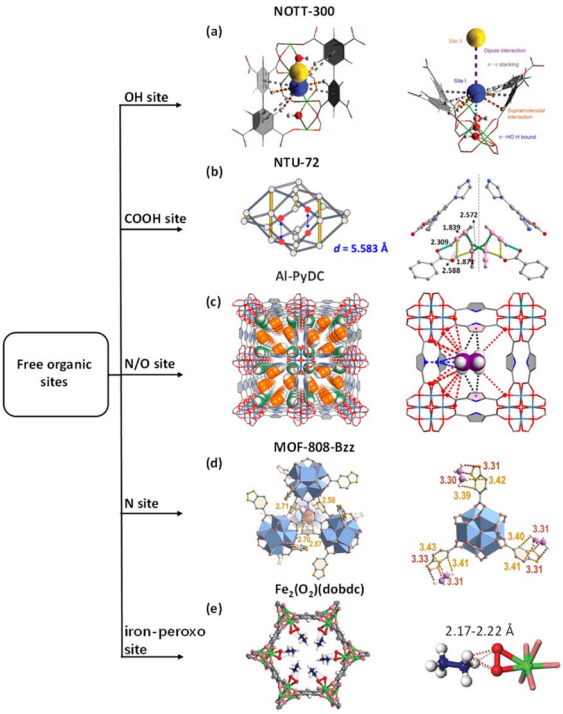

Fig. 3 (a) Schematic representation of the action of combining C_2H_2 and C_2H_4 molecules. (b) The pincer distance of NTU-72 and structure of C_2H_2- loaded NTU-72. (c) The SCXRD structure of C_2H_2-loaded Al-PyDC and the C_2H_6 binding site in gas-loaded Al-PyDC. (d) C_2H_4 binding sites I and sites II in MOF-808-Bzz. (e) Structure of $Fe_2(O_2)$(dobdc)⊃C_2D_6. Reprinted with permission from ref. 80. Copyright 2015 Springer Nature Limited, ref. 81. Copyright 2023 The Royal Society of Chemistry, ref. 83. Copyright 2023 Springer Nature Limited, ref. 53. Copyright 2023 John Wiley & Sons, ref. 46. Copyright 2018 The American Association for the Advancement of Science, respectively.

the strength of the interactions between open metal sites and hydrocarbons typically increases in the order of C_2H_6 < C_2H_4 < C_2H_2. Based on the same 6-c platform, we replaced the functional group of COOH by –CH_3 and CH_3.[48] The varied pore environment and organic sites endow NTU-73-CH_3 with remarkable capability for the direct production of poly-grade C_2H_4 from ternary C2 hydrocarbons under ambient conditions. Comparably, the precursor framework of NTU-73-COOH cannot purify C_2H_4, while NTU-73-CF3 exhibits only negligible capability in this regard. This is primarily attributable to the modified binding sites in the NTU-73 series, which not only eliminate the channel obstruction caused by the formed C_2H_2 tetramer, but also enhance the interactions of host-C_2H_2/C_2H_6. These interaction changes were clearly observed by gas-loaded structures, and TJT-100 also demonstrates the ability for C_2H_4 purification from ternary (C_2H_2/C_2H_6/C_2H_4) mixtures by utilizing the abundant O sites.[82]

To further promote the host-C_2H_6 and host-C_2H_2 interactions, multiple supramolecular binding sites have been designed in the MOFs with suitable pore sizes. For example, Al-PyDC was assembled with ligands containing N and a large number of polar O sites, providing abundant supramolecular binding sites for C_2H_6, while the electronegative O and N sites

Open Access Article. Published on 02 June 2025. Downloaded on 5/21/2026 10:40:29 PM. This article is licensed under a Creative Commons Attribution-NonCommercial 3.0 Unported Licence.

form hydrogen bonds with C_2H_2, as confirmed by gas loaded structural analysis.[83] This unique design endows Al-PyDC with the capacity to effectively purify C_2H_4 from mixtures containing C_2H_2 and C_2H_6 in one step. Furthermore, this MOF has been shown to be highly stable under harsh conditions (Fig. 3c).

By expanding the dimensions of the individual organic sites to nitrogen-containing heterocyclic ligands, including indole-5-carboxylic acid (ind), benzimidazole-5-carboxylic acid (bzz), and indazole-5-carboxylic acid (izo), the functionalized MOF-808 materials attain a uniform distribution and specific configuration of such extensive binding sites. MOF-808-Bzz has multiple strong supramolecular interactions, providing an excellent geometric configuration for C_2H_6, resulting in the highest C_2H_2/C_2H_4 (1/99, v/v) and C_2H_6/C_2H_4 (50 : 50, v/v) selectivity among these four materials (Fig. 3d).[53]

To achieve efficient C_2H_4 and C_2H_6 separation, an inverse interaction, namely the stronger host–C_2H_6 interaction, has been considered. Inspired from the structures of metalloenzymes, $Fe_2(O_2)$(dobdc) exhibited a preferential binding of C_2H_6 over C_2H_4.[46] High-resolution neutron powder diffraction (NPD) measurements revealed that the peroxo site binds C_2D_6 through a C–D/O interaction, of which the D···O distance varies in a narrow range of 2.17 to 2.22 Å. In addition, the nonplanar C_2D_6 molecule matches better to the pore surface in $Fe_2(O_2)$(dobdc) than the planar C_2D_4 molecule, resulting in stronger hydrogen bonds with the Fe-peroxo site and stronger van der Waals interactions with the ligand surface (Fig. 3e).

In light of the terminal acidic H on C_3H_4, the basic organic site strategy has also been explored in the design of MOFs for the removal of trace C_3H_4 from C_3H_6. Taking the pore-partitioned MOF as a platform, aminophthalic acid (NH_2-BDC) was selected to construct the framework.[84] The amino sites, which are densely arranged, possess a distinctive capacity to recognise the acetylic and methyl hydrogen atoms of C_3H_4, resulting in the formation of short hydrogen bonds. Moreover, the customised nanospace induces C_3H_4···C_3H_4 molecules to aggregate together with short H···C distances. Although the NH_2 group also interacts with C_3H_6, the interaction distance is longer, yielding a sharp adsorption difference (84.5 $cm^3\ g^{-1}$) at about 1 kPa, 298 K. Furthermore, such an interaction difference was also finely illustrated by *in situ* infrared spectroscopy measurement.

2.1.3 Multiple sites. MOFs with multiple sites show a promising future in the field of gas separation, due to the systematically tuned chemical properties, the associated pore size changes and the excellent stability. Typically, the fluorine atom of the inorganic fluorinated anions, supported as the pillar of the MOF framework, has high electronegativity, high ionisation potential and low polarizability, which can drastically change the gas adsorption characteristics of the MOFs.[85]

To further promote the ability to selectively capture C_2H_2 with a terminal acidic H, the weakly basic hybrid anion MF_6^{2-} (M = Si, Ti and Zr) was selected. As a typical example, SIFSIX-1-Cu [SIFSIX, hexafluorosilicate (SiF_6^{2-}); 1, 4,4′-bipyridine)] was prepared.[34] The prototypical primitive cubic network has previously been reported for high volumetric CH_4 and CO_2 uptake.[86,87] Notably, the periodically arrayed SiF_6^{2-} allowed preferential binding of C_2H_2 molecules through strong C–H···F H-bonding (2.017 Å) and van der Waals (vdW) interactions with the organic linkers. Constrained by the narrow pores, the four neighbouring adsorbed molecules assemble to form a gas cluster through multiple $H^{\delta+}\cdots C^{\delta-}$ dipole–dipole interactions, further increasing the energy for adsorption. Comparably, the calculated H-bond distances between C_2H_4 and SiF_6^{2-} sites are longer than those between C_2H_2 and SiF_6^{2-} sites. This unique interaction allows SIFSIX-1-Cu to show balanced performance between C_2H_2 uptake and C_2H_2/C_2H_4 selectivity (Fig. 4a). This idea has been further expanded in the family of cubic net of SIFSIX-1-Cu, SIFSIX-2-Cu (2: 4.4′-dipyridylacetylene), SIFSIX-2-Cu-i, SIFSIX-3-Cu (3: pyrazine), SIFSIX-3-Zn, SIFSIX-3-Ni, and TIFSIX-2-Cu-i (TIFSIX = TiF_6^{2-}) by changing the length of the linkers, the node, and/or the framework interpenetration for separation of C_2H_4 from ternary ($C_2H_2/C_2H_6/C_2H_4$) or quaternary ($CO_2/C_2H_2/C_2H_6/C_2H_4$) mixtures (Fig. 4a).[88]

By changing pyridine to imidazole at the coordination sites of the linear ligand, a new MOF (NTU-67) with a trap-and-flow

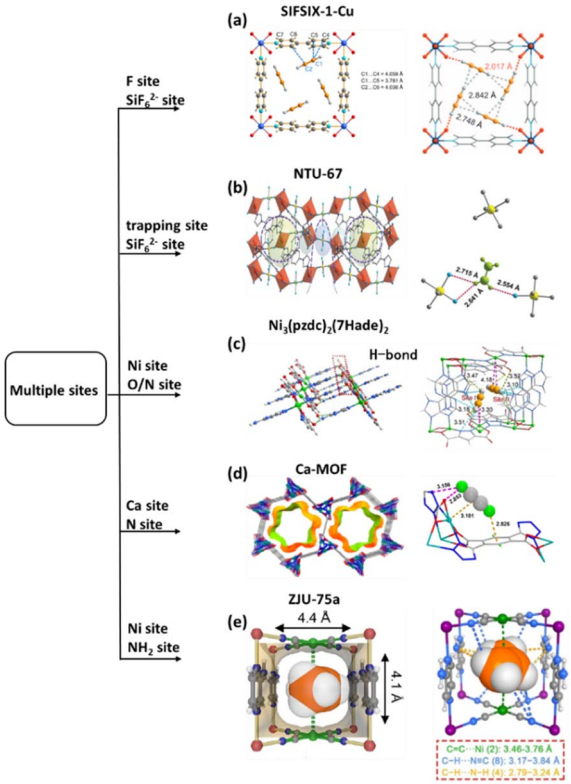

Fig. 4 (a) Optimized C_2H_2 configuration and adsorption binding sites in SIFSIX-1-Cu. (b) View of the inner space in channel A, and view of the structure of a molecular trap with pure gas of NTU-67⊃C_2H_4. (c) Coordination environment of $Ni_3(pzdc)_2(7Hade)_2$, binding configurations of C_2H_2, and the open Ni^{2+} strong polarization capacity and the calculated C≡C–H bond angle. (d) Coordination environment of Ca^{2+} ions and preferential adsorption sites for C_2H_2. (e) Densely arranged high-density strong binding sites and C_3H_6 adsorption sites based on theoretical calculations. Reprinted with permission from ref. 34. Copyright 2016 The American Association for the Advancement of Science, ref. 36. Copyright 2022 John Wiley & Sons, ref. 85. Copyright 2020 John Wiley & Sons, ref. 89. Copyright 2021 American Chemical Society, ref. 90. Copyright 2023 John Wiley & Sons, respectively.

© 2025 The Author(s). Published by the Royal Society of Chemistry

Open Access Article. Published on 02 June 2025. Downloaded on 5/21/2026 10:40:29 PM. This article is licensed under a Creative Commons Attribution-NonCommercial 3.0 Unported Licence.

channel structure was prepared by crystal conversion. With the narrowest window aperture of 3.4 Å, the flow channel acted as a sieve channel for faster diffusion of the linear molecules of C_2H_2/CO_2 (3.3 Å) and the butterfly-like molecule of C_2H_4 (4.2 Å). Meanwhile, the confined nanospace regulated by three SiF_6^{2-} anions and six imidazoles in another channel works as a molecular trap for adsorbed molecules. Crystallographic study under pure gas revealed that the linear C_2H_2 interacts with SiF_6^{2-} anions and imidazole carbon to form short hydrogen bonds in the range of 2.470–2.984 Å. In addition, the existing hydrogen bonds between the adsorbed C_2H_2 molecules enable the formation of gas clusters, which benefits the C_2H_2 uptake at very low pressure. For CO_2, they are observed in the molecular trap around the SiF_6^{2-} anions, forming a typical dipolar–dipolar (Si–F$\cdots$C=O: δ^+–$\delta^-\cdots\delta^+ = \delta^-$) interaction. However, relatively longer hydrogen bonds of F$\cdots$H– $C_{C_2H_4}$ (2.554–2.715 Å) were observed for C_2H_4. Notably, the competitive binding of the gases was validated by crystallographic study under mixed gas. Therefore, NTU-67 was able to directly harvest highly-pure C_2H_4 from the ternary ($CO_2/C_2H_2/C_2H_4$) mixtures (Fig. 4b).[36]

To investigate the combined effect of open metal sites and electronegative sites in a single domain, a super-microporous MOF, $Ni_3(pzdc)_2(7Hade)_2$ was designed and prepared. This structure features S-shaped one-dimensional ultramicroporous channels decorated with a high-density of open Ni sites and electronegative oxygen and nitrogen sites. First-principles density functional theory (DFT) calculations revealed that C_2H_2 interacts with the Ni site. The slight bending of the C≡C–H bond angle suggests that the unsaturated Ni^{2+} site can polarize the C_2H_2 molecule. In addition, the highly polar $H_{C_2H_2}$ interacts with the basic or electronegative O and N sites on the pore surface through electrostatic interactions at very short distances of 3.10–3.60 Å. In contrast, π-complexation occurs between Ni and C_2H_4 with a longer distance of 4.00–4.40 Å, despite the vdW interaction between C_2H_4 and the pore surface being very similar in type and geometry to that observed for C_2H_2. Therefore, the difference in the synergistic effect significantly improves the adsorption capacity and selectivity of C_2H_2 from C_2H_4 containing mixtures (Fig. 4c).[85]

Another example is Ca-MOF, derived from a N, O-donor ligand 2,5-di(2*H*-tetrazol-5-yl) pyrophosphate.[89] This material exhibits unique metal carboxylate-nitrogen heterocyclic oxide units, and a high density of open metal sites and organic functional sites that enable it to selectively adsorb and separate C_2H_2. This interaction of the open metal sites with the π-electron of the C_2H_2 molecules is a key feature, while the organic groups play a regulatory role in the pore structure and surface properties through organic sites. This group forms hydrogen bonds and other interactions with C_2H_2, thereby generating additional binding forces. Monte Carlo simulations revealed that C_2H_2 forms strong C–H$\cdots$O/N bonds with benzene rings and interacts with Ca^{2+} sites through M$\cdots\pi$ interactions. In comparison, C_2H_4 lacks C–H$\cdots\pi$ interaction (Fig. 4d). Additionally, $CuTiF_6$-TPPY (TPPY: 5,10,15,20-tetra(4-pyridyl)-21h,23h-porphyrin) with semi-cage-like 1D channels decorated with synergistic binding sites of TiF_6^{2-} and TPPY exhibits a noticeable adsorption of C_2H_2 and C_2H_6 over C_2H_4.[67] Therefore, efficient single-step C_2H_4 purification from a $C_2H_2/C_2H_4/C_2H_6$ mixture has been achieved based on this MOF. Similar to the structure of Fe(pyrazine)$Pt(CN)_4$, a new MOF Co(pyz-NH_2)$[Ni(CN)_4]$ (ZJU-75a, pyz-NH_2 = 2-aminopyrazine) has been prepared for the separation of C_3H_6/C_3H_8.[90] The open Ni site and the organic NH_2 sites point into the narrow channel (4.4 Å), allowing multiple interactions with C_3H_6, including double π-complexation interactions (3.46 and 3.76 Å) with face-to-face packed Ni sites and multiple supramolecular interactions with N sites (C–H$\cdots N_{CN}$: 3.17–3.84 Å and C–H$\cdots N_{NH_2}$: 2.79–3.24 Å). In contrast, only weak supramolecular interactions (C–H$\cdots N_{CN}$: 3.07–3.81 Å) and C–H$\cdots N_{NH_2}$: 2.63–3.55 Å) were observed in host@C_3H_8, due to the lack of a double bond in C_3H_8 (Fig. 4e).

2.1.4 Molecular sieving. Based on the molecular size or shape, molecular sieve separation that allows smaller molecules to pass, but not large ones, has been considered as an effective strategy for adsorption separation of light hydrocarbons. Complete separation ensures the purity of the adsorbed gas and enables infinite selectivity. However, the molecular sizes and shapes of light hydrocarbons are very similar, making it challenging to construct MOFs with open pores that are located between the molecular diameters of the gases, particularly those with the same number of carbon atoms.

As a typical example, $[Ca(C_4O_4)(H_2O)]$ (UTSA-280), synthesized from calcium nitrate and squaric acid, has two parallel 1D open cylindrical channels with similar cross-sectional areas of about 14.4 $Å^2$.[70] Importantly, this value is larger than the minimum cross-sectional area of C_2H_4 (13.7 $Å^2$), but smaller than that of C_2H_6 (15.5 $Å^2$). Therefore, it exhibits exclusive C_2H_4 adsorption, but not of C_2H_6 at 298 K. This observation was further confirmed by the adsorption isotherms of the two gases at 273 and 195 K. Further diffraction experiments and calculations show that the C_2H_4 molecules adopt a head-to-head configuration inside the 1D channel, associated with weak C–H$\cdots$O hydrogen bonding, π$\cdots$π stacking and vdW interactions with the rings of the ligand or coordinated water molecules. However, C_2H_6, regardless of its orientation, is strongly restricted by the aperture of the channel (Fig. 5a).

Moving to the target of C_3H_6/C_3H_8 mixtures, the two have <0.4 Å size difference, and design and construction of the sieving channel becomes more challenging. Selecting or tailoring the length of the ligands is not effective, as the required change is located in a wider range. Inspired by the sub-Å level size change of the hybrid ions, a chemically stable fluorinated MOF, KAUST-7, was prepared according to the reticular chemistry approach.[32] Initially, by changing the SiF_6^{2-} pillar in SIFSIX-3-Ni (adsorbs both C_3H_6 and C_3H_8 due to the free rotation of the pyrazine ligands) to a slightly bigger cation $NbOF_5^{2-}$, the short proximal distance between adjacent F atoms provides a plausible window opening of 3.0–4.8 Å, associated with the restricted rotation and tilting of the pyrazine linker. Therefore, KAUST-7 displayed full exclusion of C_3H_8 from C_3H_6-containing mixtures. Sieving separation of C_3H_6/C_3H_8 has also been observed in Y-abtc (abtc = 3,3′,5,5′-azobenzenete tracarboxylates), which has cage-like pores connected through small windows of 4.72 Å (Fig. 5b).

Open Access Article. Published on 02 June 2025. Downloaded on 5/21/2026 10:40:29 PM.
This article is licensed under a Creative Commons Attribution-NonCommercial 3.0 Unported Licence.

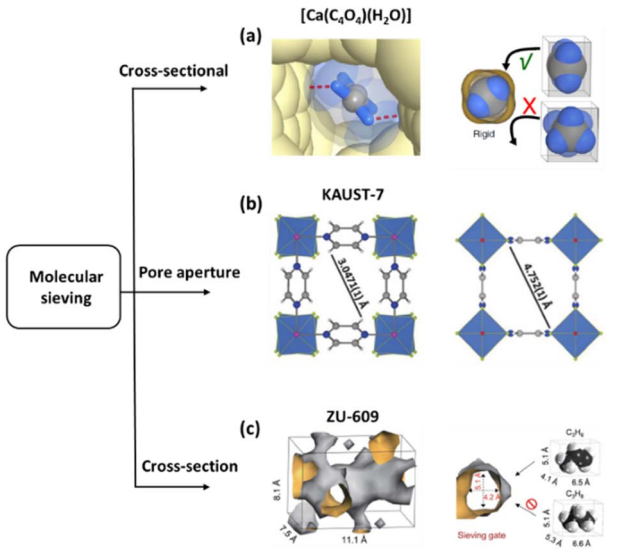

Fig. 5 (a) Preferential binding site for C_2H_4 molecules, and size/shape sieving based on the minimum cross-sectional areas of C_2H_4 and C_2H_6 molecules. (b) Crystal structure of NbOFFIVE-1-Ni, and simulation of the maximum open structure of NbOFFIVE-1-Ni. (c) Sieving gate of ZU-609 and the molecular sizes of propylene and propane. Reprinted with permission from ref. 70. Copyright 2018 Springer Nature Limited, ref. 32. Copyright 2016 The American Association for the Advancement of Science, ref. 33. Copyright 2023 The American Association for the Advancement of Science, respectively.

Although the strategy of molecular sieving can provide complete separation of the mixtures, the narrow pore strongly restricts molecule diffusion, a long-standing issue of adsorption separation. ZU-609, a 2D network composed of an inorganic metal node and organic linkers (EDS2−, 1,2-ethanedisulfonate; dps, 4,4′-dipyridyl sulfide), exhibits a large 1D channel with a size of 7.5–11.1 Å.[33] Meanwhile, such a channel was connected by a narrow neck (4.2 × 5.1 Å). This cross-sectional area falls just between the molecular dimensions of C_3H_6 and C_3H_8. In other words, by incorporating a molecular sieve gate and a fast diffusion channel in a single domain, ZU-609 exhibits precise exclusion of C_3H_8 from C_3H_6-containing mixtures, as well as fast C_3H_6 adsorption kinetics. Particularly, the diffusion coefficient of this MOF is 1–2 orders of magnitude higher than that of KAUST-7 and Co-gallate. The rapid diffusion and high sorption were finely supported by *in situ* PXRD analysis and dispersion corrected calculation (Fig. 5c).

2.1.5 Diffusion controlled. The strategy of molecular sieving with accelerated adsorption–diffusion undoubtedly has significant advantages in adsorption science; however, precise design and avoidance of sieving losses, given the flexible nature of the target MOF, are major challenges. Synergistic thermodynamic and kinetic adsorption, mainly determined by strong binding sites and pore size/shape, holds unique advantages. For instance, based on the bis(5-methyl-1*H*-1,2,4-triazol-3-yl) methane ligand (btm), $[Zn_2(btm)_2]$ (MAF-23) was prepared. However, the methylene group in the framework cannot distinguish the C2/C3 hydrocarbons.[88] After heating this MOF under oxygen flow, almost half of the btm ligands were oxidized, forming a new ligand bis(5-methyl-1,2,4-triazol-3-yl) methanone (H_2btk). Due to the similar properties between the methylene group and carbonyl group, the channel size/shape of MAF-23-O is basically the same as that of the precursor framework. MAF-23-O demonstrated faster adsorption of C_3H_6 than that of C_3H_8; this is because the lone pair of the carbonyl oxygen interacts with the sp^2 C–H bond of C_3H_6, but not for C_3H_8 (Fig. 6a). In addition, this work also highlights the importance of post-synthetic modification, a reliable strategy for achieving the desired structure–property relationship compared to direct synthesis from the corresponding building blocks.

To further tune the synergistic effect of thermodynamic and kinetic adsorption performance of C_3H_6 from C_3H_8, a group of MOFs were synthesized using chiral ligands. With L-malic acid, the L-mal-MOF has a homogeneous one-dimensional pore structure measured to be 5.3 × 5.5 Å. In contrast, the racemic material DL-mal-MOF synthesized from a mixture of D/L-malic acid ligands exhibited periodic contraction–expansion pore structures, forming quasi-discrete pore structures. This difference was caused by the different orientations of the chiral group in the nanosapce. Similar to MAF-23-O, abundant oxygen atoms were found in these contraction–expansion pore structures. Adsorption isotherms showed that the DL-mal-MOF has a significantly higher equilibrium-kinetic combined selectivity of C_3H_6/C_3H_8, which was further illustrated by energy fluctuations and corresponding binding energy during the diffusion of the C_3H_6 and C_3H_8 molecules in such quasi-discrete pore structures.[27] This result suggests that the narrow-neck channel, along with the O-rich environment, may make the MOF a C_3H_6/C_3H_8 separator (Fig. 6b). Utilizing a similar concept, a phosphate anion (PO_4^{3-}) functionalized MOF $ZnAtzPO_4$ with a narrow (4.94 Å)-neck (3.82 Å) channel, has been reported for C_2H_4/C_2H_6 separation (Fig. 6c).[35]

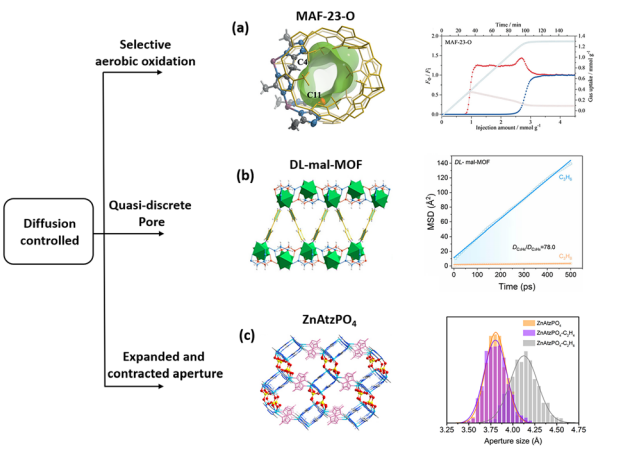

Fig. 6 (a) Crystal and pore structures of MAF-23-O, and breakthrough curves and adsorption kinetic curves using an equimolar C_3H_6/C_3H_8 mixture at 298 K and 1 atm. (b) Structure of DL-mal-MOF and MD-derived self-diffusion rates of C_3H_6 and C_3H_8. (c) Three-dimensional structure of $ZnAtzPO_4$ and distribution of the aperture size of the bottleneck. Reprinted with permission from ref. 88. Copyright 2019 John Wiley & Sons, ref. 27. Copyright 2023 The American Chemical Society, ref. 35. Copyright 2020 Science, respectively.

© 2025 The Author(s). Published by the Royal Society of Chemistry

Open Access Article. Published on 02 June 2025. Downloaded on 5/21/2026 10:40:29 PM. This article is licensed under a Creative Commons Attribution-NonCommercial 3.0 Unported Licence.

2.2 Oriented design strategies in soft MOFs

Soft MOFs, a kind of crystalline porous solid with reversible phase transformation, have been considered as the most interesting discovery in materials chemistry in the last two decades. The combination of diverse structural nature and an external stimulus (such as gas adsorption, temperature, pressure, light, and electric field) creates emergent softness of the frameworks; particularly, some of them can show fully different structural responses to the gases, even if they have very similar properties. This unique characteristic thereafter sheds light on the development of adsorption based light hydrocarbon separation technology with significant vitality. According to the modified parts of the framework, they can be broadly divided into three types: global softness, local softness and confined softness. However, the design and construction of the desired softness for the accurate detection of light hydrocarbons, as well as the thorough understanding of the softness involved, remains a critical challenge.

2.2.1 Global softness of the framework. The global softness of MOFs refers to their ability to exhibit significant structural flexibility and adaptability, usually caused by layer sliding, framework expansion, bond formation and breaking, *etc.* Their ability to structurally adapt enhances their performance and opens up opportunities for the design of new MOFs tailored to specific industrial needs. With the discovery of the first soft MOF ZIF-7 (gate-opening mechanism) for C_2H_4 and C_2H_6 separation,[38] the design or tuning of structural softness, usually including a rapid change, step change and gradual change, for light hydrocarbon separation became a hot topic, as it is significant for exclusive molecular recognition.

2.2.1.1 Rapid change. Typically, an ultramicroporous MOF UTSA-300 ([Zn(dps)$_2$(SiF$_6$)], dps = 4,4′-dipyridylsulfide) with 2D channels of about 3.3 Å was reported. Interestingly, the fully activated framework transformed into a closed pore phase with 0D nanospaces. This is due to the conformational changes of the dps ligands and the rotation of the SiF_6^{2-} ions, leading to a shrinkage of the framework. However, this 0D nanospace starts to open under C_2H_2 at 273 K, but not for C_2H_4 and CO_2. Neutron powder diffraction and modelling studies pointed out that two F atoms from the two adjacent SiF_6^{2-} ions bind a C_2H_2 molecule (*via* short hydrogen bonds) in a head-on configuration, leading to a recovery of the pore system from 0D to 2D.[91] The framework change allows UTSA-300a to selectively capture C_2H_2 from C_2H_4 or CO_2 containing mixtures.

In contrast, NTU-65, the global soft framework demonstrated different structural changes, resulting in efficient C_2H_4 purification ability from $C_2H_2/CO_2/C_2H_4$.[92] The as-synthesized NTU-65, constructed from 1,4-di(1*H*-imidazole-1-yl)benzene, Cu^{2+} and SiF_6^{2-}, exhibits a 3D framework with pcu topology. The two adjacent, rather than the two opposite, F atoms on SiF_6^{2-} join the coordination of the framework, while other F atoms form hydrogen bonds with the ligands. In addition, NTU-65 has two types of nanochannels with opening sizes of 2.6 × 3.4 and 5.2 × 6.3 Å^2. Therefore, the activated framework showed sharply different PXRD and parameters of the unit cell, indicating the global framework change. Interestingly, this activated framework showed a temperature-dependent response for C_2H_2, CO_2, and C_2H_4 at 195 K, but only for C_2H_2 at 298 K. On further temperature optimization to 263 K, C_2H_2 and CO_2 were adsorbed, resulting in a one-step purification of C_2H_4 (Fig. 7a).

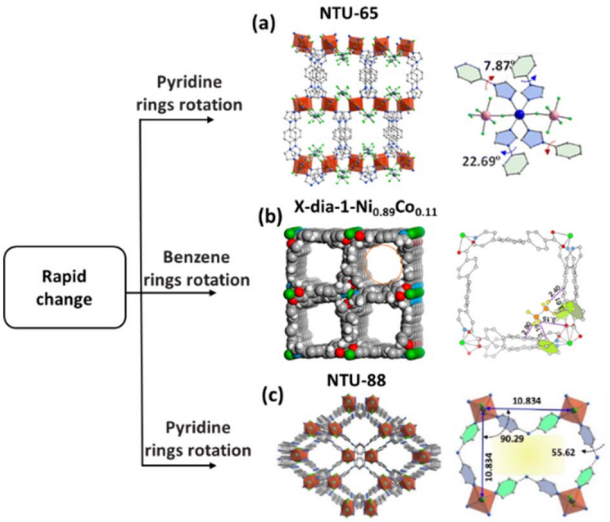

Fig. 7 (a) The crystal structure of NTU-65 *via* the *c* axis and benzene ring rotation of NTU-65. (b) The crystal structure of X-dia-1-$Ni_{0.89}Co_{0.11}$ and C_2H_4 and C_2H_6 binding sites at X-dia-1-$Ni_{0.89}Co_{0.11}$. (c) The crystal structure of NTU-88 *via* an axis and open phase of NTU-88o under C_3H_4 at 100 kPa. Reprinted with permission from ref. 92. Copyright 2020 John Wiley & Sons, ref. 56. Copyright 2024 American Chemical Society, ref. 69. Copyright 2023 John Wiley & Sons, respectively.

In addition, sudden pore opening of X-dia-1-Ni occurs on C_2H_6, but not on C_2H_4, affording direct harvesting of C_2H_4 in the adsorption step.[56] The pressure of C_2H_6 triggered sudden opening can be finely tuned through partial Co^{2+} doping, due to the better shape-fitting between the host and C_2H_6 under increased pressure. Further modelling calculation results confirmed that the open phase of X-dia-1-Ni exhibited strong C_2H_6 interaction through multiple C–H···O bonding with distances of 2.40 and 3.61 Å, whereas only two C–H···O bonds with distances of 3.75 and 3.83 Å were observed between the host and C_2H_4 (Fig. 7b).

On the base of an NTU-65 precursor with Cu–F (from SiF_6^{2-}) and Cu–N (from ligand) coordination bonds, the same group developed a new approach to fine regulate the gradient gate-opening in a series of MOFs (NTU-65-FeZr, NTU-65-FeTi, NTU-65-CoZr and NTU-65-CoTi) *via* node substitution.[51] Due to the systemically altered strength of the coordination bond, the sole structural response toward C_3H_4 in NTU-65-FeZr gradually evolves into a sequential response to C_3H_4 (1.6 kPa), C_3H_6 (19.4 kPa), and C_3H_8 (57.2 kPa) in NTU-65-CoTi at 273 K, as the incorporation of multiple nodes determines the energy barrier of the global softness of the framework. This unique phenomenon allows NTU-65-CoTi to show sieve separation of C_3H_4/C_3H_6/C_3H_8 in one step.

Notably, co-adsorption is a kind of common phenomenon once the inherent large pore has been opened by the molecule

Open Access Article. Published on 02 June 2025. Downloaded on 5/21/2026 10:40:29 PM. This article is licensed under a Creative Commons Attribution-NonCommercial 3.0 Unported Licence.

with strong host–guest interactions, which then leads to issues with selectivity and separation efficiency. To tackle this problem, we designed a rotational shutter (a rotated pyridyl ring) in NTU-88, a soft MOF composed of 4,4′-dipyridylnitride and $NiCl_2$.[69] The 2D coordination framework connected by halogen bonds exhibits a zig-zag channel with a rhomboid pore of 5.3 × 8.8 Å. But, the structure of the fully activated framework exhibits significant changes, particularly the sharply tailored open size of the channel (1.6 Å). However, this framework demonstrated quick C_3H_4 uptake, but no C_3H_6 uptake. Structural models under typical pressure and modelling calculations showed that a rotation of the pyridine rings in L was observed in the open phase of this MOF, creating an open pore with a maximum size of 4.4 Å, very close to the molecular size of C_3H_4 (4.4 Å), but smaller than that of C_3H_6 (5.4 Å). Thus, this is a rare soft example that can comprehensively suppress co-adsorption (Fig. 7c).

2.2.1.2 Stepwise change. It is worth noting that the adsorption isotherms of these corresponding MOFs show a clear step in a slightly wider pressure range. However, the guest- or stimuli-triggered phase transition in soft MOFs passes through a closed phase, an intermediate phase and then an open phase. Such stepwise phase transitions represent a novel and responsive platform for molecular recognition, even for light hydrocarbons. As an early example, the MIL-53-series demonstrates stepwise adsorption isotherms of CO_2 and alkanes.[93,94] A similar stepwise N_2 adsorption isotherm was also found in a flexible framework Co(BDP).[95,96] However, the stepwise structural change dominated by coordination bonds usually requires high energy input (high gas pressure), which could not distinguish the small difference in the light hydrocarbons. Inspired by the stepwise isotherms of CO_2 in a partially interpenetrated MOF, MFM-202, an interpenetrated dia framework, showed a stepwise C_2H_2 uptake at 195 K.[97] However, the unique function of such a stepwise change was not investigated in detail.

As an early reported soft MOFs, ELM-11 adopts a 2D square-grid coordination framework. The *trans*-axial positions of the metal centres were occupied by two BF^{4-} anions. Interestingly, the author found S-shaped adsorption isotherms of CO_2, N_2, O_2, Ar, and CH_4, caused by stepwise layer expansion. Utilizing this characteristic, ELM-11 was found to have a stepwise C_2H_2 uptake and trace C_2H_4 adsorption, resulting in efficient separation performance, when the partial pressure of C_2H_2 changed from 50 kPa to 10 kPa.[98]

To develop the function of the MOFs that involves stepwise opening, $Zn_2(bpdc)_2(bpee)$, (bpdc = 4,4′-biphenyldicarboxylate; bpee = 1,2-bipyriylethylene) was investigated.[71] The framework showed emerging stepwise adsorption isotherms of short alkanes at 298 K, as well as C2 hydrocarbons. Raman spectra of the C_2H_6 loaded sample revealed that the methyl group of C_2H_6 interacts with the uncoordinated $C{=}O_{COO}$ on the bpdc ligand, causing a decrease in the dihedral angle ($\Delta\phi = -2.0°$) between the two rings of the bpdc ligand. Comparably, the dihedral angle increases ($\Delta\phi = 1.5°$) when C_2H_4 was adsorbed, reflecting a competitive alternative binding site with similar binding strength to that of the H-bonding. In other words, a higher pressure of C_2H_4 (π orbital plays a minimal role) is required to open the gate of such a framework. Furthermore, the chain length of short alkanes is crucial for the gate opening of the pressure dependence (C2 < C3 < C4). Therefore, tuning the H-bond strength is shown to be a strategy for optimizing the MOFs with the desired gate-opening pressure (Fig. 8a).

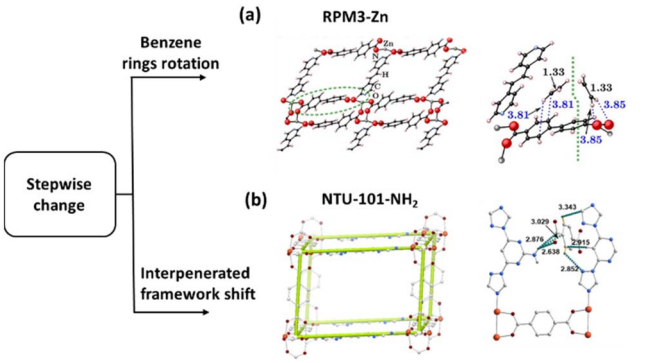

Fig. 8 (a) The lateral perspective of the RPM3-Zn structure and C_2H_2, C_2H_4 and C_2H_6 binding sites at $Zn_2(bpdc)_2(bpee)$. (b) The crystal structure of NTU-101-NH_2. Reprinted with permission from ref. 71. Copyright 2012 American Chemical Society, ref. 62. Copyright 2025 John Wiley & Sons, respectively.

Inspired by this finding and also by the dynamics of the interpenetrated MOF, we recently presented an approach to control the temperature-dependent dynamics in hydrogen-bonded interpenetrated frameworks. NTU-101-NH_2, a single H-bond linked interpenetrated porous framework, exhibited stepwise structural dynamics in response to CO_2.[62] Importantly, this MOF showed gas and pressure dominated dynamics towards C_2H_6 (37 kPa, 328 K) and showed an inverse ability for C_2H_6/C_2H_4 separation at an elevated temperature of 328 K. This was due to the shift of the dynamics towards C_2H_6 (37 kPa, 328 K) and C_2H_4 (53 kPa, 328 K). This is because the displacement of the interpenetrating frameworks here requires a relatively weak stimulus, allowing the adsorption to be optimised in a higher temperature range. However, NTU-101, the precursor framework linked by three H-bonds, shows structural dynamics at very low temperatures. Therefore, hydrogen-bonded frameworks were expected to pave the way for the design of soft families capable of challenging separations at higher temperatures (Fig. 8b).

2.2.1.3 Gradual change. Sudden pore opening and stepwise pore opening both result from overcoming the clearly defined host–guest interactions, but the change is not always a sudden transition from a closed phase to an open phase. During the adsorption process, the pores or structure of MOF materials can be gradually adjusted to match the size and shape of the adsorbate molecules, resulting in a progressively enhanced host–guest interaction. This characteristic is different from the structural response of MOFs with a sudden global change and gradual global change.

Yet an earlier framework of CPL-1, one of the attractive adsorbents, has bridging pillar ligands and 2D porous sheets. The formed small channel with a pore size of 4.0 × 6.0 $Å^2$ features abundant O atoms in a one-to-one fashion.[99]

© 2025 The Author(s). Published by the Royal Society of Chemistry

Open Access Article. Published on 02 June 2025. Downloaded on 5/21/2026 10:40:29 PM. This article is licensed under a Creative Commons Attribution-NonCommercial 3.0 Unported Licence.

Interestingly, the structure was shown to change gradually under increased pressure of C_2H_2, as the gradually enhanced host–C_2H_2 interaction promotes the changes in the structure.[100] The same group then investigated the separation potential of CPL-1 on C_2H_4 and C_2H_6.[101] The flexibility of the framework allowed stepped adsorption isotherms, particularly for C_2H_4 in the pressure range of 200 to 400 kPa, at 273 K; however, the C_2H_6 uptake is very low in the measured region. Shifting the target to the C3 hydrocarbons, CPL-1 showed a gradually changing thermo-responsive gate-opening behavior towards C_3H_6 in the temperature range of 273 to 288 K, but no structural response was found under C_3H_8.[102]

Due to the global framework change, the temperature assistant framework response usually occurred at relatively low temperature. To overcome this issue, a microporous MOF, $[Zn_3OH)_2(btca)_2]$ (JNU-1, H_2btca = benzotriazole-5-carboxylic acid), with gas-induced fit was synthesized. The activated JNU-1 exhibits a 1D microporous channel of 8 Å diameter with an accessible open zinc site.[103] A self-adaption framework change was observed upon increasing C_2H_2 loading, namely a gradually closed form. Gas-loading crystal analysis and modelling calculations showed a side-on configuration of the trapped C_2H_2 interacting with two adjacent open Zn sites. Furthermore, one C_2H_2 molecule interacts with other two additional molecules bound to Zn sites *via* diploe interactions. The gradual increase in adsorption leads to enhanced host–guest interactions, which in turn trigger framework shrinkage. This phenomenon is distinctly different from the general observation of gradual pore enlargement of the framework associated with increased pressure of the adsorbed gas (Fig. 9a).

For the gradual change in the framework, we have recently found a new system that exhibits a subtle expansion and contraction of the channel neck. NTU-68 was prepared *via* crystal conversion of NTU-65 in boiling water.[40] Crystal analysis (from 200 to 340 K) revealed that the distance of the channel neck defined by F–F gradually expanded and then contracted to around 4 Å (turning point: 328 K), which falls between the centre dimensions of C_3H_6 (3.44 Å) and C_3H_8 (4.02 Å). Therefore, an unprecedented phenomenon of thermodynamically dominant C_3H_6 uptake, but kinetically regulated C_3H_8 adsorption behaviour, was observed. The calculated energy profile reveals that the maximum energy for passing through the cell is 42.8 kJ mol^{-1}. However, C_3H_8 has to overcome two strong interactions, corresponding to 46.3 and 63.8 kJ mol^{-1}, respectively, as C_3H_8 diffusion requires a configuration change. This temperature-dependent gradual change allows an enhancement in separation efficiency as the temperature increases from 273 to 298 K (Fig. 9b).

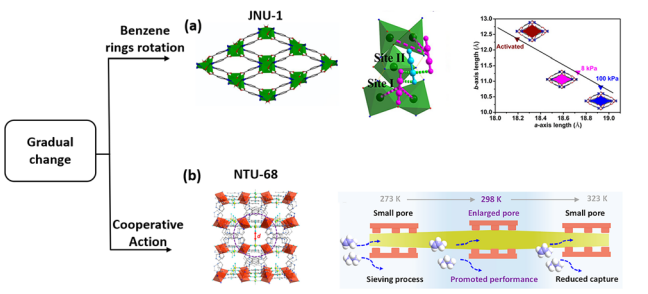

Fig. 9 The structure of JNU-1 (a) and illustration of the accelerated separation process in NTU-68a (b). Reprinted with permission from ref. 103. Copyright 2019 John Wiley & Sons, ref. 40. Copyright 2023 American Chemical Society, respectively.

2.2.2 Local softness of the framework. Compared with the global softness of the MOF, the concept of local softness is defined as the partial movement of the MOF framework. Local softness, particularly in the context of a functional ligand, exhibits a unique advantage in its capacity for adaptive environmental adjustment, enabling precise recognition of guest molecules. This process results in a molecular sieving effect analogous to that of traditional MOFs. In other words, it is conceptually feasible to identify small differences in light hydrocarbon components by utilizing the local structural changes. The small changes in energy barriers offer prospects for expeditious material regeneration in the ensuing phase; nevertheless, they concomitantly engender challenges in precise structure design, and no commensurate theoretical framework has been formulated to date.[104] In the following section, a comparison is made between the local dynamics of the ligand (local node change usually causes global change) in the MOFs for light hydrocarbon separation and the more typical local dynamics of the ligand in other materials.

A coordination framework was synthesised and prepared from a butterfly-type ligand comprising isophthalic acid and phenothiazine-5,5-dioxide (OPTz) moieties (OPTz-IPA).[72] After activation, the framework features a nanocage connected by eight nanochannels. Interestingly, one OPTz moiety and one isophthalic unit adopt a face-to-face configuration, forming a gate of 3 Å inside the channel. Therefore, the thermal flipping of the OPTz units provides a gate function that enables different kinetic responses towards C_2H_4 and C_2H_6, as well as O_2/Ar. It is worth noting that the ability for preferred adsorption is strongly temperature-dependent, of which the T_{max} is as low as 270 K for the adsorption separation of C_2H_4 and C_2H_6. The function of such thermal local-dynamics was extended into the separation of water isotopologues, which have extremely similar physicochemical properties (Fig. 10a).[105]

Recently, a 3D porous MOF, named JNU-3, was prepared by using a branched ligand with carboxylate, triazole and pyridine coordination sites. JNU-3 possesses a 1D channel with dimensions of approximately 4.5 A × 5.3 Å. The yielded cross-sectional area (23.85 Å^2) is slightly larger than that of the minimum cross-sections of C_3H_6 (19.34 Å^2) and C_3H_8 (18.17 Å^2). In addition, a molecular pocket with an aperture size of 3.7 Å is lined up on both sides of the 1D channel. Given the larger kinetic parameters of C_3H_6 and C_3H_8, it appears improbable that these pockets can accommodate them. However, the tilting and rotation of the "guard" moiety of aromatic rings on the ligand can enlarge the aperture (4.4 for C_3H_6 and 4.7 Å for C_3H_8) of the pocket, facilitating the adsorption of C_3H_6 and C_3H_8. Consequently, the unique structure can be regarded as an orthogonal-array dynamic molecular sieve, allowing both fast adsorption–desorption kinetics and large capacity. The presence of a gas-responsive pocket has been demonstrated to facilitate the

Open Access Article. Published on 02 June 2025. Downloaded on 5/21/2026 10:40:29 PM. This article is licensed under a Creative Commons Attribution-NonCommercial 3.0 Unported Licence.

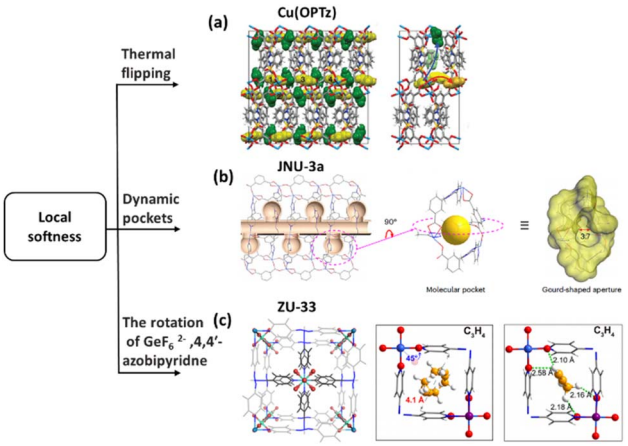

Fig. 10 (a) Simulation of the structure of activated Cu(OPTz)-loaded C_2H_4 and the diffusion structure between the interlayer and intralayer. (b) Crystal structure of JNU-3a with molecular pockets and schematic diagram of molecular pockets. (c) The structure of ZU-33 and bonding sites for loaded C_3H_4 and C_3H_4(PD). Reprinted with permission from ref. 72. Copyright 2019 American Association for the Advancement of Science, ref. 106. Copyright 2024 Springer Nature Limited, ref. 107. Copyright 2022 Springer Nature Limited, respectively.

purification of C_2H_4 from C2–C4 mixtures in one-step (Fig. 10b).[106] In addition, this strategy has been expanded in HAF-1, which features channels and shrinkage throats, the latter being defined as narrower channels that connect the main channels and a molecular pocket.[55]

As a molecule separator, GeFSIX-14-Cu-i (ZU-33) can also exhibit an adaptable response to guest molecules.[107] The coordination of 4,4′-azopyridine with a GeF_6^{2-} anion provides ZU-33 with local rotational flexibility, which plays a crucial role in the recognition of C_2H_2, C_3H_4, and C_3H_4 (PD), and avoids the competitive adsorption of olefins and paraffins. The responsive properties to different stimuli endow this MOF with multiple regulations for challenging separations (Fig. 10c).

2.2.3 Softness of the confined moiety in the framework. Except the softness of the global framework and also the local moiety, we recently found a new kind of softness of the confined moiety in a rigid framework.[37] The new MOF, (NTU-85) has a super-tetrahedral cluster ($Cu_{10}O_{13}$) and one-dimensional (1D) nanochannels consisting of lattice water molecules. Of particular significance is the observation that the lattice water molecules can be categorised into two distinct types: four molecules interact with the inner surface of the nanochannel *via* short hydrogen bonds, while a single molecule occupies the centre of the four water molecules and forms hydrogen bonds over a greater distance. In this regard, the central lattice water was accurately removed, resulting in the formation of a 1D water nanotube with an internal diameter of 4.5 Å within the rigid framework. The slight expansion and contraction of the water nanotube contributes exclusive C_3H_6 adsorption, but not C_3H_8 adsorption. This finding opens the route for establishing confined chemistry in MOFs (Fig. 11).

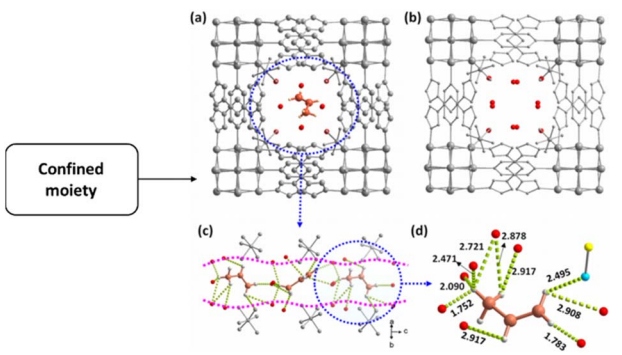

Fig. 11 Crystal structure of loaded C_3H_6 and C_3H_8 samples: (a) NTU-85-WNT⊃C_3H_6 and (b) NTU-85-WNT⊃C_3H_8 and (c, d) detailed H-bonding interactions of C_3H_6 in one-dimensional nanochannels. Reprinted with permission from ref. 37. Copyright 2023 American Chemical Society.

3. Applications

In recent years, there has been significant research interest in the field of adsorption separation of light hydrocarbons using MOFs. According to the demand for highly pure olefins, the separation process can be broadly classified into olefin-selective adsorption and alkane-selective adsorption.[108–112] To obtain pure olefins from an olefin-selective adsorption process, further desorption–adsorption cycles *via* inert gas sweeping or a vacuum pump are required. In contrast, alkane-selective adsorption has been shown to produce pure olefins directly, a process that is notably more energy efficient. This section will discuss recent research advances in the purification of C_2H_4 and C_3H_6 from light hydrocarbon mixtures, particularly those with the same carbon numbers, in recent years.[2,111,113] Furthermore, we compared MOFs with framework dynamics induced by light hydrocarbons (Table 4), and the separation performance and the isosteric heat of adsorption (Q_{st}) of MOFs used for light hydrocarbon separation (Table 5).

3.1 C_2H_4 harvesting from the desorption process

3.1.1 C_2H_4/C_2H_6 feed gas. As a molecular sieving MOF, UTSA-280 demonstrated high C_2H_4 capacity, up to 2.5 mmol g^{-1}, at 298 K and 1 bar, whereas only a trace amount of C_2H_6 (0.098 mmol g^{-1}) was adsorbed.[70] Therefore, the calculated C_2H_4/C_2H_6 selectivity is very high. In the breakthrough experiments, the packed samples exhibited full capture of C_2H_4 from equimolar C_2H_4/C_2H_6 mixtures, while highly pure C_2H_6 was released initially. Enriched C_2H_4 can be recovered with high purity during the regeneration step, yielding a productivity of C_2H_4 as high as 1.86 mol kg^{-1}. Notably, the sieving effect of C_2H_4/C_2H_6 remains unaffected by the presence of additional components in the feed gas. Nevertheless, the role of coordinated water in preserving the structural integrity and enhancing the separation performance was found to be crucial (Fig. 12a).

ZU-901 exhibits a unique 'S' shaped C_2H_4 adsorption curve, providing a high C_2H_4 working capacity of up to 1.36 mmol g^{-1}, at 273 K and 1 bar.[116] Interestingly, the material showed a C_2H_4 uptake of 0.19 mmol g^{-1} at 0.1 bar and 273 K, followed by a rapid increase to 1.55 mmol g^{-1} at 1 bar, signifying the C_2H_4

© 2025 The Author(s). Published by the Royal Society of Chemistry

Open Access Article. Published on 02 June 2025. Downloaded on 5/21/2026 10:40:29 PM. This article is licensed under a Creative Commons Attribution-NonCommercial 3.0 Unported Licence.

Table 4 Light hydrocarbon-induced framework dynamics of the representative MOFs

MOFs	Reasons for phase changing	P_{gas} for phase changing (kPa)	Temperature (K)	Ref.
ZIF-7	Configuration change in benzimidazole	C_2H_6: 0.0008 C_2H_4: 0.0012	298	38
NTU-88	Pyridine ring rotation	C_3H_4: 1.7 C_3H_6: no change	273	69
GeFSIX-dps-Zn GeFSIX-dps-Cu	Pyridine ring rotation	C_3H_4: 0.13 C_3H_4: 0.015	298	114
NTU-65-CoTi	Benzene ring rotation	C_3H_4: 1.6 C_3H_6: 19.4 C_3H_8: 57.2	273	51
$Zn_2(bpdc)_2(bpee)$	bpdc benzene ring rotation	C_2H_2: 0.2 C_2H_4: 0.4 C_2H_6: 0.26	298	71
MFM-202	Benzene ring rotation	C_2H_2: 2.7 C_2H_4: 4.0 C_2H_6: no change	195	97
NTU-101-NH_2	Shifting of the interpenetration framework	C_2H_6: 36 C_2H_4: 57	293	62
X-dia-1-Ni	Pyridine ring and pyridine ring rotation	C_2H_6: 51.7	273	56
ZU-13	Pyridine ring rotation	C_3H_4: 0.05	298	115
NTU-68	Benzene ring rotation	Gradual change		40
Cu(OPTz)	Phenothiazine-5,5-dioxide rotation	Gradual change		72
TYUT-17	3-Methylisonicotinic rotation	C_2H_6: <0.1	298	66
JNU-3	Pyridine ring rotation	Gradual change		65
ZU-33	4,4′-azopyridine ligand and GeF_6^{2-} anion rotation	CH_2=C=CH_2: 0.002	298	107
NTU-85	Dynamic of water nanotubes	Gradual change	298	37

working capacity of 1.36 mmol g^{-1}. A similar adsorption phenomenon was observed upon increasing the temperature and pressure, to 298 K and 3 bar, respectively. Comparably, the C_2H_6 capacity of ZU-901 is as low as 0.26 mmol g^{-1} under both conditions. In breakthrough experiments, the clear separation interval confirmed the ability for C_2H_4/C_2H_6 separation. Thanks to the relatively low binding energy, adsorbed C_2H_4 can be rapidly regenerated and collected with >95% purity. Aspen adsorption simulation revealed that 99.51% purity of C_2H_4 could be obtained with 75% recovery from a two-bed pressure swing adsorption process. In addition, this material can be prepared *via* stirred, associated with mother liquor circulation (Fig. 12b). Meanwhile, some other MOFs, such as $Co(aip)(pyz)_{0.5}$ (Fig. 12c)[117] and MOF-808-Bzz,[53] have been observed to demonstrate selective capture of C_2H_6 from C_2H_4-containing mixtures. Furthermore, we have summarized the top ten C_2H_4/C_2H_6 adsorption ratios, as illustrated in Fig. 16a. Notably, MAF-42 achieves an impressive adsorption ratio, up to 301 at 1 bar.[118] This summary serves as a valuable reference for efficient light hydrocarbon separation techniques.

3.2 C_2H_4 harvesting from the adsorption process

3.2.1 C_2H_2/C_2H_4 feed gas. Utilizing the interlayer and intralayer space, ZUL-100 and ZUL-101, which were synthesized from $NbOF_5^{2-}$ and three different organic ligands, showed highly selective capture of C_2H_2 (selectivity: 175) from a C_2H_2/C_2H_4 mixture (1/99, v/v).[119] In the breakthrough experiments, both ZUL-100 and ZUL-101 have excellent separation performance. Notably, under humid conditions, they have been shown to achieve high-performance separation of trace amounts of C_2H_2, and to directly obtain polymer-grade C_2H_4 with a yield of 121.2 mmol g^{-1} and 103.6 mmol g^{-1}, respectively (Fig. 13a).

Cu(OH)INA exhibited remarkable C_2H_2 adsorption capacity performance within the temperature range of 272–313 K, even at lower pressures.[120] At 0.01 bar and 298 K, the adsorption amount of C_2H_2 reached 44.01 cm^3 cm^{-3}, while the adsorption amount of C_2H_4 was found to be considerably lower. The adsorptive selectivity was calculated to be 105–41 and 71–35 at two distinct temperatures (298 K and 313 K), which confirmed the potential of the material for C_2H_2/C_2H_4 (1/99, v/v) separation. Breakthrough experiments further validated the material's separation ability by obtaining high purity C_2H_4 (>99.99%) with a productivity of 167 mL cm^{-3}. Moreover, after the increase in flow rate, the separation efficiency (165 mL cm^{-3}) remained close to that of the low flow rate. Furthermore, the large-scale synthesis, at least, can be scaled up to 8 L under stirring and 1.31 kg of product (91% yield) can be obtained (Fig. 13b).

Despite the fact that many of the MOFs have been the focus of research in regard to their potential for selective C_2H_2/C_2H_4 capture, only a limited number of them have been shown to achieve a balance between C_2H_2 uptake and C_2H_2/C_2H_4 selectivity. SIFSIX-2-Cu-i with periodic SiF_6^{2-} ions demonstrated a high C_2H_2 adsorption capacity (2.1 mmol g^{-1}, 0.05 bar, 298 K) and selectivity (39.7 to 44.8).[34] In contrast, SIFSIX-1-Cu exhibited exceptionally high C_2H_2 uptake (8.5 mmol g^{-1}) at 298 K and 1.0 bar, yet the superior C_2H_4 uptake resulted in moderately high

Open Access Article. Published on 02 June 2025. Downloaded on 5/21/2026 10:40:29 PM.
This article is licensed under a Creative Commons Attribution-NonCommercial 3.0 Unported Licence.

Table 5 Typical MOFs for separation of light hydrocarbons

MOFs	Feed gas	Velocity of feed gas (mL min^{-1}) and working temperature (K)	Q_{st} (kJ mol^{-1})	Purity and productivity	Ref.
UTSA-280	C_2H_4/C_2H_6 (1/1, v/v)	2.0, 298	C_2H_4: 34.1	Highly pure C_2H_4, 1.86 mol kg^{-1}	70
ZU-901	C_2H_6/C_2H_4 (1/1, v/v)	1.7, 273	C_2H_4: 24.85	C_2H_4, 95%, —	123
$Co(aip)(pyz)_{0.5}$	C_2H_4/C_2H_6 (1 : 1, v/v)	1.0, 298	C_2H_4: 33.6	C_2H_4 > 97%, 19.1 L kg^{-1}	117
$Fe_2(O_2)(dobdc)$	C_2H_6/C_2H_4 (1/1, v/v)	5.0, 298	C_2H_6: 66.8	C_2H_4, 99.99%, 0.79 mmol g^{-1}	46
Ni-MOF 2	C_2H_6/C_2H_4 (1/1, v/v)	2.0, 298	C_2H_6: 23.6 C_2H_4: 21.4	C_2H_4 > 99.95%, 12 L kg^{-1}	68
TYUT-17	C_2H_6/C_2H_4 (1/9, v/v)	2.0, 298	C_2H_6: 27.1 C_2H_4: 21.4	C_2H_4 > 99.99%, 77.4 L kg^{-1}	66
ZUL-100	C_2H_2/C_2H_4 (1/99, v/v)	1.25, 298	C_2H_2: 65.3 C_2H_4: <40	C_2H_4 > 99.9999%, 121.2 mmol g^{-1}	119
Cu(OH)INA	C_2H_2/C_2H_4 (1/99, v/v)	2.0, 298	C_2H_2: 36.1 C_2H_4: 29.6	C_2H_4 > 99.99 %, 167 mL cm^{-3}	120
MOF-303	$C_2H_2/C_2H_4/C_2H_6$ (1/9/90, v/v/v)	1.25,296	C_2H_2: 31.7 C_2H_4: 24.3 C_2H_6: 25.1	C_2H_4 > 99.95%, 1.35 mmol g^{-1}	123
Al-PyDC	C_2H_2/C_2H_4 (1/99, v/v)	1.25, 296	C_2H_2: 35.3 C_2H_4: 27.8 C_2H_6: 30.1	C_2H_4 > 99.999%, 7.93 mmol g^{-1}	83
MOF-808-Bzz	$C_2H_2/C_2H_4/C_2H_6$ (1/1/1, v/v/v)	1.0, 298	C_2H_2: 32.36 C_2H_4: 26.43 C_2H_6: 29.87	C_2H_4 ≥ 99.95%, —	53
MAC-4	$C_2H_6/C_3H_6/C_2H_4$ (2/10/25, v/v/v)	7.0, 298	C_2H_6: 22.7 C_2H_4: 17.1 C_3H_6: 25.3	C_2H_4 ≥ 99.9% 27.4 L kg^{-1} $^1C_3H_6$ ≥ 99.5% 36.2 L kg^{-1}	132
MOF-1	$C_2H_6/C_2H_2/C_2H_4$ (3/3/10, v/v/v)	7.0, 298	C_2H_6: 31.8 C_2H_4: 28.7 C_3H_6: 23.2	C_2H_4 > 99.9 %, 4.6 L kg^{-1}	133
Ni-dcpp-bpy	C_2H_2/CH_4 (1/1, v/v)	6.0, −298	C_2H_2: 33.8 C_2H_4: 26.7	C_2H_4 > 99.9 %, 6.1 L kg^{-1}	134
SNNU-33	C_2H_2/CH_4 (5/2, v/v)	5.0, 298	C_2H_2: 40.4 C_2H_4: 32.9	CH_4 > 99.95%, 3.5 mmol g^{-1}	135
NU-57	C_3H_8/C_3H_6 (1/1, v/v)	3.0, 298	C_3H_8: 33.0 C_3H_6: 28.5	C_3H_6 > 99.5%, 34.2 L kg^{-1}	130
JNU-3a	C_3H_6/C_3H_8 (1/1, v/v)	1.0, 298	C_3H_8: 34.6 C_3H_6: 38.9	C_3H_6 > 99.5%, 34.2 L kg^{-1}	65
HIAM-301	C_3H_6/C_3H_8 (95/5, v/v)	5.0, 298	C_3H_6: 27.0	C_3H_6 > 99.6%, 38.5 cm^3 g^{-1}	64
ZJU-75	C_3H_6/C_3H_8 (1/1, v/v)	2.0, 296	C_3H_8: 33.1 C_3H_6: 65.9	C_3H_6 > 99.5% 18.7 L kg^{-1}	90
FDC-4	C_3H_6/C_3H_8 (1/1, v/v)	4.0, 300	C_3H_6: 35.0	C_3H_6 99.7%, 19.5 L kg^{-1}	74
GeFSIX-dps-Cu	C_3H_4/C_3H_6 (1/9, v/v) and C_2H_2/C_2H_4 (1/9, v/v)	2.0, 298	C_2H_2: 56.3	C2–C3 alkynes > 99.99%, —	114
Sql-NbOFFIVE-bpe-Cu-AB	C_3H_6/C_3H_8 (1/99, v/v)	1.0, 298	C_3H_4:69.0 C_3H_6 : 53.0	C_3H_6 > 99.9%, 118 mmol g^{-1}	136

© 2025 The Author(s). Published by the Royal Society of Chemistry

Open Access Article. Published on 02 June 2025. Downloaded on 5/21/2026 10:40:29 PM.
This article is licensed under a Creative Commons Attribution-NonCommercial 3.0 Unported Licence.

Table 5 (*Contd.*)

MOFs	Feed gas	Velocity of feed gas (mL min^{-1}) and working temperature (K)	Q_{st} (kJ mol^{-1})	Purity and productivity	Ref.
Zn-BPZ-TATB	$C_2H_6/C_3H_6/C_2H_4$ (2/10/25,[54] v/v/v)	8.0, 298	C_2H_6: 23.1 C_2H_4: 18.3 C_3H_6: 28.1	C_3H_6 99.5%, 38.2 L kg^{-1} C_2H_4 99.9%, 12.7 L kg^{-1}	3
Zn-MOF	C_3H_6/C_2H_4(1/9, v/v)	5.0, 298	C_2H_4: 25.8 C_3H_6: 33.3	C_2H_4 (>99.9 %), 98.71 L kg^{-1}	137
Tb-MOF-76(NH_2)	C_2H_6/C_2H_4/Ar (5/5/90, v/v/v	7.0, 298	C_2H_4: 30.9–29.5 C_2H_6: 32.8–30.7	C_2H_4, >99.9 %, —	138
X-dia-1-$Ni_{0.89}Co_{0.11}$	(C_2H_6/C_2H_4: 1/9, v/v)	10, 298	—	C_2H_4, >99.9 %, —	56
Y-abtc	C_3H_8/C_3H_6: 5/95, v/v)	4.0, 298	C_3H_6: 57.4	C_2H_4, 99.5%, —	6
NKMOF-1-M (M = Cu or Ni)	$C_3H_4/CH_2{=}C{=}CH_2/C_3H_6$ (0.5/0.5/99, v/v/v)	2.0, 298	C_3H_4: 65.1 (Ni), 67.2 (Cu) $CH_2{=}C{=}CH_2$: 54.0 (Ni), 45.2 (Cu) C_3H_6: 38.0 (Ni), 37.2 (Cu)	C_3H_6 99.996%, —	52
Ca-based MOF	$C_3H_4/CH_2{=}C{=}CH_2/C_3H_6$ (0.5 : 0.5 : 99, v/v/v)	2.7, 298	C_3H_4: 55.5 $CH_2{=}C{=}CH_2$: 51.7	C_3H_6 99.95%, —	139
ZNU-2	C_3H_4/C_3H_6 (1/9 or 1/99, v/v)	2.0, 298	C_3H_4: 43.2 C_3H_6: 35.5	C_3H_6 > 99.996%, 37.8 or 52.9 mol kg^{-1}	140
NTU-88	C_3H_4/C_3H_6 (1/1, v/v)	2.0, 298	C_3H_4: 44	C_3H_6 > 99.95%, —	69
NTU-101-NH_2	C_3H_4/C_3H_6 (1/99, v/v)	4.0, 298	C_3H_4: 43.5	C_3H_6, 99.95%, 15.7 mL g^{-1}	62
JNU-9-CH_3	$C_3H_4/CH_2{=}C{=}CH_2/C_3H_6/C_3H_8$ (1/1/1/1, v/v/v/v)	2.0, 298	C_3H_4: 34.6 $CH_2{=}C{=}CH_2$: 31.9 C_3H_6: 27.4 C_3H_8: 31.1	$C_3H_6 \geq$ 99.99%, —	60
PCP-IPA	C_3H_6/C_3H_8 (1/1, v/v)	3.7, 298	C_3H_8: 50.94 C_3H_6: 43.36	C_3H_6 (99.99%), 15.2 L kg^{-1}	129
$CuZrF_6$-TPA	$C_3H_4/CH_2{=}C{=}CH_2$(1/1, v/v)	0.8, 298	C_3H_4: 46.1 $CH_2{=}C{=}CH_2$: 37.1	$CH_2{=}C{=}CH_2$ > 99.95%, 4.7 mol L^{-1}	141
NbOFFIVE-1-Ni	C_3H_6/C_3H_8 (1/1, v/v)	4.0, 298	C_3H_6: 57.4	C_3H_6, ~0.6 mol kg^{-1}	32
NTU-85-WNT	C_3H_6/C_3H_8 (1/1, v/v)	0.5, 298	C_3H_6:49.9	C_3H_6, > 99.8%, 1.6 mL mL^{-1}	37
NTU-68	C_3H_6/C_3H_8 (1 : 1, v/v)	1.0, 298	C_3H_6: 42.8	C_3H_8 > 99.95%, —	40
DL-mal-MOF	C_3H_6/C_3H_8 (1/1 or 95/5 v/v)	2.0, 298	C_3H_6: 64.4	Highly pure C_3H_6, 2.1 L kg^{-1}	27

© 2025 The Author(s). Published by the Royal Society of Chemistry

Open Access Article. Published on 02 June 2025. Downloaded on 5/21/2026 10:40:29 PM.
This article is licensed under a Creative Commons Attribution-NonCommercial 3.0 Unported Licence.

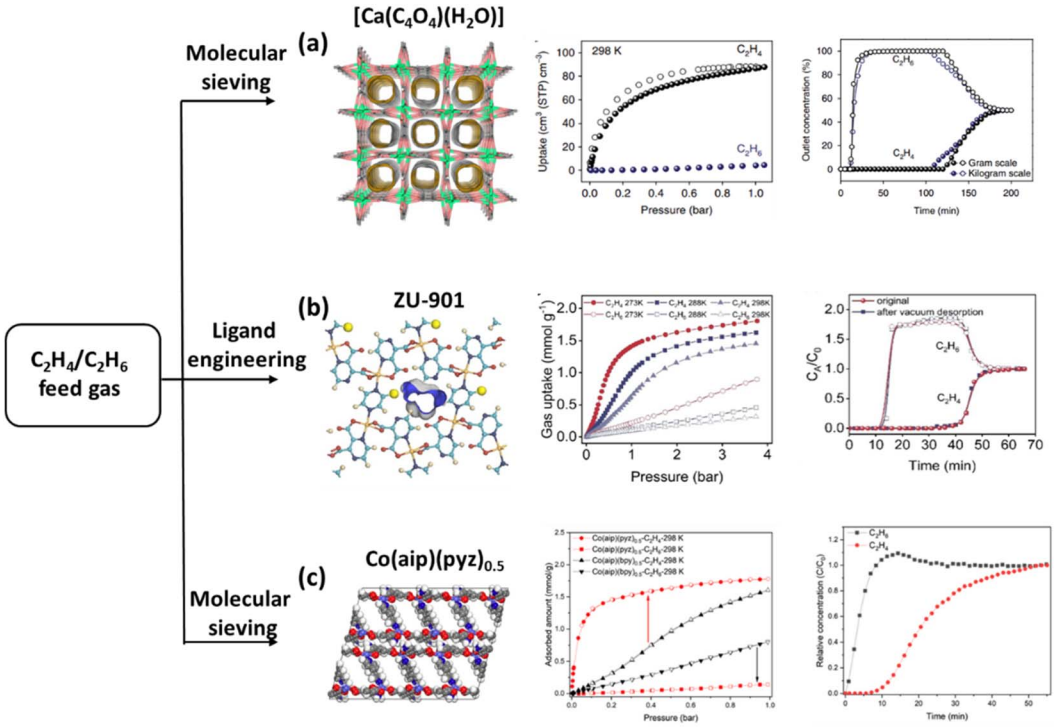

Fig. 12 (a) The crystal structure of guest-free UTSA-280, single-component sorption isotherms of C_2H_4 and C_2H_6 at 298 K and breakthrough curves from different scales for an equimolar C_2H_4/C_2H_6 mixture at 298 K and 1 bar. (b) The internal structures of ZU-901, adsorption isotherms of C_2H_4 and C_2H_6 at different temperatures and high pressure, and breakthrough curve of the fresh and regenerated sample *via* vacuum desorption. (c) The structures of $Co(aip)(pyz)_{0.5}$, C_2H_4 and C_2H_6 adsorption isotherms of $Co(aip)(pyz)_{0.5}$ at 298 K, and experimental column breakthrough curves for C_2H_4/C_2H_6 equimolar binary mixtures at 298 K. Reprinted with permission from ref. 70. Copyright 2018 Springer Nature Limited, ref. 116. Copyright 2023 John Wiley & Sons, ref. 117. Copyright 2023 Elsevier Inc, respectively.

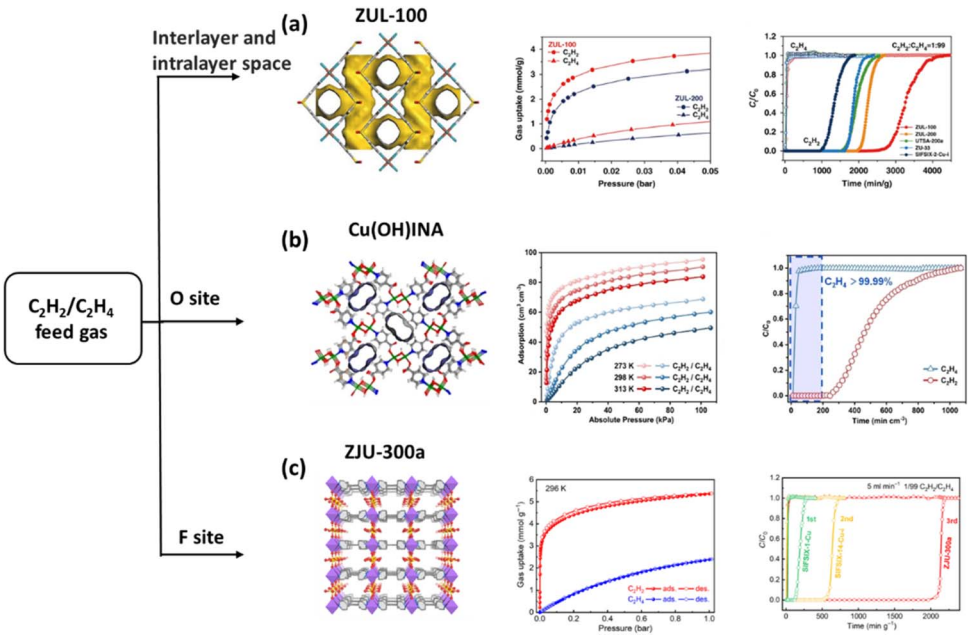

Fig. 13 (a) Pore geometry of ZUL-100 with an intralayer, C_2H_2 and C_2H_4 adsorption isotherms at 298 K, and experimental column breakthrough curves for the C_2H_2/C_2H_4 mixture at 298 K and 1 bar. (b) Structure and one-dimensional channel of Cu(OH)INA, adsorption isotherms of C_2H_2 and C_2H_4 at various temperatures, and breakthrough experiment with a C_2H_2/C_2H_4 mixture at a flow rate of 2 mL min^{-1} at 298 K. (c) Single-crystal structure of ZJU-300, adsorption isotherms for C_2H_2 and C_2H_4 at 296 K, and experimental column breakthrough curves for 1/99 C_2H_2/C_2H_4 separation at a flow rate of 5 mL min^{-1} under ambient conditions. Reprinted with permission from ref. 119. Copyright 2020 Springer Nature Limited, ref. 120. Copyright 2024 John Wiley & Sons, ref. 121. Copyright 2023 The American Association for the Advancement of Science, respectively.

© 2025 The Author(s). Published by the Royal Society of Chemistry

Open Access Article. Published on 02 June 2025. Downloaded on 5/21/2026 10:40:29 PM. This article is licensed under a Creative Commons Attribution-NonCommercial 3.0 Unported Licence.

C_2H_2/C_2H_4 separation selectivity (7.1 to 10.6). These values reflected the emerging separation performance of C_2H_2/C_2H_4. In the breakthrough experiments, highly-pure C_2H_4 broke the sample beds of SIFSIX1-Cu and SIFSIX-2-Cu-i at first, while 0.38 and 0.73 mmol g^{-1} of C_2H_2 was captured by from the 1/99 mixture, respectively. After replacing the linear ligand from a 2-c to 4-c linker, ZJU-300 with densely decorated SiF_6^{2-} ions also exhibited a promising C_2H_2 uptake of 3.23 mmol g^{-1} (0.01 bar, 296 K). This result is substantially higher than that of all the SIFSIX materials (Fig. 13c).[121]

When the pressure was increased to 1 bar, the C_2H_2 uptake increased to 5.4 mmol g^{-1}, while the C_2H_4 uptake was only 2.39 mmol g^{-1}. It is noteworthy that the C_2H_2/C_2H_4 (1/99) selectivity is as high as 1672. This observation was subsequently confirmed through dynamic breakthrough experiments, which revealed that the C_2H_4 productivity reached 436.7 mmol g^{-1}. Moreover, the material maintained good stability under humidity and an acidic gas atmosphere.

3.2.2 C_2H_4/C_2H_6 feed gas. $Fe_2(O_2)$(dobdc) demonstrates a superior C_2H_6 (74.3 cm^3 g^{-1}) adsorption capacity in comparison to that of C_2H_4 (57.3 cm^3 g^{-1}) at 298 K and 1 bar, providing an increased C_2H_6/C_2H_4 (v/v: 1/1) selectivity (from 3.5 to 4.4) under increased pressure.[46] Thus, in the breakthrough experiment, the C_2H_6/C_2H_4 mixture can be completely separated to yield 99.95% pure C_2H_4, up to 2172 mmol per liter (C_2H_6/C_2H_4, 50/50) and 6855 mmol per liter (C_2H_6/C_2H_4, 10/90). Importantly, the material can be readily regenerated for cycling separations. Encouraged by this finding, breakthrough experiments were performed on multi-components. The highly efficient separation performance suggests that $Fe_2(O_2)$(dobdc) is an effective separator for C_2H_4 purification when the concentration of C_2H_6 is low, as well as the existence of CH_4, H_2, and C_2H_2 impurities (Fig. 14a).

The two isostructural MOFs Ni-MOF-1 and Ni-MOF-2 have also been investigated for C_2H_6/C_2H_4 separation.[63] For Ni-MOF-1, nearly the same adsorption isotherms of C_2H_6 (113 cm^3 g^{-1}) and C_2H_4 (116 cm^3 g^{-1}) were observed at 298 K and 1 bar. However, Ni-MOF 2 demonstrated a substantially higher adsorption of C_2H_6 (133 cm^3 g^{-1}) over C_2H_3 (105 cm^3 g^{-1}). Along with an uptake difference of 40 cm^3 g^{-1} at 0.5 bar, Ni-MOF 2 can efficiently separate the equimolar C_2H_6/C_2H_4 mixture gas in dynamic penetration experiments, yielding a C_2H_4 productivity of 12 L kg^{-1}. In addition, cycling experiments demonstrated that Ni-MOF-2 has good reproducibility for this separation (Fig. 14b).

Different from the previously mentioned rigid MOFs, TYUT-17, a flexible-robust framework, exhibited a selective adsorption tendency for C_2H_6.[66] TYUT-17 demonstrated a higher

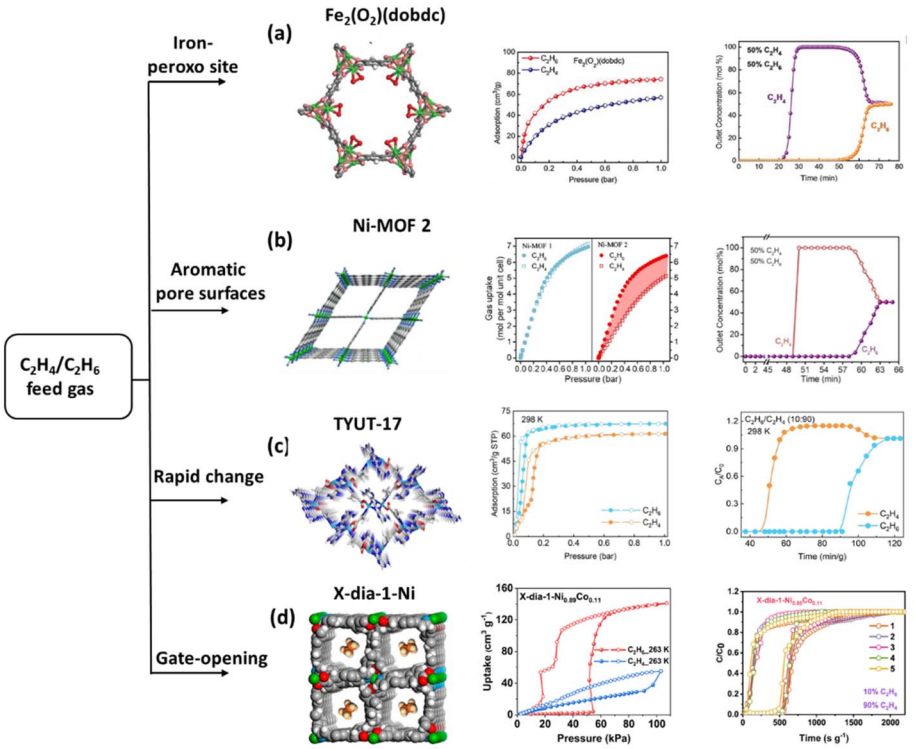

Fig. 14 (a) Structures of $Fe_2(O_2)$(dobdc), adsorption isotherms of C_2H_6 and C_2H_4 at 298 K, and experimental column breakthrough curves for a C_2H_6/C_2H_4 mixture at 298 K and 1.01 bar. (b) The three-dimensional open framework of Ni-MOF 2, C_2H_4 and C_2H_6 single-component adsorption isotherms at 298 K, and dynamic breakthrough curves of equimolar C_2H_6/C_2H_4 gas mixtures at 298 K and 1 bar. (c) The structure TYUT-17, single-component gas adsorption isotherms at 298 K, and breakthrough curves of TYUT-17 for C_2H_6/C_2H_4 (v/v, 10/90) mixtures at 298 K and 1 bar. (d) C_2H_6 adsorption induced the structural transformation of X-dia-1-Ni, C_2H_4 and C_2H_6 adsorption isotherms for X-dia-1-$Ni_{0.89}Co_{0.11}$ at 273 K, and cyclic breakthrough separation experiments for C_2H_4/C_2H_6 (1/9) mixtures performed at 100 kPa and 263 K. Reprinted with permission from ref. 46. Copyright 2018 The American Association for the Advancement of Science, ref. 63. Copyright 2023 John Wiley & Sons, ref. 66. Copyright 2024 John Wiley & Sons, ref. 56. Copyright 2024 American Chemical Society, respectively.

Open Access Article. Published on 02 June 2025. Downloaded on 5/21/2026 10:40:29 PM. This article is licensed under a Creative Commons Attribution-NonCommercial 3.0 Unported Licence.

adsorption capacity of 62.6 cm^3 g^{-1} for C_2H_6, at 298 K and 0.1 bar; however, the C_2H_4 uptake was found to be 18.7 cm^3 g^{-1}, providing an exceptional C_2H_6/C_2H_4 selectivity (6.4) and uptake ratio (3.3). It was observed that an increase in temperature resulted in a shift of the gate-opening phenomenon to a high-pressure region, but the $P_{C_2H_4}$ always lagged behind the $P_{C_2H_6}$, indicating the reality of sample regeneration. Following the introduction of a feed gas comprising C_2H_6/C_2H_4 mixtures to the packed TYUT-17, the observation of different retention times indicated unambiguous separation. The productivity of C_2H_4 of >99.9% purity was recorded at 77.4 L kg^{-1}. Furthermore, the gate-opening of TYUT-17 facilitated the separation of the C_2H_6/C_2H_4 mixture at 313 K (Fig. 14c).

To promote the separation temperature, an implication of saving energy in the separation process, we developed two hydrogen-bonded interpenetrated frameworks, NTU-101 and NTU-101-NH_2.[62] A three H-bond linked interpenetrated porous framework, NTU-101 exhibited a structural response to C_2H_6 and C_2H_4 in the temperature range of 288 to 303 K. Comparably, the single H-bond connected framework of NTU-101-NH_2 exhibited a structural response to C_2H_6 and C_2H_4 in a wider temperature range of 288 to 333 K, particularly the gate-opening pressure under C_2H_6 is always earlier than that of C_2H_4. Consequently, NTU-101-NH_2 is capable of separating the C_2H_6/C_2H_4 (1/9, v/v) mixtures at a relative higher temperature of 328 K. To our knowledge, this is the first example that can selectively capture C_2H_6 from C_2H_4 at such a higher temperature and yielded a productivity of polymer-grade C_2H_4, of up to 15.7 mL g^{-1}. Meanwhile, the robust NTU-101-NH_2 can be prepared on a large scale through the stirring method at room temperature.

In addition, the flexible dia coordination network of X-dia-1-$Ni_{0.89}Co_{0.11}$ exhibited preferred gate-opening for C_2H_6, but not for C_2H_4 at 263 K.[56] The unique structural change driven the C_2H_6 adsorption sharply increased at a pressure of 50 kPa, and the maximum adsorption capacity reached 131.4 cm^3 g^{-1}. However, the structure did not show evident gate-opening, thus providing a low C_2H_4 uptake of 44.8 cm^3 g^{-1}. The ability for harvesting high-purity (99.9%) C_2H_4 directly was validated by dynamic breakthrough experiments at 263 K (C_2H_6/C_2H_4: 1/9, v/v) (Fig. 14d).

3.2.3 $C_2H_2/C_2H_4/C_2H_6$ feed gas. The harvesting of highly pure C_2H_4 from the ternary mixture of $C_2H_2/C_2H_4/C_2H_6$ requires the MOFs to have the ability to selectively adsorb C_2H_2 and C_2H_6 simultaneously. An earlier example of this was exhibited by TJT-100, due to the hierarchy of weak sorbent–sorbate interactions.[82] To promote the separation performance, three isostructural MOFs, named NPU-1, NPU-2 and NPU-3, were synthesized from an Mn6 cluster, rigid dicarboxylate ligands and a 3-connected pyridyl-based tritopic ligand.[122] With the smallest pore size among the three, NPU-1 exhibited the largest uptakes for C_2H_2 (5.1 mmol g^{-1}), C_2H_6 (4.5 mmol g^{-1}) and C_2H_4 (4.2 mmol g^{-1}). The adsorption selectivities for C_2H_6/C_2H_4 (1/1, v/v) and C_2H_2/C_2H_4 (1/1, v/v) were calculated to be 1.32 and 1.4, respectively. The preferential uptake of C_2H_2 and C_2H_6 allows this MOF to produce highly pure C_2H_4 from equimolar ternary mixtures in one-step. The stability of this separation was

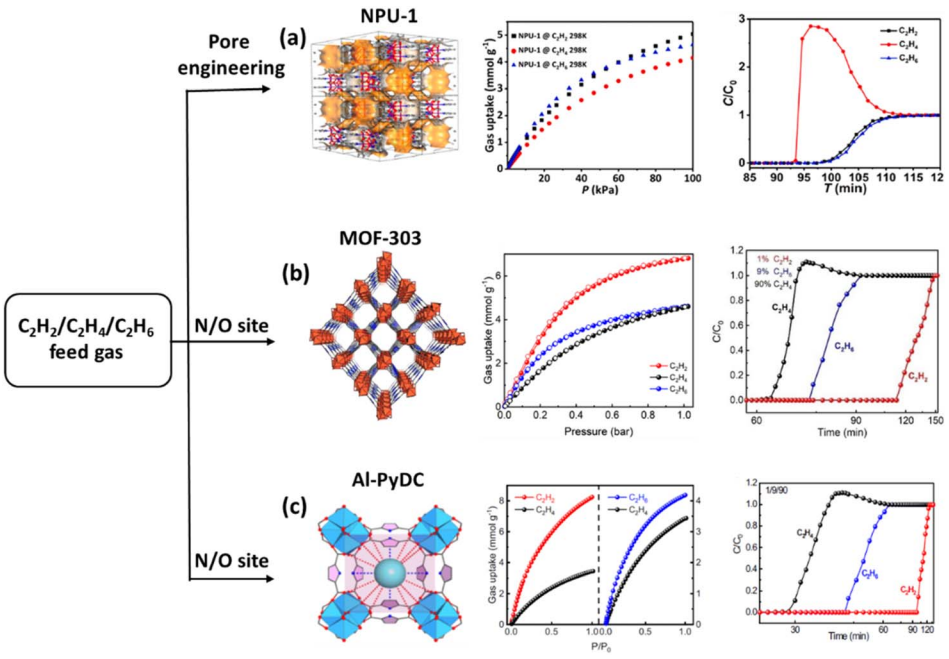

Fig. 15 (a) NPU-1 three-dimensional structure; C2 gas sorption isotherms of NPU-1 at 298 K; and experimental breakthrough curves at 298 K for C2 (1 : 1 : 1mixture) separation. (b) The framework of MOF-303, C2 adsorption isotherm of MOF-303 at 296–313 K, and experimental column breakthrough curves of MOF-303 for C2 mixtures under ambient conditions. (c) Multiple supramolecular binding sites in the pores of Al-PyDC, C2 adsorption isotherms of Al-PyDC at 296 K, and experimental column breakthrough curves of Al-PyDC for C2 mixtures under ambient conditions. Reprinted with permission from ref. 122. Copyright 2021 American Chemical Society, ref. 123. copyright 2023 John Wiley & Sons, ref. 83. Copyright 2023 Springer Nature Limited, respectively.

© 2025 The Author(s). Published by the Royal Society of Chemistry

Open Access Article. Published on 02 June 2025. Downloaded on 5/21/2026 10:40:29 PM. This article is licensed under a Creative Commons Attribution-NonCommercial 3.0 Unported Licence.

validated through cycling experiments. Based on the packing of the C_2H_2-selective MOF and C_2H_6-selective MOF, the same group developed a synergistic sorbent separation technology for purification of C_2H_4 from $C_2H_2/C_2H_4/C_2H_6$ mixtures.[88] This technology may pave the way for the development of new separation systems based on reported MOFs for challenging separations (Fig. 15a).

The aluminium-based MOF (MOF-303) is a stable, low-cost, and easily scalable separation material.[123] It also demonstrated preferred C_2H_2 (7.94 mmol g^{-1}) and C_2H_6 (5.01 mmol g^{-1}) adsorption compared with that of C_2H_4. In the dynamic breakthrough experiment, the binary mixture C_2H_2/C_2H_4 (1/99, v/v) can be separated, with an outlet effluent C_2H_4 yield of 5.07 mmol g^{-1} and a purity greater than 99.95%. Furthermore, the yield of the C_2H_4/C_2H_6 binary mixture is also as high as 0.56 mmol g^{-1}, and the purity is greater than 99.95%. In the ternary mixture (1/9/90, v/v/v), the productivity of C_2H_4 is as high as 1.35 mmol g^{-1} (>99.95%), exhibiting excellent separation performance (Fig. 15b).

The low polarity O/N supramolecular binding sites allow Al-PyDC to show both higher C_2H_2 (8.24 mmol g^{-1}) and C_2H_6 (4.20 mmol g^{-1}) uptakes in comparison to C_2H_4 (3.44 mmol g^{-1}) at 296 K and 1 bar,[83] along with both a good C_2H_2/C_2H_4 (1/99, v/v) selectivity of 4.3 and C_2H_6/C_2H_4 (50/50, v/v) selectivity of 1.9. In the dynamic breakthrough experiments, both C_2H_2/C_2H_4 and C_2H_6/C_2H_4 binary mixtures can be separated. Therefore, Al-PyDC can separate the $C_2H_2/C_2H_4/C_2H_6$ ternary mixtures for getting polymer-grade C_2H_4 in one-step with a productivity of 1.61 mmol g^{-1}. Furthermore, the system demonstrates consistent recyclability over 20 cycles, exhibiting no decline in performance under acidic gas conditions (Fig. 15c).

3.3 C_3H_6 harvesting from the desorption process

3.3.1 C_3H_6/C_3H_8 feed gas. The harvesting of pure C_3H_6 at the desorption process from C_3H_6/C_3H_8 feed gas requires a MOF that exhibits superior C_3H_6 uptake attributable to either stronger interaction sites or a favoured C_3H_6 trap.[109,124,125] Typically, based on the sieving effect, KAUST-7 exhibits specific adsorption of C_3H_6 but did not permit C_3H_8 to diffuse/adsorb into the pore system at 298 K up to 1 bar, as evidenced by fully overlaid adsorption isotherms between pure C_3H_6 and equimolar C_3H_6/C_3H_8.[32] Breakthrough experiments further demonstrated that KAUST-7 flowed directly out of the packed column, while C_3H_6 penetrated after ~480 s, followed by further desorption to obtain pure C_3H_6, and the recovery is ~2 mol per kg per hour at standard ambient temperature and pressure. In addition, KAUST-7 possesses a noticeably high chemical (tolerance to water vapor and hydrogen sulfide) and thermal stability (Fig. 17a). Another example of sieving separation is ZU-609 with local sieving channels, which has the potential to separate C_3H_6 from C_3H_6/C_3H_8 mixtures due to the presence of molecular sieving gates and fast diffusion channels in the local sieving channels and the similar size of the molecular sieving gates to the size of the C_3H_6 molecules.[33] The single-component adsorption isotherms indicated sieving performance for C_3H_6 and C_3H_8 with an uptake ratio of 22.3 at 298 K and 1 bar. Breakthrough experiments confirmed the superior adsorption performance of ZU-609 on C_3H_6 with a dynamic adsorption capacity of about 1.64 mmol g^{-1} and a yield of 32.2 L kg^{-1} for obtaining high-purity (99.9%) C_3H_6 (Fig. 17f).

In the presence of an orthogonal-array dynamic molecular sieve, both stepwise C_3H_6 and C_3H_8 adsorption isotherms were observed in JUN-3a.[65] The rapid uptake at low pressure gradually diminished and the step shifted to higher pressures following increased pressure, a phenomenon attributable to the local dynamic of the molecular pocket. Importantly, at an earlier gate opening pressure, the C_3H_6 uptake reached 58.6 cm^3 g^{-1} at 303 K and 1 bar, which is considerably than that of C_3H_8 (42.5 cm^3 g^{-1}). The density of C_3H_6 was calculated to be 404 g L^{-1} based on the pore volume, reflecting its good packing ability of C_3H_6 compared to the density of gaseous C_3H_6 (1.707 g L^{-1}). Breakthrough curves revealed that JNU-3a can separate equimolar C_3H_6/C_3H_8 at 303 K. C_3H_8 was eluted from the packed column at about 70 min, while C_3H_6 penetrated through the column after 35 min. In the desorption stage, JNU-3a was able to obtain high-purity C_3H_6 with a productivity of 34.2 L kg^{-1} (Fig. 17b).

In the context of quasi-discrete cavities, DL-mal-MOF demonstrated rapid and different uptakes of C_3H_6 and C_3H_8 in the low pressure region, with uptake values of up to 1.68 mmol g^{-1} and 1.21 mmol g^{-1} at 298 K and 1 kPa.[27] In contrast, both L-mal-MOF and D-mal-MOF exhibited nearly the same adsorption isotherms for C_3H_6 and C_3H_8. Remarkably, DL-mal-MOF demonstrated both a high Henry's selectivity of 5.86 and kinetic selectivity of 114.2. The observed disparity in diffusion rates facilitates the dynamic separation of C_3H_6/C_3H_8 mixtures (50/50, or 95/5, v/v) at 298 K. During the desorption stage, the polymer-grade C_3H_6 was attained, with a yield of 2.1 L kg^{-1} (Fig. 17c).

Dependent on the cooperative global and local dynamics, FDC-4 exhibited gate-opening during C_3H_6 adsorption, yielding an uptake of 122 cm^3 g^{-1} at 300 K.[74] However, C_3H_8 adsorption in this narrow channel adopts a diffusion controlled manner, thereby resulting in the very low uptake of C_3H_8 being observed. The substantial differences in both uptake capacity and adsorption kinetics enabled the dynamic separation of an equimolar C_3H_6/C_3H_8 mixture, thereby revealing sieving performance and producing C_3H_6 (19.5 L kg^{-1}) with a purity of 99.7% (Fig. 17d).

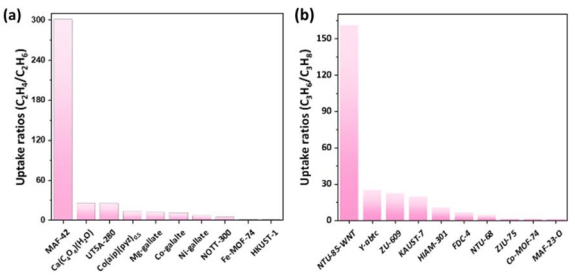

Fig. 16 The top ten in terms of uptake ratios for C_2H_4/C_2H_6 (a) and C_3H_6/C_3H_8 (b).

Open Access Article. Published on 02 June 2025. Downloaded on 5/21/2026 10:40:29 PM.
This article is licensed under a Creative Commons Attribution-NonCommercial 3.0 Unported Licence.

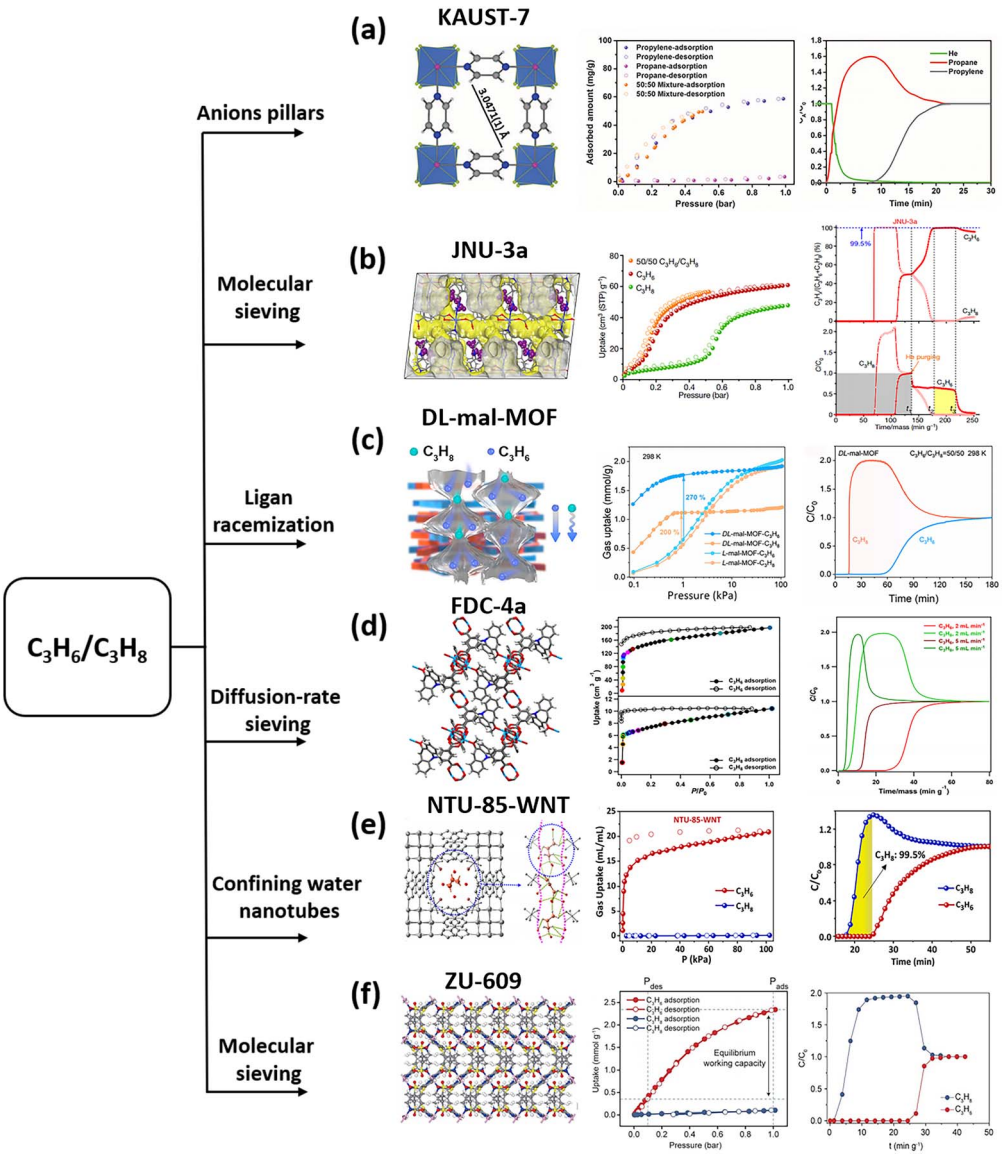

Fig. 17 (a) The crystal structure of KAUST-7, adsorption isotherms for pure C_3H_8, pure C_3H_6, and C_3H_6/C_3H_8 equimolar mixtures at 298 K, and breakthrough experimental curves of equimolar C_3H_6/C_3H_8 mixtures at 298 K. (b) The crystal structure of C_3H_6@JNU-3a, adsorption isotherms for pure C_3H_8, pure C_3H_6, and C_3H_6/C_3H_8 equimolar mixtures at 303 K, and breakthrough experimental curves of equimolar C_3H_6/C_3H_8 mixtures at 303 K. (c) The ligand racemization strategy is illustrated, adsorption isotherms of C_3H_6 and C_3H_8 on DL-mal-MOF and breakthrough experimental curves of C_3H_6/C_3H_8 (50/50, v/v) mixtures at 298 K. (d) The crystal structure of FDC-4a, adsorption isotherms for C_3H_6 and C_3H_8 at 240 K, and breakthrough experimental curves of equimolar C_3H_6/C_3H_8 mixtures at 300 K. (e) The crystal structure of NTU-85-WNT⊃C_3H_6, hydrogen bond interactions of C_3H_6 in one-dimensional nanochannels, adsorption isotherms for C_3H_6 and C_3H_8 at 298 K, and breakthrough experimental curves of equimolar C_3H_6/C_3H_8 mixtures at 300 K. (f) The crystal structure of ZU-609, adsorption isotherms for pure C_3H_8 and C_3H_6 at 298 K, and breakthrough experimental curves of equimolar C_3H_6/C_3H_8 mixtures at 298 K and 1 bar. Reprinted with permission from ref. 32. Copyright 2016 Science, ref. 65. Copyright 2021 Springer Nature Limited, ref. 27. Copyright 2023 American Chemical Society, ref. 74. Copyright 2024 Springer Nature Limited, ref. 37. Copyright 2023 American Chemical Society, ref. 33. Copyright 2024 Science, respectively.

NTU-85-WNT, characterized by localized dynamics of a water nanotube within a rigid framework, exhibited rapid C_3H_6 uptake within the initial pressure range, and reached 20.9 mL mL^{-1}.[37] Conversely, C_3H_8 uptake was observed to be negligible (0.13 mL mL^{-1}). The clear cut-off adsorption yields an extremely high adsorption selectivity of 1570 at 298 K and 1 bar. This sieving phenomenon is very similar to that of the rigid separator of KAUST-1, but the underlying mechanism is totally different. Breakthrough experiments substantiated the exclusive adsorption of C_3H_6 by NTU-85-WNT, with C_3H_8 eluting out of the packed column initially. The confined effect of the water nanotube enables the harvesting of adsorbed C_3H_6 at the desorption stage with a high purity of 98.8%. However, the lower porosity of the water nanotube limits the C_3H_6 productivity (1.6 mL mL^{-1}) at a certain content (Fig. 17e).

The same group developed a new concept of delicate softness in a temperature-responsive MOF (NTU-68) for efficient separation of C_3H_6/C_3H_8 in the next year.[40] Quantitatively, NTU-68

© 2025 The Author(s). Published by the Royal Society of Chemistry

Open Access Article. Published on 02 June 2025. Downloaded on 5/21/2026 10:40:29 PM. This article is licensed under a Creative Commons Attribution-NonCommercial 3.0 Unported Licence.

exhibited a pronounced uptake of C_3H_6 (33.3 $cm^3\ g^{-1}$ at 298 K) at 2 kPa, which exceeds the total uptake of KAUST-7 at 1 bar. The calculated density of C_3H_6 is as high as 565.9 mL mL^{-1}, closely approaching the density of liquid C_3H_6 (606 mL mL^{-1}). In contrast, the MOF exhibited a markedly lower C_3H_8 uptake (7.5 $cm^3\ g^{-1}$) at 298 K and 1 bar. As illustrated by the changing trend (in the temperature range of 273 to 323 K), the temperature-responsive delicate softness around the channel neck results in a thermodynamic preferred C_3H_6 adsorption (the higher the temperature, the lower the uptake), but a kinetic dominated C_3H_8 uptake (the higher the temperature, the higher the uptake). Consequently, the breakthrough separation efficiency of this mixture was found to be twofold enhanced upon increasing the temperature from 273 to 298 K. Notably, the separation process remained unaffected by the presence of general impurities.

The ftw-type MOFs consisting of a hexanuclear cluster M6 (M = Zr^{4+}, Hf^{4+}, Ce^{4+}, Y^{3+}) and a four-coordination linker have potential for molecular sieving due to the large cage-like cavities interconnected by narrow windows. For example, the iso-configurational MOFs ftw-MOF-ABTC and HIAM-301 both exhibit excellent molecular sieving in the separation of C_3H_6/C_3H_8 mixtures, but the mechanisms of separation are different.[64,126] The MOF-ABTC achieves molecular sieving by adjusting the length of the ligand only to change the window size and thus its pore size. In contrast, HIAM-301 has a highly distorted pore due to the inconsistency of the plane created by the mutual rotation of the octahedra and the large aspect ratio of the H_4eddi linker; in addition, the use of Y_6 clusters instead of Zr_6 clusters changes the framework from electrically neutral to an anionic framework and the presence of counterions in the cavities provides additional pore size modulation. The two synergistically regulate the pore size of HIAM-301 to achieve efficient sieving of C_3H_6/C_3H_8. In terms of separation performance, HIAM-301 showed better separation performance compared to ftw-MOF-ABTC, with 3.16 mmol g^{-1} adsorption for C_3H_6 and negligible adsorption for C_3H_8 (<0.3 mmol g^{-1}) at 298 K and 1 bar, enabling the complete separation of C_3H_6 and C_3H_8. Breakthrough experiments at room temperature also showed that the dynamic adsorption capacity of HIAM-301 for C_3H_6 is 46.4 $cm^3\ g^{-1}$, which enabled the production of polymer-grade C_3H_6. The single-component adsorption curves and breakthrough experiments of ftw-MOF-ABTC showed that the differences in adsorption amounts of ftw-MOF-ABTC for C_3H_6 and C_3H_8 are not significant (2.3 mmol g^{-1}, 2.46 mmol g^{-1}), but the adsorption kinetics of C_3H_6 is faster than that of C_3H_8 under the low-pressure condition, so that C_3H_6/C_3H_8 is effectively separated in the breakthrough experiment (Fig. 18a and b). Furthermore, we also compared the top ten C_3H_6/C_3H_8 adsorption ratios, as shown in Fig. 16b, where NTU-85-WNT reaches an adsorption ratio of 160, which has the potential to completely separate the C_3H_6/C_3H_8 mixture.[37] This summary provides a reference for efficient light hydrocarbon separation.

In addition, other MOFs, such as ZJU-75, MAF-23-O, Y-abtc, and Co-MOF-74, have been observed to exhibit preferential adsorption of C_3H_8 from mixtures containing C_3H_6.[6,22,88,90] However, due to the closed separation mechanism discussed above, we will not discuss them further.

3.3.2 C_3H_4($CH_3C{\equiv}CH$)/C_3H_6/C_3H_8 feed gas. The purification of C_3H_6 from ternary or quaternary C3 hydrocarbons has been considered as the most challenging process in gas separation.[127] To recognize the extremely small molecular difference, we developed a group of soft PCPs (NTU-65-FeZr, NTU-65-FeTi, NTU-65-CoZr and NTU-65-CoTi)[51] on the basis of a global soft framework of NTU-65 that has a Cu^{2+} node and electronegative site of a SiF_6^{2-} anion. The changed strength of the coordination bonds, derived from the changed metal node and the multiple sites, endowed the framework with the capacity to show a system structure response: from solely the C_3H_4 response at 17.1 kPa in NTU-65-FeZr to the sequential response

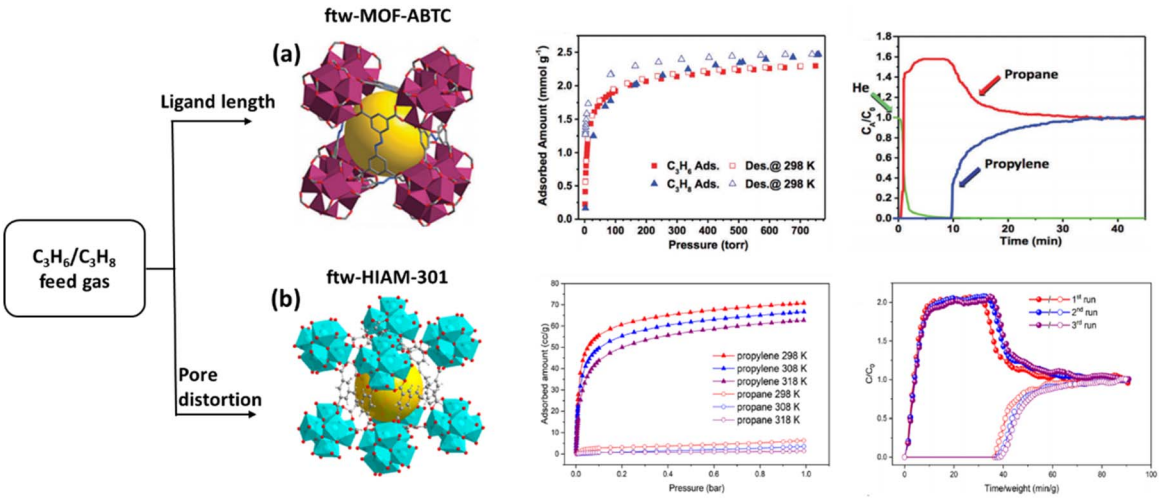

Fig. 18 (a)The crystal structure of ftw-MOF-ABTC, adsorption isotherms for pure C_3H_8 and C_3H_6 at 298 K, and breakthrough experimental curves of equimolar C_3H_6/C_3H_8 mixtures at 298 K. (b) The crystal structure of ftw-HIAM-301, adsorption isotherms for pure C_3H_8 and C_3H_6 at different temperatures, and breakthrough experimental curves of equimolar C_3H_6/C_3H_8 mixtures at room temperature. Reprinted with permission from ref. 126. Copyright 2018. The Royal Society of Chemistry, ref. 64. Copyright 2021 American Chemical Society, respectively.

Open Access Article. Published on 02 June 2025. Downloaded on 5/21/2026 10:40:29 PM. This article is licensed under a Creative Commons Attribution-NonCommercial 3.0 Unported Licence.

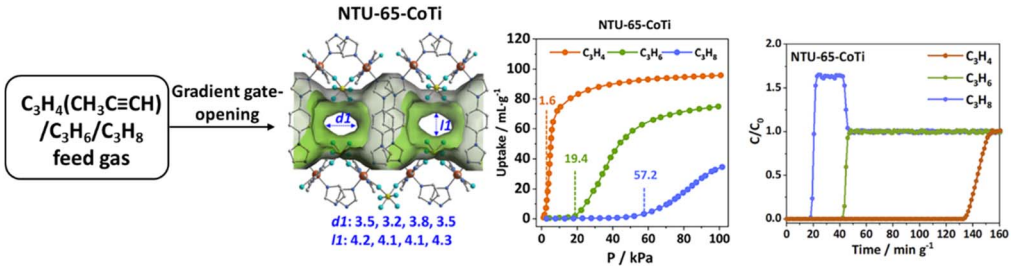

Fig. 19 The crystal structure of NTU-65-CoTi, adsorption isotherms for C_3H_4, C_3H_6 and C_3H_8 at 273 K, and breakthrough experimental curves of C_3H_6/C_3H_8 (0.5/49.75/49.75, v/v/v, 2 mL min^{-1}) mixtures at 273 K. Reprinted with permission from ref. 51. Copyright 2024 The Royal Society of Chemistry.

of C_3H_4 at 1.6 kPa, C_3H_6 response at 19.4 kPa and finally C_3H_8 at 57.2 kPa in NTU-65-CoTi at 273 K. Therefore, such unprecedented gradient structural-response driven NTU-65-CoTi is capable of separating $C_3H_4/C_3H_6/C_3H_8$ (0.5/49.75/49.75, v/v/v, 2 mL min^{-1}) mixtures. Based on breakthrough results, two beds were connected for the adsorption cycle. From bed B, C_3H_6 with a purity of 99.5% can be harvested at the desorption stage, while C_3H_8 with highly purity can be obtained at the adsorption stage (Fig. 19).

3.4 C_3H_6 harvesting from the adsorption process

3.4.1 C_3H_4 ($CH_3C{\equiv}CH$ and/or $CH_2{=}C{=}CH_2$)/C_3H_6 feed gas. To remove the trace amount of C_3H_4 from C_3H_6, a stronger host–C_3H_4 interaction is imperative. This is necessary to ensure that C_3H_6, in its highly pure state, can be effectively harvested from the adsorption process. Typically, ZNU-2, an ultra-stable MOF with cage-like pores (decorated with TiF_6^{2-} anions) interconnected with each other by contracted necks, has been reported for selective C_3H_4 capture from C_3H_4/C_3H_6 mixtures. Single gas adsorption isotherms revealed that ZNU-2 demonstrated both high C_3H_4 uptake at 0.01 bar (3.9 mmol g^{-1}) and 1 bar (7.7 mmol g^{-1}) at 298 K, while the uptake of C_3H_6 reached 0.61 and 5.3 mmol g^{-1}, respectively. Therefore, with the combination of a C_3H_4/C_3H_6 selectivity (1/99, v/v) of 12.5, the separation potential, a concept developed by Krishina, of ZNU-2 is as high as 31.0 mmol g^{-1}, the maximum value among the

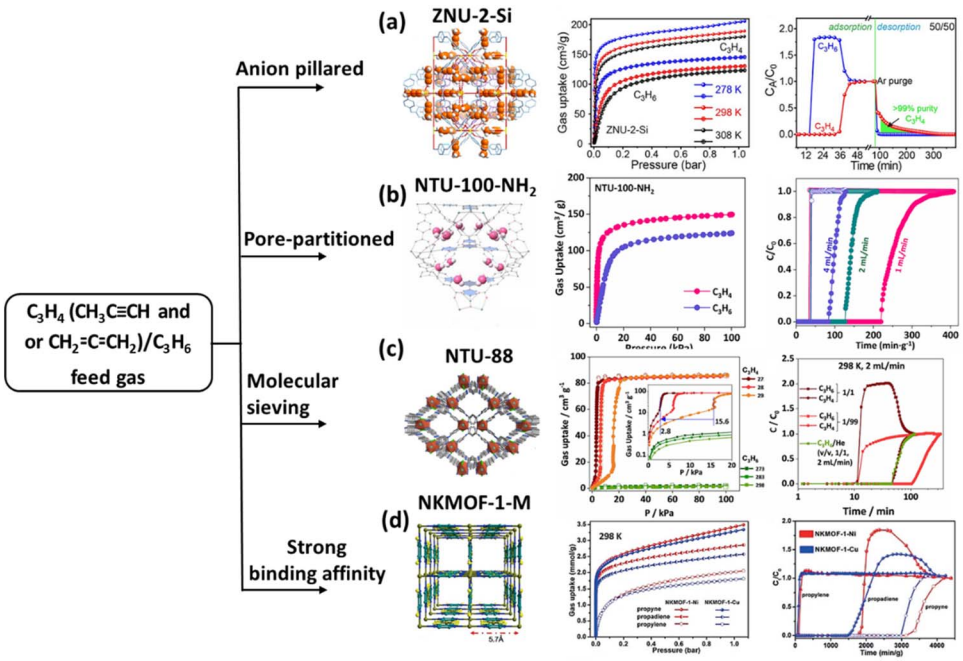

Fig. 20 (a) The crystal structure of C_3H_4 loaded ZNU-2-Si, C_3H_4 and C_3H_6 adsorption isotherms for ZNU-2-Si at 278, 298 and 308 K, and breakthrough experimental curves of equimolar $C_3H_4/C_3H_6/C_3H_8$ mixtures at 298 K. (b) The crystal structure of NTU-100-NH_2, C_3H_4 and C_3H_6 adsorption isotherms for ZNU-2-Si at 278, 298 and 308 K, and breakthrough experimental curves of equimolar C_3H_4/C_3H_6 mixtures at different inlet rates at 298 K. (c) The crystal structure of NTU-88, adsorption isotherms for C_3H_4 and C_3H_6 at different temperatures, and breakthrough curves of NTU-88 for C_3H_4/C_3H_6 and C_3H_4/He at 298 K. (d) The 3D structure of NKMOF-1-M (M = Ni or Cu), adsorption isotherms for C_3H_4, $CH_2{=}C{=}CH_2$ and C_3H_6 and breakthrough experimental curves of C_3H_4, $CH_2{=}C{=}CH_2$ and C_3H_6 (0.5/0.5/99, v/v/v) mixtures at 298 K. Reprinted with permission from ref. 128. Copyright 2023 The Royal Society of Chemistry, ref. 84. Copyright 2024 John Wiley & Sons, ref. 69. Copyright 2023 John Wiley & Sons, ref. 52. Copyright 2019 John Wiley & Sons, respectively.

© 2025 The Author(s). Published by the Royal Society of Chemistry

Open Access Article. Published on 02 June 2025. Downloaded on 5/21/2026 10:40:29 PM.
This article is licensed under a Creative Commons Attribution-NonCommercial 3.0 Unported Licence.

MOFs. After the introduction of the C_3H_4/C_3H_6 (1/99, v/v) feed gas into the packed column, pure C_3H_6 broke out at first, while C_3H_4 was detected about 150 min later. The clear separation interval indicates a productivity of C_3H_6 of 42.0 mol kg^{-1}. Similarly, an anionic pillared caged MOF, ZNU-2-M (M = Si, Ti, Nb) was also developed for light hydrocarbon separations (Fig. 20a).[128]

NTU-100-NH_2, a highly porous MOF, possesses densely decorated NH_2 sites within its framework, resulting in a strong interaction with C_3H_4. This interaction enables a remarkable uptake capacity of up to 84.5 cm^3 g^{-1} at 1 kPa and 298 K, which is almost two times higher than that of NTU-100-NO_2, the same framework with decorated NO_2.[84] Furthermore, NTU-100-NH_2 exhibited significantly improved adsorptive selectivity (1.4 to 11.3) and diffusion selectivity (0.13 to 3.15). Therefore, NTU-100-NH_2 has been shown to possess the capacity to remove trace amounts of C_3H_4 from C_3H_4/C_3H_6 (1/99, v/v) mixtures at room temperature, while also being capable of producing polymer-grade C_3H_6 directly. Further breakthrough experiments revealed that the productivity of pure C_3H_6 remained almost unchanged at different sweep rates (1, 2, and 4 mL min^{-1}) even with wet feed gas (Fig. 20b).

The phenomenon of co-adsorption has been frequently observed in the context of adsorption separation mechanisms that are reliant upon the interaction between the host and guest molecules. NTU-88, the framework with rotational pyridyl rings that was reported by us, exhibited sieving separation of C_3H_4/C_3H_6.[69] At 298 K, a two-step C_3H_4 adsorption process, with a steep increase occurring at 15.6 kPa and a maximum uptake of 86.0 cm^3 g^{-1} was observed. Furthermore, the shutter rotating pressure was observed to shift to a very low value of 2.9 kPa at 273 K. However, the total uptake remained constant within the temperate range of 273 to 328 K. In contrast, negligible C_3H_6 uptake was observed in NTU-88 within these wide temperature ranges. The observation of nearly the same elution times for C_3H_4/He and C_3H_4/C_3H_6 in the dynamic separation process indicates that the co-adsorption of C_3H_4 and C_3H_6 was strongly restricted in NTU-88. Furthermore, breakthrough experiments demonstrated that NTU-88 has excellent ability for selective capture of C_3H_4 from C_3H_4/C_3H_6 mixtures, yielding highly-pure C_3H_6 with a productivity of 4.10 mmol g^{-1} at 273 K. Notably, this MOF can be scale-up synthesized *via* room temperature stirring of the related reagents in methanol in a very short time (Fig. 20c).

NKMOF-1-M (M = Cu or Ni) displayed the preferred adsorption of trace C_3H_4 from C_3H_6. Both MOFs demonstrated high adsorption of C_3H_4, including $CH_3C{\equiv}CH$ and $CH_2{=}C{=}CH_2$ (over 3.0 mmol g^{-1} at 298 K, 1 bar), which is considerably higher than that of C_3H_6 (over 1.8 mmol g^{-1}). Importantly, the steep curves observed at pressures below 1 kPa, across a wide temperature range, indicated strong binding affinity for C_3H_4. Therefore, their adsorption selectivity is very high, over 100. Breakthrough experiments showed that NKMOF-1-Ni can selectively capture trace amounts of C_3H_4, yielding highly pure C_3H_6 (99.996%, 230 mmol L^{-1}) from the feed gas of $CH_3C{\equiv}CH/CH_2{=}C{=}CH_2/C_3H_6$ (0.5/0.5/99) mixtures at room temperature. A similar phenomenon has been observed in ultra-microporous MOF-NKMOF-M (Fig. 20d).[52]

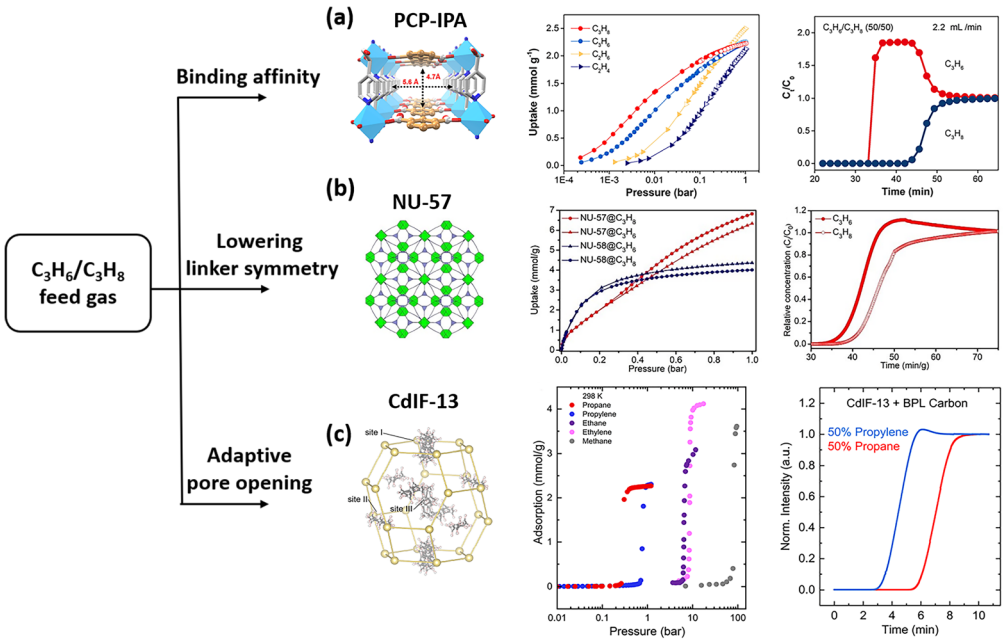

Fig. 21 (a) The 3D structure of PCP-IPA, the adsorption isotherms of different light hydrocarbons at 298 K, and breakthrough experimental curves of equimolar C_3H_6/C_3H_8 mixtures at 298 K and 1 bar. (b) The structure of NU-57, the adsorption isotherms of C_3H_6 and C_3H_8 for NU-57 and NU-58, and breakthrough experimental curves of equimolar C_3H_6/C_3H_8 mixtures at 298 K. (c) The crystal structure of C_3H_8 loaded CdIF-13, adsorption isotherms for C_3H_6 and C_3H_8 at 298 K, and breakthrough experimental curves of equimolar C_3H_6/C_3H_8 mixtures at 298 K and 1 bar. Reprinted with permission from ref. 129. Copyright 2022 Springer Nature Limited, ref. 130. Copyright 2025 John Wiley & Sons, ref. 43. Copyright 2023 American Chemical Society, respectively.

Open Access Article. Published on 02 June 2025. Downloaded on 5/21/2026 10:40:29 PM.
This article is licensed under a Creative Commons Attribution-NonCommercial 3.0 Unported Licence.

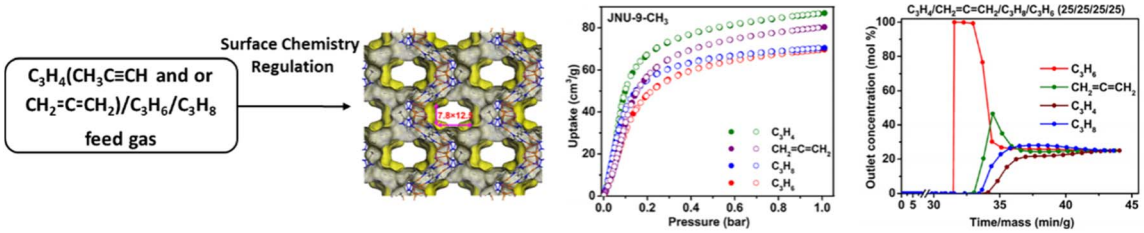

Fig. 22 The crystal structure of JNU-9-CH_3, adsorption isotherms for C_3H_4, CH_2=C=CH_2, C_3H_6 and C_3H_8 at 298 K, and breakthrough experimental curves of C_3H_4, CH_2=C=CH_2, C_3H_6 and C_3H_8 (25/25/25/25, v/v/v) mixtures at 298 K. Reprinted with permission from ref. 60. Copyright 2024 American Chemical Society.

3.4.2 C_3H_6/C_3H_8 feed gas. Selective alkane trapping has been considered as an energy-saving method for olefin purification. Featuring parallelly aligned and extended isophthalic acids, serving as a paraffin nano-trap, PCP-IPA has been investigated for selective C_3H_8 capture for harvesting high-purity C_3H_6 directly.[129] Due to the rigidity of the framework, type-I C_3H_6 and C_3H_8 adsorption isotherms were observed. C_3H_8 uptake was always higher than that of C_3H_6 in the pressure range of 0–1 bar. Thereby, the calculated selectivity of C_3H_8/C_3H_6 (1/1, v/v) was determined to be 2.48, at 298 K and 1 bar, including a separation potential of 1.2 mol L^{-1}. Breakthrough results (C_3H_8/C_3H_6: 1/1, v/v) confirmed the separation ability under dynamic conditions, that is highly-pure C_3H_6 broke the column at 34.8 min, while C_3H_8 eluted out at 43.9 min. The productivity of C_3H_6 (99.99%) was 15.23 L kg^{-1} (Fig. 21a).

A desymmetrization approach was utilised in the preparation of NU-57, which realized inversion C_3H_8/C_3H_6 separation. The maximum C_3H_8 uptake of NU-57 was found to be superior to that of C_3H_6, despite the adsorption isotherms of C_3H_8 and C_3H_6 demonstrating almost complete overlap in the low-pressure region.[130] In addition, the Q_{st} values of NU-57 for C_3H_8 and C_3H_6 were 33.0 kJ mol^{-1} and 28.5 kJ mol^{-1}, respectively, suggesting a stronger interaction between the framework and C_3H_8 molecules than C_3H_6 molecules. Harvesting of pure C_3H_6 from C_3H_8-containing mixtures was confirmed by breakthrough experiments. A similar approach was adopted in Cu-ASY,[131] a new MOF that incorporates infinite Cu-carboxylate rods which can separate C_3H_8/C_3H_6 mixtures with a C_3H_6 productivity of 2.2 L kg^{-1} (Fig. 21b).

In addition to the aforementioned rigid frameworks, which have been demonstrated to be capable of performing inversion C_3H_8/C_3H_6 separation, a soft framework has also been shown to be effective for this task. CdIF-13, prepared from Cd^{2+} and benzimidazolate, exhibited guest-induced structural changes.[43] At 298 K, step-shaped C_3H_8 adsorption isotherms revealed that gate opening of CdIF-13 occurred at 0.3 bar, which is far earlier than that of C_3H_6 (0.8 bar). Comparatively, the isostructural ZIF-7 displayed a very small difference in gate-opening pressure of C_3H_8 (0.008 bar) and C_3H_6 (0.020 bar) at 298 K. Therefore, highly pure C_3H_6 was harvested by using a double column packed with CdIF-13 and BPL carbon from equimolar C_3H_8/C_3H_6 feed gas (Fig. 21c).

3.4.3 C_3H_4(CH_3C≡CH and or CH_2=C=CH_2)/C_3H_6/C_3H_8 feed gas. The purification of C_3H_6 from four-component mixtures (C_3H_4/CH_2=C=$CH_2/C_3H_6/C_3H_8$) represents the most challenging process in light hydrocarbon separations. JNU-9-CH_3, a hydrolytically stable Cu_4I_4-triazolate MOF with a spatial distribution of polar and nonpolar sites, was designed.[60] The densely packed and readily accessible iodine and nitrogen sites in the 1D channel allowed JNU-9-CH_3 to show the single gas uptakes in a sequence of C_3H_8 > CH_3C≡CH > CH_2=C=CH_2 > C_3H_6. The calculated selectivity of the C_3H_8/C_3H_6 (1/1, v/v) mixture is 1.5 at 298 K and 1 bar, while the selectivities of CH_3C≡CH/C_3H_6 (1/1, v/v) and CH_2=C=CH_2/C_3H_6 (1/1, v/v) are 2.1 and 1.3, respectively. Breakthrough experiments showed that JNU-9-CH_3 is able to separate such equimolar quaternary hydrocarbons, yielding highly pure C_3H_6 of 102.7 mmol L^{-1} (Fig. 22). In addition, the velocity of the feed gas exerts minimal influence on the separation performance.

4. Large-scale synthesis

Since their first appearance, MOFs have undergone remarkable development and have demonstrated excellent performance in the field of gas separation. If MOFs with gas separation functions can be synthesized on a large scale, it will undoubtedly lead to a significant reduction in production costs and bring significant benefits for the application of MOFs in the market. Despite considerable efforts, only a few of the MOF products with unique structures and potential applications have been synthesized on a large scale. The synthesis of MOFs on a large scale is still challenging due to the high cost of some of the organic ligands and metal salts that are essential components in the synthesis of MOFs. Ensuring consistent quality and reproducibility, a key requirement for large-scale production, remains a formidable task. It is therefore widely recognised in the scientific community that the large-scale synthesis of MOFs should focus on the following key aspects. First, the material cost must be reduced, which can be achieved by exploring alternative raw materials or more efficient synthesis routes. Second, higher yields should be achieved to meet the growing demands of various industries. Thirdly, a relatively fast and simple synthesis process is highly desirable, which can increase production efficiency and reduce production time. Fourthly, the synthesis process should have less impact on the environment, in line with the principles of sustainable development.[142,143]

In addressing the complex issues hindering large-scale synthesis of MOFs, researchers have developed a range of

© 2025 The Author(s). Published by the Royal Society of Chemistry

Open Access Article. Published on 02 June 2025. Downloaded on 5/21/2026 10:40:29 PM. This article is licensed under a Creative Commons Attribution-NonCommercial 3.0 Unported Licence.

Table 6 Advantages and drawbacks of common synthesis methods

Methods	Pros.	Cons.
Room temperature stirring	Green, simple, and low energy	Not universally applicable for MOF preparation
Mechanochemistry	Environmental friendly, simple, and low-cost	Damaged material and high impurity content
Solvothermal	Simple	Long-reaction-cycle High cost of the reactor
Flow chemistry	High-yield production with excellent batch consistency	Clog-prone piping
Electrochemistry	High purity	A relatively high cost

methods, including room-temperature stirring, solvothermal, mechanochemical synthesis, continuous flow production and electrochemical which have been explored with the aim of improving production efficiency.[144–147] These large-scale synthesis methods have their own advantages and shortcomings, which are detailed in Table 6. The employment of such methodologies has yielded encouraging outcomes with regard to enhancing the efficiency of the production process. In the context of MOF production, it is imperative to give due consideration to both extrinsic and intrinsic factors. Poor management of these factors can lead to increased costs in the production process, which is a significant concern for both academic research and industrial applications. Despite the difficulties in large-scale production of MOFs, companies such as BASF, Framergy, Nuada or MOF apps are now able to produce a range of MOFs. MIL-100 (Fe), UiO-66 (Zr), Al-fum MOF, ZIF-8, ZIF-67, HKUST-1, PCN-250 (Fe) or MIL-127 (Fe) can be produced on a kilogram scale.[148] CALF-20, a MOF material that can efficiently capture CO_2, in the presence of moisture after combustion,[149] is now being produced by BASF on a multi-ton scale. The success of large-scale synthesis of these examples has shed light on the large-scale synthesis of MOFs (Fig. 23).

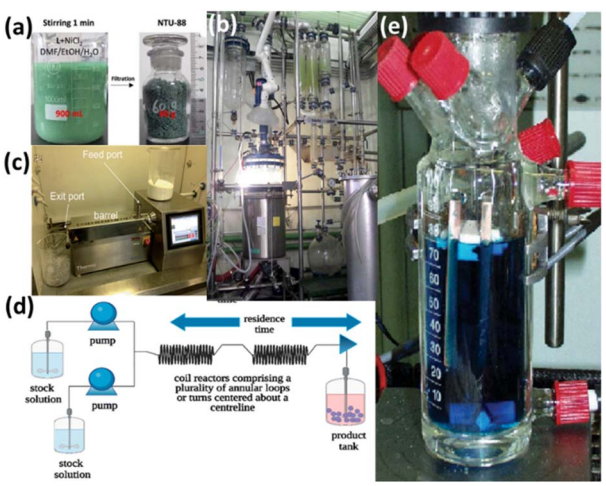

Fig. 23 (a) Large-scale preparation of NTU-88 *via* room temperature stirring. (b) Large-scale preparation of Uio-66 using solvothermal methods. (c) Key components of the twin-screw extruder. (d) Demonstration of the continuous flow method for synthesizing MOFs. (e) Synthesis of MOFs using Cu as the electrode material by the electrochemical synthesis method. Reprinted with permission from ref. 69. Copyright 2023 John Wiley & Sons, ref. 162. Copyright 2015 Elsevier, ref. 152. Copyright 2015 The Royal Society of Chemistry, ref. 163. Copyright 2022 The Royal Society of Chemistry, ref. 164. 2006. Copyright The Royal Society of Chemistry, respectively.

4.1 Room-temperature stirring

As an alternative fast and simple method, room-temperature stirring has been a well-established for material synthesis in laboratory and industry, due to its significant advantages of cost-effectiveness, safety, scalability, versatility, simple operation, and almost negligible energy consumption. For MOF synthesis, the main procedure involves the dissolution of suitable organic ligands and metal salts separately in appropriate solvents, followed by the gradual pouring of one of the above solutions into another under stirring conditions, or the simultaneous pouring of both solutions into a third vessel. The gentle nature of this method renders it less likely to result in the rapid precipitation of reactants, thus necessitating extended periods to achieve complete crystallisation at room temperature in comparison to methods conducted at elevated temperatures. The incorporation of reaction promoters, such as formic acid, acetic acid, triethylamine, or ammonia water, has been demonstrated to effectively modulate the reaction rate. It is also crucial to ensure the homogeneity of the mixture throughout the reaction vessel to avoid the formation of undesirable particles due to localised supersaturation.

NKMOF-8-Br and NKMOF-8-Me, which possess excellent separation performance for C_2H_6/C_2H_4, can be efficiently prepared through room temperature stirring of ligands, CuI, and triethylamine (TEA) in acetonitrile at room temperature within 3 minutes. Both MOFs have high yields (>90%). Notably, the acetonitrile solution can be readily recycled through filtration and then reused in the following reaction cycles without the need for further purification.[150] We have recently achieved large-scale synthesis of a series of light hydrocarbon separators, including NTU-88 (60.0 g, stirring in 1 min) and NTU-101-NH_2 (50.5 g, 5 min stirring) *via* room temperature stirring of N containing ligands and Cu^{2+} or Ni^{2+}.[62,69] For them, ammonia or triethylamine was gently added into the stirring system. Meanwhile, a MOF of CeBTB (H_3BTB: 1,3,5-Tri(4-carboxyphenyl) benzene) with a carboxylate ligand can also be synthesized by such a method.[151] Differently, the promoter 1-methylimidazole was used to regulate the deprotonation ability of H_3BTB. CeBTB (uniform size of 150 nm) can be conveniently prepared in a 1 L beaker. As a C_3H_6/C_3H_8 separator, ZJU-75 can

Open Access Article. Published on 02 June 2025. Downloaded on 5/21/2026 10:40:29 PM. This article is licensed under a Creative Commons Attribution-NonCommercial 3.0 Unported Licence.

also be readily scaled up through room temperature stirring of $K_2[Ni(CN)_4]\cdot nH_2O$ pyz-NH_2 and $Co(NO_3)_2\cdot 6H_2O$ in water/ethanol solution.[90] Further kilogram-scale synthesis has also been achieved in this case, giving a high yield of 75% within 8 hours. The calculated space-time yield was found to be 158 kg per m^3 per day. It is interesting that MOF-303 can be prepared in water as the sole solvent and can be readily scaled up to the kilogram level with a yield of up to 93%, but a reflux reaction apparatus is required.[123]

4.2 Mechanochemical synthesis

The concept of mechanochemistry is regarded as one of the important innovations that have had a profound impact on the world.[152] The application of mechanical forces can break the intramolecular bonds between reactants, thereby facilitating the formation of new bonds. This process is accompanied by the transformation of mechanical energy into thermal energy through the process of heating.[153] The mechanochemical synthesis has been shown to be solvent-free or to require only a minimal amount of solvent, thereby minimising its environmental impact. Furthermore, mechanochemistry has been demonstrated to exhibit advantages over the above-mentioned strategies, including reduced reaction times and enhanced efficiency.[154–156] This characteristic is of particular significance for poorly soluble metal precursors or ligands, as it circumvents the issues associated with solubility whilst concomitantly minimizing environmental damage. By reducing the reliance on solvents, there is the potential to substantially reduce production costs, a highly desirable outcome in both academic research and industrial production.

A mixture of dried copper acetate and isonicotinic acid was subjected to 10 minutes of milling, resulting in the formation of copper(II) isonicotinic acid and the trapping of acetic acid and water molecules within the pores of the resultant product.[157] Notwithstanding the potential of mechanical milling for the synthesis of MOFs, the majority of extant research has focused on gram-scale feeds. In order to find ways to scale-up this technique, a ThermoFisher Process-11 Twin Screw Extruder, a machine with a screw configuration of a sequence of alternating conveying and kneading zones, was used.[152] Through the feed port, the MOF precursor can be introduced into a heatable drum containing screws and the exit port can be connected to a mold for collecting the final material, yielding continuous synthesis of various metal complexes, including Ni(salen), $Ni(NCS)_2(PPh_3)_2$, HKUST-1, ZIF-8, and MAF-4 Al(fumarate)(OH). It is important to note that the space time yields for these methods are as high as 144×10^3 kg m^{-3} per day, which is significantly greater than the yields for other methods of MOF synthesis. Recent breakthroughs in mechanochemical synthesis have demonstrated the remarkable efficiency of a novel "cage-on-MOF" strategy, enabling the rapid preparation of 28 distinct MOF@PCC composites within just 5 min.[158] Particularly noteworthy is the exceptional performance of these materials, with MOF-808@PCC-4 showing dramatic enhancements in CO_2/C_2H_2 separation (exhibiting a 64% increase in C_2H_2 uptake capacity and 166% improvement in IAST selectivity in breakthrough tests), while MIL-101@PCC-4 achieved outstanding C_2H_2 adsorption reaching 6.11 mmol g^{-1} with an IAST selectivity of 2.59. This mechanochemical approach represents a significant advancement compared to conventional solution-based post-synthetic modification methods, which typically require time-consuming heating procedures and multiple purification steps. The "cage-on-MOF" methodology not only achieves gram-scale synthesis (up to 100 g batches) with near-quantitative yields, but also maintains excellent crystallinity and porosity control while completely eliminating organic solvent consumption-offering a synthesis efficiency approximately 300 times greater than that of traditional solution-phase methods while ensuring consistent material quality.

Although mechanochemistry has evident advantages, this strategy is not universally applicable as the generation of excessive mechanical energy may lead to the amorphization of MOFs and the subsequent decomposition and damage of the material.[159] In addition, the formation of new bonds is often inconsistent, leading to the production of various impurities that cannot be easily removed. Furthermore, mechanical synthesis is often not suitable for MOFs with high coordination numbers that require a relatively slow and well-controlled crystallization process.

4.3 Solvothermal and hydrothermal synthesis

In 1995, Nalco Chemical Company and the Yaghi group produced the first MOF materials using solvothermal synthesis. A certain proportion of organic ligands and metal salts are dissolved in different solvents, after which the solutions are mixed in a sealed reaction vessel, and then the nucleation and growth of crystals is promoted by heating.[160] This method is by far the most widely used method for producing MOF crystals in laboratories.[161]

However, there are significant limitations for the large-scale production of MOFs. In particular, increasing the size of the reaction vessel leads to a significant reduction in the surface-to-volume ratio, which further reduces the efficiency of the reaction, but also requires, for example, the use of hundreds of liters of solvent per batch. In addition, the reaction time is too long, given the high temperature and pressure involved. Finally, the cost of the pressure vessel, especially those for hundreds of liters, is very high.

4.4 Flow chemistry synthesis

Flow chemistry is a process in which the solutions of various components are passed through a reaction apparatus, leading to the occurrence of chemical reactions.[163,165,166] This process contrasts with traditional batch-reaction devices, in which different components are placed in separate vessels and react over time. Consequently, flow chemistry can be regulated precisely through parameter change and device design, thereby ensuring reproducibility of high-quality products. In the context of flow chemistry, the most salient benefit of this process is that the rapid separation of MOF crystals and related solvents facilitates the recycling of solvents. This, in turn, has a number

© 2025 The Author(s). Published by the Royal Society of Chemistry

Open Access Article. Published on 02 June 2025. Downloaded on 5/21/2026 10:40:29 PM. This article is licensed under a Creative Commons Attribution-NonCommercial 3.0 Unported Licence.

of significant benefits, such as environmental friendliness, capital investment and energy input (hot solvent will be transferred into the reactor in time).

The utilisation of both a stirred tank reactor and a plug flow reactor has become a widespread practice in the field of flow synthesis. For instance, a microwave-assisted flow chemistry method has been employed to synthesize UiO-66 with a significantly enhanced reaction rate when compared to conventional solvothermal synthesis.[162] In addition, MOF-5 with a space time yield of 0.1 ton per m^3 per day, has been synthesised *via* a flow chemistry method.[167] After optimization, the flow system, operated at 140 °C and residence time ≥5.5 h, reached a steady state that can continuously produce high surface area MOF-5. In other words, parameter optimization in flow chemistry plays an important role in the manufacture of MOFs with controlled quality.

Following the modification of the heating reactor to incorporate a microwave-assisted heating reactor, a notable enhancement in the rate of MOF growth, accompanied by excellent reproducibility, has been observed in the case of MOF-74(Ni).[168] The raw materials of MOF-74(Ni) were introduced into a microwave reactor to facilitate initial nucleation. The solution was subsequently introduced into a reactor for a duration of 8 minutes to complete the growth of the crystals. This process resulted in enhanced crystallinity, accompanied by a space time yield of 2160 kg per m^3 per day. Using a similar system, UiO-66, HKUST-1 and MIL-53(Al) were obtained in 7, 1 and 4 minutes of residence time, resulting in high space time yields of 7204 kg per m^3 per day, 64 800 kg per m^3 per day and 3618 kg per m^3 per day, respectively.[146] In such a system, the separation of the nucleation and growth steps has been shown to accelerate the reaction rate and ensure the quality of the resulting MOFs.

However, it was also noted that the flow chemistry synthesis suffers from a problem of reactor/pipeline fouling and clogging. During the reaction process, precipitates are often generated, and the clogging caused by these precipitates can accumulate in the system. As a consequence, the efficiency and quality of the product are affected. In order to address this issue, it is imperative to implement regular cleaning procedures or to undertake a redesign of the reactor components, such as the introduction of a match screw inside the tube, in order to maintain the functionality of the flow system.

4.5 Electrochemical synthesis

In comparison with the conventional solvothermal synthesis method, the electrochemical synthesis has milder reaction conditions, a significantly reduced reaction time, and the process of MOF synthesis can be regulated by modulating the voltage.[148] With regard to electrochemical synthesis, the methods can be categorised into three distinct classifications depending on the direction of electron transfer and the location where the nucleation process occurs: (1) surface electrode nucleation, including anodic dissolution and cathodic deposition, (2) indirect bipolar electrodeposition and (3) electrophoretic deposition.[169] The researchers in PASF immersed a copper plate as an anode into an organic solution containing 1,3,5-benzenetricarboxylic acid. When a specific current was applied, Cu ions were transferred from the surface of the anode to the solution and reacted with the organic linker in the solution, ultimately producing an octahedral powder of HKUST-1. Notably, the surface area of the electrochemical synthesis material is 1820 $m^2\ g^{-1}$, which is larger than that of HKUST-1 synthesised by the solvothermal method (1550 $m^2\ g^{-1}$). Recently, a mechanism for the anodic solvation synthesis of HKUST-1 was proposed, which consists of initial nucleation; growth of HKUST-1 islands; intergrowth; and crystal detachment.[170]

Despite the advances achieved thus far, numerous challenges have been encountered when attempting to realise large-scale production. Initially, a large-scale electrochemical synthesis device is required; however, this task involves complex issues. For example, the electrodes must be uniformly arranged over a large area, and the circulation and stirring of the electrolyte must be well-controlled, which pose significant technical difficulties. Furthermore, when reaction control is considered during large-scale synthesis, ensuring the homogeneity of parameters such as electric field, temperature, and electrolyte concentration throughout the entire reaction system is extremely challenging, as doing so would produce products of unstable quality and poor consistency.

In a word, room-temperature stirring is one of the most practical and effective methods for large-scale synthesis of MOFs, especially holding a unique position in the large-scale synthesis of MOFs for light hydrocarbon separation. Secondly, mechanochemical methods have emerged and shown potential in the large-scale synthesis of light hydrocarbon separation MOFs. Although solvothermal, electrochemical and flow chemistry methods have made some progress in the large-scale synthesis of some MOFs, they still need to be studied more in the large-scale synthesis of light hydrocarbon separation MOFs. It is believed that in the near future, in terms of light hydrocarbon separation, the large-scale production methods are more diversified, the industrialization conditions will be more mature, and the large-scale production of high-efficiency, low-cost and sustainable high-quality light hydrocarbon separation MOFs will be realized. It is encouraging to see that companies like BASF are already striving for excellence and have achieved exciting results in the large-scale production of MOFs. It is encouraging that companies like BASF are already pursuing excellence and achieving exciting results in the large-scale production of MOFs. It is expected that this trend will continue, leading to significant progress in the large-scale production and application of MOFs not only in light hydrocarbon separation but even in other areas.

5. Conclusion and outlook

The development of high-performance MOFs for light hydrocarbon separation has witnessed remarkable progress, driven by innovative design strategies and engineering advancements. Rigid MOFs, functionalized with tailored binding sites, enable selective guest interactions through precise control of pore environments, while flexible MOFs leverage dynamic structural

Open Access Article. Published on 02 June 2025. Downloaded on 5/21/2026 10:40:29 PM. This article is licensed under a Creative Commons Attribution-NonCommercial 3.0 Unported Licence.

responses under external stimuli to achieve molecular recognition. These advancements, coupled with emerging scale-up synthesis techniques, underscore the potential of MOFs to revolutionize industrial separation processes. However, critical challenges remain in achieving cost-effective, one-step separation processes, precise material design for specific applications, and scalable production. Addressing these challenges will require interdisciplinary collaboration and sustained innovation in both fundamental research and applied technologies.

To propel MOFs toward practical implementation in light hydrocarbon separation, future research should prioritize the following directions.

5.1 Pore aperture engineering

Precise control over pore size and geometry is essential for molecular sieving. While rigid MOFs allow tunability *via* ligand and metal node selection, flexible MOFs offer dynamic pore adjustment in response to guest molecules. Integrating computational tools—such as artificial intelligence (AI) and molecular simulations—will accelerate the prediction of optimal MOF architectures for target separations. These approaches can minimize trial-and-error experimentation and guide the design of frameworks with pore environments tailored to specific gas pairs.

5.2 Enhanced host–guest interactions

Synergistic integration of multiple interaction mechanisms (*e.g.*, van der Waals forces, open metal sites, hydrogen bonding, and π-complexation) within a single MOF can amplify selectivity. Future work should focus on multifunctional frameworks that combine complementary binding sites, such as Lewis acidic metal clusters and functionalized organic linkers, to enable multi-mechanism adsorption. Additionally, exploring stimuli-responsive systems (*e.g.*, light- or temperature-triggered structural changes) could further refine dynamic separation processes.

5.3 Elucidating mechanisms

A deeper understanding of the interplay between thermodynamic equilibria and kinetic diffusion is critical. Advanced characterization techniques (*e.g.*, *in situ* spectroscopy and *operando* diffraction) combined with molecular dynamics (MD) simulations can unravel molecular transport pathways and adsorption site competition. Investigating the nano-confinement effects within MOF pores may also reveal strategies to manipulate guest molecule behavior, particularly under industrially relevant high-temperature conditions.

5.4 Scalability and stability

Bridging the gap between laboratory synthesis and industrial deployment demands scalable, low-cost production methods. Room temperature stirring synthesis and solvent-free routes should be optimized to reduce energy consumption and material waste. Concurrently, improving MOF stability under harsh operational conditions (*e.g.*, moisture, high pressure, and thermal cycling) is imperative for long-term viability.

5.5 Interdisciplinary collaboration

Cross-disciplinary efforts integrating chemistry, materials science, chemical engineering, and data science will be vital to overcome existing barriers. Partnerships with industry can accelerate technology transfer, while open-access databases for MOF properties and performance metrics will streamline material discovery.

In conclusion, MOFs represent a transformative platform for light hydrocarbon separation, offering unprecedented control over molecular recognition and process efficiency. While challenges in design precision, stability, and scalability persist, the convergence of computational modeling, advanced synthesis, and mechanistic insights holds immense promise. By addressing these hurdles through targeted research and collaborative innovation, MOFs may soon transition from academic breakthroughs to industrial mainstays, ushering in a new era of sustainable and energy-efficient chemical separations.

Data availability

No primary research results, software or code have been included and no new data were generated or analysed as part of this review.

Author contributions

J. D. conceived the idea of this project. H. Z., J. T. and C. Y. collected literatures, wrote and revised the paper. All authors offered constructive comments on the manuscript.

Conflicts of interest

The authors declare no conflicts of interest.

Acknowledgements

We are thankful for the financial support from the National Natural Science Foundation of China (22171135 and 22471235), the Natural Science Foundation of Jiangsu Province (BK20231269), the Outstanding Graduate Student Innovation Project of Xinjiang University (51252500201) and the State Key Laboratory of Materials-Oriented Chemical Engineering (SKL-MCE-23A18).

References

1 D. S. Sholl and R. P. Lively, *Nature*, 2016, **532**, 435–437.
2 W. D. Fan, X. Wang, X. R. Zhang, X. P. Liu, Y. T. Wang, Z. X. Kang, F. N. Dai, B. Xu, R. M. Wang and D. F. Sun, *ACS Cent. Sci.*, 2019, **5**, 1261–1268.
3 G.-D. Wang, Y.-Z. Li, W.-J. Shi, L. Hou, Y.-Y. Wang and Z. Zhu, *Angew. Chem., Int. Ed.*, 2023, **62**, e202311654.

© 2025 The Author(s). Published by the Royal Society of Chemistry

Open Access Article. Published on 02 June 2025. Downloaded on 5/21/2026 10:40:29 PM. This article is licensed under a Creative Commons Attribution-NonCommercial 3.0 Unported Licence.

4 S. A. Chernyak, M. Corda, J. P. Dath, V. V. Ordomsky and A. Y. Khodakov, *Chem. Soc. Rev.*, 2022, **51**, 7994–8044.
5 P. Hu, J. L. Hu, H. Liu, H. Wang, J. Zhou, R. Krishna and H. B. Ji, *ACS Cent. Sci.*, 2022, **8**, 1159–1168.
6 H. Wang, X. Dong, V. Colombo, Q. Wang, Y. Liu, W. Liu, X.-L. Wang, X.-Y. Huang, D. M. Proserpio, A. Sironi, Y. Han and J. Li, *Adv. Mater.*, 2018, **30**, 1805088.
7 J. Q. Liu, Y. J. Liu, D. K. Talay, E. Calverley, M. Brayden and M. Martinez, *Carbon*, 2015, **85**, 201–211.
8 Q. Z. Xue, X. F. Li, X. Chang, C. C. Ling, L. Zhu and W. Xing, *Appl. Surf. Sci.*, 2018, **444**, 772–779.
9 Y. F. Yuan, Y. S. Wang, X. L. Zhang, W. C. Li, G. P. Hao, L. Han and A. H. Lu, *Angew. Chem., Int. Ed.*, 2021, **60**, 19063–19067.
10 Y. Chai, X. Han, W. Li, S. Liu, S. Yao, C. Wang, W. Shi, I. da-Silva, P. Manuel, Y. Cheng, L. D. Daemen, A. J. Ramirez-Cuesta, C. C. Tang, L. Jiang, S. Yang, N. Guan and L. Li, *Science*, 2020, **368**, 1002–1006.
11 J. G. Min, K. C. Kemp and S. B. Hong, *Sep. Purif. Technol.*, 2020, **250**, 117146.
12 H. Li, M. Eddaoudi, M. O'Keeffe and O. M. Yaghi, *Nature*, 1999, **402**, 276–279.
13 X. Wang, W. Lu, Z. Y. Gu, Z. Wei and H. C. Zhou, *Chem. Commun.*, 2016, **52**, 1926–1929.
14 K. S. Walton, *Nat. Chem.*, 2014, **6**, 277–278.
15 S. Krause, V. Bon, I. Senkovska, U. Stoeck, D. Wallacher, D. M. Tobbens, S. Zander, R. S. Pillai, G. Maurin, F. X. Coudert and S. Kaskel, *Nature*, 2016, **532**, 348–352.
16 S. H. Yang, X. Lin, W. Lewis, M. Suyetin, E. Bichoutskaia, J. E. Parker, C. C. Tang, D. R. Allan, P. J. Rizkallah, P. Hubberstey, N. R. Champness, K. M. Thomas, A. J. Blake and M. Schröder, *Nat. Mater.*, 2012, **11**, 710–716.
17 L. Wen, P. Cheng and W. B. Lin, *Chem. Sci.*, 2012, **3**, 2288–2292.
18 S. Kitagawa, R. Kitaura and S. Noro, *Angew. Chem., Int. Ed.*, 2004, **43**, 2334–2375.
19 H. Sato, W. Kosaka, R. Matsuda, A. Hori, Y. Hijikata, R. V. Belosludov, S. Sakaki, M. Takata and S. Kitagawa, *Science*, 2014, **343**, 167–170.
20 J. Duan, M. Higuchi, R. Krishna, T. Kiyonaga, Y. Tsutsumi, Y. Sato, Y. Kubota, M. Takata and S. Kitagawa, *Chem. Sci.*, 2014, **5**, 660–666.
21 Z.-J. Liang, F.-D. Dong, L. Ye, K. Zheng, D.-Y. Hu, X. Feng, W.-Y. Su, Z.-S. Wang, M.-Y. Zhou, Z.-L. Fang, D.-D. Zhou, J.-P. Zhang and X.-M. Chen, *Chem. Sci.*, 2025, **16**, 3307–3312.
22 Y. S. Bae, C. Y. Lee, K. C. Kim, O. K. Farha, P. Nickias, J. T. Hupp, S. T. Nguyen and R. Q. Snurr, *Angew. Chem., Int. Ed.*, 2012, **51**, 1857–1860.
23 Y.-L. Peng, T. Wang, C. Jin, C.-H. Deng, Y. Zhao, W. Liu, K. A. Forrest, R. Krishna, Y. Chen, T. Pham, B. Space, P. Cheng, M. J. Zaworotko and Z. Zhang, *Nat. Commun.*, 2021, **12**, 5768.
24 X. W. Gu, J. X. Wang, E. Y. Wu, H. Wu, W. Zhou, G. D. Qian, B. L. Chen and B. Li, *J. Am. Chem. Soc.*, 2022, **144**, 2614–2623.
25 Z. Z. Lu, H. G. W. Godfrey, I. da Silva, Y. Q. Cheng, M. Savage, P. Manuel, S. Rudic, A. J. Ramirez-Cuesta, S. H. Yang and M. Schroder, *Chem. Sci.*, 2018, **9**, 3401–3408.
26 S. Horike, Y. Inubushi, T. Hori, T. Fukushima and S. Kitagawa, *Chem. Sci.*, 2012, **3**, 116–120.
27 X. Huang, F. Chen, H. Sun, L. Yang, Q. Yang, Z. Zhang, Y. Yang, Q. Ren and Z. Bao, *J. Am. Chem. Soc.*, 2023, **146**, 617–626.
28 C.-X. Chen, Z.-W. Wei, T. Pham, P. C. Lan, L. Zhang, K. A. Forrest, S. Chen, A. M. Al-Enizi, A. Nafady, C.-Y. Su and S. Ma, *Angew. Chem., Int. Ed.*, 2021, **60**, 9680–9685.
29 H. Angewandte ChemieChen, B. Wang, B. Zhang, J. Chen, J. Gui, X. Shi, W. Yan, J. Li and L. Li, *Chem. Sci.*, 2023, **14**, 7068–7075.
30 Q. Min Wang, D. Shen, M. Bülow, M. Ling Lau, S. Deng, F. R. Fitch, N. O. Lemcoff and J. Semanscin, *Microporous Mesoporous Mater.*, 2002, **55**, 217–230.
31 E. D. Bloch, W. L. Queen, R. Krishna, J. M. Zadrozny, C. M. Brown and J. R. Long, *Science*, 2012, **335**, 1606–1610.
32 A. Cadiau, K. Adil, P. M. Bhatt, Y. Belmabkhout and M. Eddaoudi, *Science*, 2016, **353**, 137–140.
33 J. Cui, Z. Zhang, L. Yang, J. Hu, A. Jin, Z. Yang, Y. Zhao, B. Meng, Y. Zhou, J. Wang, Y. Su, J. Wang, X. Cui and H. Xing, *Science*, 2024, **383**, 179–183.
34 X. Cui, K. Chen, H. Xing, Q. Yang, R. Krishna, Z. Bao, H. Wu, W. Zhou, X. Dong, Y. Han, B. Li, Q. Ren, M. J. Zaworotko and B. Chen, *Science*, 2016, **353**, 141–144.
35 Q. Ding, Z. Zhang, C. Yu, P. Zhang, J. Wang, X. Cui, C.-H. He, S. Deng and H. Xing, *Sci. Adv.*, 2020, **6**, eaaz4322.
36 Q. Dong, Y. Huang, K. Hyeon-Deuk, I. Y. Chang, J. Wan, C. Chen, J. Duan, W. Jin and S. Kitagawa, *Adv. Funct. Mater.*, 2022, **32**, 2203745.
37 Q. Dong, Y. Huang, J. Wan, Z. Lu, Z. Wang, C. Gu, J. Duan and J. Bai, *J. Am. Chem. Soc.*, 2023, **145**, 8043–8051.
38 C. Gücüyener, J. van den Bergh, J. Gascon and F. Kapteijn, *J. Am. Chem. Soc.*, 2010, **132**, 17704–17706.
39 A. N. Hong, H. Yang, T. Li, Y. Wang, Y. Wang, X. Jia, A. Zhou, E. Kusumoputro, J. Li, X. Bu and P. Feng, *ACS Appl. Mater. Interfaces*, 2021, **13**, 52160–52166.
40 Y. Huang, J. Wan, T. Pan, K. Ge, Y. Guo, J. Duan, J. Bai, W. Jin and S. Kitagawa, *J. Am. Chem. Soc.*, 2023, **145**, 24425–24432.
41 Y. Jiang, J. Hu, L. Wang, W. Sun, N. Xu, R. Krishna, S. Duttwyler, X. Cui, H. Xing and Y. Zhang, *Angew. Chem., Int. Ed.*, 2022, **61**, e202200947.
42 J. Luo, G. Yang, G. Zhang, Z. Huang, J. Peng, Y. Luo, X. Wang, C. Yang, J. Jiang, D. Cao, B. Chen, H. Tang and J. Xiao, *Chem*, 2024, **10**, 3148–3158.
43 R. A. Klein, L. W. Bingel, A. Halder, M. Carter, B. A. Trump, E. D. Bloch, W. Zhou, K. S. Walton, C. M. Brown and C. M. McGuirk, *J. Am. Chem. Soc.*, 2023, **145**, 21955–21965.
44 B. Li, X. Cui, D. O'Nolan, H.-M. Wen, M. Jiang, R. Krishna, H. Wu, R.-B. Lin, Y.-S. Chen, D. Yuan, H. Xing, W. Zhou, Q. Ren, G. Qian, M. J. Zaworotko and B. Chen, *Adv. Mater.*, 2017, **29**, 1704210.
45 K. Li, D. H. Olson, J. Seidel, T. J. Emge, H. Gong, H. Zeng and J. Li, *J. Am. Chem. Soc.*, 2009, **131**, 10368–10369.

© 2025 The Author(s). Published by the Royal Society of Chemistry

Open Access Article. Published on 02 June 2025. Downloaded on 5/21/2026 10:40:29 PM. This article is licensed under a Creative Commons Attribution-NonCommercial 3.0 Unported Licence.

46 L. Li, R.-B. Lin, R. Krishna, H. Li, S. Xiang, H. Wu, J. Li, W. Zhou and B. Chen, *Science*, 2018, **362**, 443–446.
47 L. Li, R.-B. Lin, R. Krishna, X. Wang, B. Li, H. Wu, J. Li, W. Zhou and B. Chen, *J. Am. Chem. Soc.*, 2017, **139**, 7733–7736.
48 Y. Li, Y. Wu, J. Zhao, J. Duan and W. Jin, *Chem. Sci.*, 2024, **15**, 9318–9324.
49 P.-Q. Liao, W.-X. Zhang, J.-P. Zhang and X.-M. Chen, *Nat. Commun.*, 2015, **6**, 8697.
50 C. X. Zhao, X. Liu, J. N. Liu, J. Wang, X. Wan, C. Wang, X. Y. Li, J. Shui, L. Song, H. J. Peng, B. Q. Li and Q. Zhang, *Angew. Chem., Int. Ed.*, 2023, **135**, e202313028.
51 S. Liu, Y. Huang, J. Wan, J.-J. Zheng, R. Krishna, Y. Li, K. Ge, J. Tang and J. Duan, *Chem. Sci.*, 2024, **15**, 6583–6588.
52 Y. L. Peng, C. He, T. Pham, T. Wang, P. Li, R. Krishna, K. A. Forrest, A. Hogan, S. Suepaul, B. Space, M. Fang, Y. Chen, M. J. Zaworotko, J. Li, L. Li, Z. Zhang, P. Cheng and B. Chen, *Angew. Chem., Int. Ed.*, 2019, **58**, 10209–10214.
53 C. Song, F. Zheng, Y. Liu, Q. Yang, Z. Zhang, Q. Ren and Z. Bao, *Angew. Chem., Int. Ed.*, 2023, **62**, e202313855.
54 J. Cui, Z. Zhang, L. Yang, J. Hu, A. Jin, Z. Yang, Y. Zhao, B. Meng, Y. Zhou, J. Wang, Y. Su, J. Wang, X. Cui and H. Xing, *Science*, 2024, **383**, 179–183.
55 Y.-J. Tian, C. Deng, L. Zhao, J.-S. Zou, X.-C. Wu, Y. Jia, Z.-Y. Zhang, J. Zhang, Y.-L. Peng, G. Chen and M. J. Zaworotko, *Nat. Chem.*, 2025, **17**, 141–147.
56 S.-M. Wang, M. Shivanna, S.-T. Zheng, T. Pham, K. A. Forrest, Q.-Y. Yang, Q. Guan, B. Space, S. Kitagawa and M. J. Zaworotko, *J. Am. Chem. Soc.*, 2024, **146**, 4153–4161.
57 Y. Jiang, J. Hu, L. Wang, W. Sun, N. Xu, R. Krishna, S. Duttwyler, X. Cui, H. Xing and Y. Zhang, *Angew. Chem., Int. Ed.*, 2022, **134**, e202200947.
58 Y. Hu, Y. Jiang, J. Li, L. Wang, M. Steiner, R. F. Neumann, B. Luan and Y. Zhang, *Adv. Funct. Mater.*, 2023, **33**, 2213915.
59 S.-C. Xiang, Z. Zhang, C.-G. Zhao, K. Hong, X. Zhao, D.-R. Ding, M.-H. Xie, C.-D. Wu, M. C. Das, R. Gill, K. M. Thomas and B. Chen, *Nat. Commun.*, 2011, **2**, 204.
60 X.-J. Xie, Z.-H. Zhang, Q.-Y. Cao, Y.-L. Huang, D. Luo, H. Zeng, W. Lu and D. Li, *J. Am. Chem. Soc.*, 2024, **146**, 30155–30163.
61 H. Yang, F. Peng, D. E. Schier, S. A. Markotic, X. Zhao, A. N. Hong, Y. Wang, P. Feng and X. Bu, *Angew. Chem., Int. Ed.*, 2021, **60**, 11148–11152.
62 W. Yang, J. Wang, K. Tan, H. L. Zhou, M. Zhang, R. Krishna, J. Duan and L. Huang, *Angew. Chem., Int. Ed.*, 2025, **64**, e202425638.
63 Y. Ye, Y. Xie, Y. Shi, L. Gong, J. Phipps, A. M. Al-Enizi, A. Nafady, B. Chen and S. Ma, *Angew Chem. Int. Ed. Engl.*, 2023, **62**, e202302564.
64 L. Yu, X. Han, H. Wang, S. Ullah, Q. Xia, W. Li, J. Li, I. da Silva, P. Manuel, S. Rudić, Y. Cheng, S. Yang, T. Thonhauser and J. Li, *J. Am. Chem. Soc.*, 2021, **143**, 19300–19305.
65 H. Zeng, M. Xie, T. Wang, R.-J. Wei, X.-J. Xie, Y. Zhao, W. Lu and D. Li, *Nature*, 2021, **595**, 542–548.
66 L. Zhang, B. Yu, M. Wang, Y. Chen, Y. Wang, L.-B. Sun, Y.-B. Zhang, Z. Zhang, J. Li and L. Li, *Angew. Chem., Int. Ed.*, 2025, **64**, e202418853.
67 P. Zhang, Y. Zhong, Y. Zhang, Z. Zhu, Y. Liu, Y. Su, J. Chen, S. Chen, Z. Zeng, H. Xing, S. Deng and J. Wang, *Sci. Adv.*, 2022, **8**, eabn9231.
68 Y.-B. Wang, T.-F. Zhang, Y.-X. Lin, J.-X. Wang, H.-M. Wen, X. Zhang, G. Qian and B. Li, *J. Mater. Chem. A*, 2024, **12**, 25812–25819.
69 J. Wan, H. L. Zhou, K. Hyeon-Deuk, I. Y. Chang, Y. Huang, R. Krishna and J. Duan, *Angew. Chem., Int. Ed.*, 2023, **62**, e202316792.
70 R.-B. Lin, L. Li, H.-L. Zhou, H. Wu, C. He, S. Li, R. Krishna, J. Li, W. Zhou and B. Chen, *Nat. Mater.*, 2018, **17**, 1128–1133.
71 N. Nijem, H. Wu, P. Canepa, A. Marti, K. J. Balkus Jr., T. Thonhauser, J. Li and Y. J. Chabal, *J. Am. Chem. Soc.*, 2012, **134**, 15201–15204.
72 C. Gu, N. Hosono, J. J. Zheng, Y. Sato, S. Kusaka, S. Sakaki and S. Kitagawa, *Science*, 2019, **363**, 387–391.
73 Y. Wang, T. Li, L. Li, R.-B. Lin, X. Jia, Z. Chang, H.-M. Wen, X.-M. Chen and J. Li, *Adv. Mater.*, 2023, **35**, 2207955.
74 Y. Su, K.-I. Otake, J.-J. Zheng, P. Wang, Q. Lin, S. Kitagawa and C. Gu, *Nat. Commun.*, 2024, **15**, 2898.
75 S. Kitagawa and M. Kondo, *Bull. Chem. Soc. Jpn.*, 1998, **71**, 1739–1753.
76 S. Horike, S. Shimomura and S. Kitagawa, *Nat. Chem.*, 2009, **1**, 695–704.
77 U. Kökçam-Demir, A. Goldman, L. Esrafili, M. Gharib, A. Morsali, O. Weingart and C. Janiak, *Chem. Soc. Rev.*, 2020, **49**, 2751–2798.
78 J. N. Hall and P. Bollini, *React. Chem. Eng.*, 2019, **4**, 207–222.
79 L. Alaerts, M. Maes, M. A. van der Veen, P. A. Jacobs and D. E. De Vos, *Phys. Chem. Chem. Phys.*, 2009, **11**, 2903–2911.
80 S. H. Yang, A. J. Ramirez-Cuesta, R. Newby, V. Garcia-Sakai, P. Manuel, S. K. Callear, S. I. Campbell, C. C. Tang and M. Schroder, *Nat. Chem.*, 2015, **7**, 121–129.
81 Y. Duan, Y. Huang, C. Wang, Q. Wang, K. Ge, Z. Lu, H. Wang, J. Duan, J. Bai and W. Jin, *Chem. Sci.*, 2023, **14**, 4605–4611.
82 H. G. Hao, Y. F. Zhao, D. M. Chen, J. M. Yu, K. Tan, S. Q. Ma, Y. Chabal, Z. M. Zhang, J. M. Dou, Z. H. Xiao, G. Day, H. C. Zhou and T. B. Lu, *Angew. Chem., Int. Ed.*, 2018, **57**, 16067–16071.
83 E. Y. Wu, X. W. Gu, D. Liu, X. Zhang, H. Wu, W. Zhou, G. D. Qian and B. Li, *Nat. Commun.*, 2023, **14**, 6146.
84 Y. H. Huang, Y. F. Feng, Y. Li, K. Tan, J. Tang, J. F. Bai and J. G. Duan, *Angew. Chem., Int. Ed.*, 2024, **63**, e202403421.
85 Z. Q. Zhang, S. B. Peh, Y. X. Wang, C. J. Kang, W. D. Fan and D. Zhao, *Angew. Chem., Int. Ed.*, 2020, **59**, 18927–18932.
86 S. Noro, S. Kitagawa, M. Kondo and K. Seki, *Angew. Chem., Int. Ed.*, 2000, **39**, 2082–2084.
87 P. Nugent, Y. Belmabkhout, S. D. Burd, A. J. Cairns, R. Luebke, K. Forrest, T. Pham, S. Q. Ma, B. Space, L. Wojtas, M. Eddaoudi and M. J. Zaworotko, *Nature*, 2013, **495**, 80–84.

© 2025 The Author(s). Published by the Royal Society of Chemistry

Open Access Article. Published on 02 June 2025. Downloaded on 5/21/2026 10:40:29 PM. This article is licensed under a Creative Commons Attribution-NonCommercial 3.0 Unported Licence.

88 Y. Wang, N.-Y. Huang, X.-W. Zhang, H. He, R.-K. Huang, Z.-M. Ye, Y. Li, D.-D. Zhou, P.-Q. Liao, X.-M. Chen and J.-P. Zhang, *Angew. Chem., Int. Ed.*, 2019, **58**, 7692–7696.
89 G. D. Wang, Y. Z. Li, W. F. Zhang, L. Hou, Y. Y. Wang and Z. H. Zhu, *ACS Appl. Mater. Interfaces*, 2021, **13**, 58862–58870.
90 D. Liu, J. Pei, X. Zhang, X.-W. Gu, H.-M. Wen, B. Chen, G. Qian and B. Li, *Angew. Chem., Int. Ed.*, 2023, **62**, e202218590.
91 R. B. Lin, L. B. Li, H. Wu, H. Arman, B. Li, R. G. Lin, W. Zhou and B. L. Chen, *J. Am. Chem. Soc.*, 2017, **139**, 8022–8028.
92 Q. Dong, X. Zhang, S. Liu, R. B. Lin, Y. Guo, Y. Ma, A. Yonezu, R. Krishna, G. Liu, J. Duan, R. Matsuda, W. Jin and B. Chen, *Angew. Chem., Int. Ed.*, 2020, **59**, 22756–22762.
93 S. Bourrelly, P. L. Llewellyn, C. Serre, F. Millange, T. Loiseau and G. Férey, *J. Am. Chem. Soc.*, 2005, **127**, 13519–13521.
94 P. L. Llewellyn, P. Horcajada, G. Maurin, T. Devic, N. Rosenbach, S. Bourrelly, C. Serre, D. Vincent, S. Loera-Serna, Y. Filinchuk and G. Ferey, *J. Am. Chem. Soc.*, 2009, **131**, 13002–13008.
95 J. A. Mason, J. Oktawiec, M. K. Taylor, M. R. Hudson, J. Rodriguez, J. E. Bachman, M. I. Gonzalez, A. Cervellino, A. Guagliardi, C. M. Brown, P. L. Llewellyn, N. Masciocchi and J. R. Long, *Nature*, 2015, **527**, 357–361.
96 M. K. Taylor, T. Runcevski, J. Oktawiec, M. I. Gonzalez, R. L. Siegelman, J. A. Mason, J. X. Ye, C. M. Brown and J. R. Long, *J. Am. Chem. Soc.*, 2016, **138**, 15019–15026.
97 S. Gao, C. G. Morris, Z. Z. Lu, Y. Yan, H. G. W. Godfrey, C. Murray, C. C. Tang, K. M. Thomas, S. H. Yang and M. Schröder, *Chem. Mater.*, 2016, **28**, 2331–2340.
98 L. B. Upi, R. Krishna, Y. Wang, X. Q. Wang, J. F. Yang and J. P. Li, *Eur. J. Inorg. Chem.*, 2016, **2016**, 4457–4462.
99 R. Kitaura, S. Kitagawa, Y. Kubota, T. C. Kobayashi, K. Kindo, Y. Mita, A. Matsuo, M. Kobayashi, H. C. Chang, T. C. Ozawa, M. Suzuki, M. Sakata and M. Takata, *Science*, 2002, **298**, 2358–2361.
100 R. Matsuda, R. Kitaura, S. Kitagawa, Y. Kubota, R. V. Belosludov, T. C. Kobayashi, H. Sakamoto, T. Chiba, M. Takata, Y. Kawazoe and Y. Mita, *Nature*, 2005, **436**, 238–241.
101 K. Kishida, Y. Watanabe, S. Horike, Y. Watanabe, Y. Okumura, Y. Hijikata, S. Sakaki and S. Kitagawa, *Eur. J. Inorg. Chem.*, 2014, **2014**, 2747–2752.
102 Y. W. Chen, Z. W. Qiao, D. F. Lv, C. X. Duan, X. J. Sun, H. X. Wu, R. F. Shi, Q. B. Xia and Z. Li, *Chem. Eng. J.*, 2017, **328**, 360–367.
103 H. Zeng, M. Xie, Y.-L. Huang, Y. Zhao, X.-J. Xie, J.-P. Bai, M.-Y. Wan, R. Krishna, W. Lu and D. Li, *Angew. Chem., Int. Ed.*, 2019, **58**, 8515–8519.
104 A. Schneemann, V. Bon, I. Schwedler, I. Senkovska, S. Kaskel and R. A. Fischer, *Chem. Soc. Rev.*, 2014, **43**, 6062–6096.
105 Y. Su, K. Otake, J. J. Zheng, S. Horike, S. Kitagawa and C. Gu, *Nature*, 2022, **611**, 289–294.
106 H. Zeng, X.-J. Xie, T. Wang, M. Xie, Y. Wang, R.-J. Wei, W. Lu and D. Li, *Nat. Chem. Eng.*, 2024, **1**, 108–115.
107 Q. J. Wang, J. B. Hu, L. F. Yang, Z. Q. Zhang, T. Ke, X. L. Cui and H. B. Xing, *Nat. Commun.*, 2022, **13**, 2955.
108 L. B. Li, H. M. Wen, C. H. He, R. B. Lin, R. Krishna, H. Wu, W. Zhou, J. P. Li, B. Li and B. L. Chen, *Angew. Chem., Int. Ed.*, 2018, **57**, 15183–15188.
109 W.-G. Cui, T.-L. Hu and X.-H. Bu, *Adv. Mater.*, 2020, **32**, 1806445.
110 C. Y. Chuah, H. Lee and T.-H. Bae, *Chem. Eng. J.*, 2022, **430**, 132654.
111 S. Q. Yang and T. L. Hu, *Coord. Chem. Rev.*, 2022, **468**, 214628.
112 L. Wang, S. Wu, J. Hu, Y. Jiang, J. Li, Y. Hu, Y. Han, T. Ben, B. Chen and Y. Zhang, *Chem. Sci.*, 2024, **15**, 5653–5659.
113 Y. B. He, R. Krishna and B. L. Chen, *Energy Environ. Sci.*, 2012, **5**, 9107–9120.
114 T. Ke, Q. Wang, J. Shen, J. Zhou, Z. Bao, Q. Yang and Q. Ren, *Angew. Chem., Int. Ed.*, 2020, **59**, 12725–12730.
115 L. Yang, X. Cui, Y. Zhang, Q. Yang and H. Xing, *J. Mater. Chem. A*, 2018, **6**, 24452–24458.
116 C. Yu, Z. Guo, L. Yang, J. Cui, S. Chen, Y. Bo, X. Suo, Q. Gong, S. Zhang, X. Cui, S. He and H. Xing, *Angew. Chem., Int. Ed.*, 2023, **62**, e202218027.
117 S. Tu, D. X. Lin, J. J. Huang, L. Yu, Z. W. Liu, Z. Li and Q. B. Xia, *Microporous Mesoporous Mater.*, 2023, **354**, 112532.
118 X.-W. Zhang, H. He, Y.-W. Gan, Y. Wang, N.-Y. Huang, P.-Q. Liao, J.-P. Zhang and X.-M. Chen, *Angew. Chem., Int. Ed.*, 2024, **63**, e202317648.
119 J. Shen, X. He, T. Ke, R. Krishna and Q. Ren, *Nat. Commun.*, 2020, **11**, 6259.
120 X. Zhang, Q. C. Chen, X. F. Bai, Y. L. Zhao and J. R. Li, *Angew. Chem., Int. Ed.*, 2024, **63**, e202411744.
121 X.-W. Gu, E. Wu, J.-X. Wang, H.-M. Wen, B. Chen, B. Li and G. Qian, *Sci. Adv.*, 2023, **9**, eadh0135.
122 B. Zhu, J.-W. Cao, S. Mukherjee, T. Pham, T. Zhang, T. Wang, X. Jiang, K. A. Forrest, M. J. Zaworotko and K.-J. Chen, *J. Am. Chem. Soc.*, 2021, **143**, 1485–1492.
123 H. M. Wen, C. Y. Yu, M. Y. Liu, C. Y. Lin, B. Y. Zhao, H. Wu, W. Zhou, B. L. Chen and J. Hu, *Angew. Chem., Int. Ed.*, 2023, **62**, e202309108.
124 X. Zhao, Y. Wang, D.-S. Li, X. Bu and P. Feng, *Adv. Mater.*, 2018, **30**, 1705189.
125 Y. Y. Xue, J. Lei, H. J. Lv, P. Liang, L. Q. Li and Q. G. Zhai, *Small*, 2024, **20**, 2311555.
126 D.-X. Xue, A. Cadiau, Ł. J. Weseliński, H. Jiang, P. M. Bhatt, A. Shkurenko, L. Wojtas, C. Zhijie, Y. Belmabkhout, K. Adil and M. Eddaoudi, *Chem. Commun.*, 2018, **54**, 6404–6407.
127 L. F. Yang, X. L. Cui, Q. W. Yang, S. H. Qian, H. Wu, Z. B. Bao, Z. G. Zhang, Q. L. Ren, W. Zhou, B. L. Chen and H. B. Xing, *Adv. Mater.*, 2018, **30**, 1705374–1705381.
128 Y. J. Jiang, L. Y. Wang, T. A. Yan, J. B. Hu, W. Q. Sun, R. Krishna, D. M. Wang, Z. L. Gu, D. H. Liu, X. L. Cui, H. B. Xing and Y. B. Zhang, *Chem. Sci.*, 2023, **14**, 298–309.
129 P. Zhang, L. Yang, X. Liu, J. Wang, X. Suo, L. Chen, X. Cui and H. Xing, *Nat. Commun.*, 2022, **13**, 4928.
130 C. Zhang, F. Formalik, D. Lv, F. Sha, K. O. Kirlikovali, X. Wang, X. Tang, S. Su, H. Xie, Y. Chen, Z. Li,

Open Access Article. Published on 02 June 2025. Downloaded on 5/21/2026 10:40:29 PM. This article is licensed under a Creative Commons Attribution-NonCommercial 3.0 Unported Licence.

R. Q. Snurr and O. K. Farha, *Angew. Chem., Int. Ed.*, 2025, **64**, e202424260.
131 W. Gong, Y. Xie, A. Yamano, S. Ito, E. W. Reinheimer, J. Dong, C. D. Malliakas, D. M. Proserpio, Y. Cui and O. K. Farha, *Angew. Chem., Int. Ed.*, 2024, **63**, e202318475.
132 G. D. Wang, Y. Z. Li, R. Krishna, W. Y. Zhang, L. Hou, Y. Y. Wang and Z. Zhu, *Angew. Chem., Int. Ed.*, 2024, **63**, e202319978.
133 G.-D. Wang, Y.-Z. Li, W.-J. Shi, L. Hou, Y.-Y. Wang and Z. Zhu, *Angew. Chem., Int. Ed.*, 2022, **61**, e202205427.
134 Z.-H. Guo, X.-Q. Wu, Y.-P. Wu, D.-S. Li, G.-P. Yang and Y.-Y. Wang, *Angew. Chem., Int. Ed.*, 2025, **64**, e202421992.
135 Y.-Y. Xue, J. Lei, H.-J. Lv, P. Liang, L. Li and Q.-G. Zhai, *Small*, 2024, **20**, 2311555.
136 M.-Y. Gao, A. A. Bezrukov, B.-Q. Song, M. He, S. J. Nikkhah, S.-Q. Wang, N. Kumar, S. Darwish, D. Sensharma, C. Deng, J. Li, L. Liu, R. Krishna, M. Vandichel, S. Yang and M. J. Zaworotko, *J. Am. Chem. Soc.*, 2023, **145**, 11837–11845.
137 Y.-Z. Li, G.-D. Wang, R. Krishna, Q. Yin, D. Zhao, J. Qi, Y. Sui and L. Hou, *Chem. Eng. J.*, 2023, **466**, 143056.
138 G. D. Wang, R. Krishna, Y. Z. Li, W. J. Shi, L. Hou, Y. Y. Wang and Z. Zhu, *Angew. Chem.*, 2022, **61**, e202213015.
139 L. Li, L. Guo, F. Zheng, Z. Zhang, Q. Yang, Y. Yang, Q. Ren and Z. Bao, *ACS Appl. Mater. Interfaces*, 2020, **12**, 17147–17154.
140 Y. Jiang, L. Wang, T. Yan, J. Hu, W. Sun, R. Krishna, D. Wang, Z. Gu, D. Liu, X. Cui, H. Xing and Y. Zhang, *Chem. Sci.*, 2023, **14**, 298–309.
141 Y. Jiang, L. Wang, J. Hu, R. Krishna, B. Chen and Y. Zhang, *Adv. Mater.*, 2024, **36**, 2311140.
142 J. W. Ren, X. Dyosiba, N. M. Musyoka, H. W. Langmi, M. Mathe and S. J. Liao, *Coord. Chem. Rev.*, 2017, **352**, 187–219.
143 M. Rubio-Martinez, C. Avci-Camur, A. W. Thornton, I. Imaz, D. Maspoch and M. R. Hill, *Chem. Soc. Rev.*, 2017, **46**, 3453–3480.
144 G. R. Cai, X. Ma, M. Kassymova, K. Sun, M. L. Ding and H. L. Jiang, *ACS Cent. Sci.*, 2021, **7**, 1434–1440.
145 D. Chakraborty, A. Yurdusen, G. Mouchaham, F. Nouar and C. Serre, *Adv. Funct. Mater.*, 2024, **34**, 2309089.
146 M. Taddei, D. A. Steitz, J. A. van Bokhoven and M. Ranocchiari, *Chem.–Eur. J.*, 2016, **22**, 3245–3249.
147 T. Gao, H. J. Tang, S. Y. Zhang, J. W. Cao, Y. N. Wu, J. Chen, Y. Wang and K. J. Chen, *J. Solid State Chem.*, 2021, **303**, 122547.
148 U. Mueller, M. Schubert, F. Teich, H. Puetter, K. Schierle-Arndt and J. Pastre, *ChemInform*, 2006, **37**, 626–636.
149 J.-B. Lin, T. T. T. Nguyen, R. Vaidhyanathan, J. Burner, J. M. Taylor, H. Durekova, F. Akhtar, R. K. Mah, O. Ghaffari-Nik, S. Marx, N. Fylstra, S. S. Iremonger, K. W. Dawson, P. Sarkar, P. Hovington, A. Rajendran, T. K. Woo and G. K. H. Shimizu, *Science*, 2021, **374**, 1464–1469.
150 S. Geng, E. Lin, X. Li, W. Liu, T. Wang, Z. Wang, D. Sensharma, S. Darwish, Y. H. Andaloussi, T. Pham, P. Cheng, M. J. Zaworotko, Y. Chen and Z. Zhang, *J. Am. Chem. Soc.*, 2021, **143**, 8654–8660.
151 B. Zhou, Q. Li, Q. Zhang, J. Duan and W. Jin, *J. Membr. Sci.*, 2020, **597**, 117772.
152 D. Crawford, J. Casaban, R. Haydon, N. Giri, T. Mcnally and S. L. James, *Chem. Sci.*, 2015, **6**, 1645–1649.
153 C. Xu, S. De, A. M. Balu, M. Ojeda and R. Luque, *Chem. Commun.*, 2015, **51**, 6698–6713.
154 M. Vadivelu, S. Sugirdha, P. Dheenkumar, Y. Arun and K. Karthikeyan, *Green Chem.*, 2017, **19**, 3601–3610.
155 Y. Wang, H. Wang, Y. Jiang, C. Zhang, J. Shao and D. Xu, *Green Chem.*, 2017, **19**, 1674–1677.
156 Q. Cao, R. T. Fallis, I. A. Browne and L. Duncan, *ChemSusChem*, 2019, **12**, 2554–2557.
157 A. Pichon, A. Lazuen-Garay and S. L. James, *CrystEngComm*, 2006, **8**, 211–214.
158 Y. Liang, G. Xie, K.-K. Liu, M. Jin, Y. Chen, X. Yang, Z.-J. Guan, H. Xing and Y. Fang, *Angew. Chem., Int. Ed.*, 2025, **64**, e202416884.
159 T. D. Bennett, S. Cao, J. C. Tan, D. A. Keen, E. G. Bithell, P. J. Beldon, T. Friscic and A. K. Cheetham, *J. Am. Chem. Soc.*, 2011, **133**, 14546–14549.
160 O. M. Yaghi, R. Jernigan, H. Li, C. E. Davis and T. L. Groy, *J. Chem. Soc., Dalton Trans.*, 1997, 2383–2384.
161 S.-N. Kim, Y.-R. Lee, S.-H. Hong, M.-S. Jang and W.-S. Ahn, *Catal. Today*, 2015, **245**, 54–60.
162 T. K. Vo, V. N. Le, K. S. Yoo, M. Song, D. Kim and J. Kim, *Cryst. Growth Des.*, 2019, **19**, 4949–4956.
163 K. Pobłocki, J. Drzeżdżon, B. Gawdzik and D. Jacewicz, *Green Chem.*, 2022, **24**, 9402–9427.
164 U. Mueller, M. Schubert, F. Teich, H. Puetter, K. Schierle-Arndt and J. Pastré, *J. Mater. Chem.*, 2006, **16**, 626–636.
165 J. Britton and C. L. Raston, *Chem. Soc. Rev.*, 2017, **46**, 1250.
166 M. Guidi, P. H. Seeberger and K. Gilmore, *Chem. Soc. Rev.*, 2020, **49**, 8910.
167 C. McKinstry, R. J. Cathcart, E. J. Cussen, A. J. Fletcher, S. V. Patwardhan and J. Sefcik, *Chem. Eng. J.*, 2016, **285**, 718–725.
168 G. H. Albuquerque, R. C. Fitzmorris, M. Ahmadi, N. Wannenmacher, P. K. Thallapally, B. P. McGrail and G. S. Herman, *CrystEngComm*, 2015, **17**, 5502–5510.
169 H. Ren and T. X. Wei, *Chemelectrochem*, 2022, **9**, e202200196.
170 N. Campagnol, T. R. C. Van Assche, M. Y. Li, L. Stappers, M. Dinca, J. F. M. Denayer, K. Binnemans, D. E. De Vos and J. Fransaer, *J. Mater. Chem. A*, 2016, **4**, 3914–3925.

© 2025 The Author(s). Published by the Royal Society of Chemistry